Neural substrates of psychotic-like states and cognitive impairment in a mouse model of schizophrenia and subsequent rescue by antipsychotic drugs

Cristina Delgado Sallent

TESI DOCTORAL UPF / 2021

Thesis supervisor

Dra. Maria Victoria Puig Velasco

Neurosciences Research Programme, Hospital del Mar Medical Research Institute (IMIM)

DEPARTMENT OF EXPERIMENTAL AND HEALTH SCIENCES. UNIVERSITAT POMPEU FABRA

upf.

IMIM Parc de Salut MAR Barcelona
Institut Hospital del Mar d'Investigacions Mèdiques

AGAUR Agència de Gestió d'Ajuts Universitaris i de Recerca

Dedication and acknowledgements

Me siento afortunada de haber estado tan bien rodeada estos años durante mi doctorado. Me habéis ayudado mucho a aprender y a evolucionar. Quiero agradecer a todos, a nivel laboral, de amistad y de familia.

Primer de tot, m'agradaria agrair a la Vicky per donar-me la oportunitat de poder fer el doctorat i guiar-me durant aquesta experiencia. He evolucionat i he après molt amb tú. Espero que aquesta nova aventura a la UAB et vagi molt bé. También quiero agradecerle a Thomas todo lo que me ha enseñado, des de empezar a manipular a un ratón hasta las complejas cirugías, pasando por todo el mundo de los registros y la electrofisiología. Pau, te tengo que reconocer que no sabría codificar ni un cuarto de lo que sé si no hubieras estado allí. Has tenido siempre la paciencia conmigo, no importaba cuantas veces te preguntara y molestara, siempre estabas allí, para ayudar-me a hacer la magia. Muchas gracias! Maria, moltes gracies a tu també, per ser la primera que em va ajudar i ensenyar quan vaig entrar al lab i sobretot, per ser la meva consellera. No se que hauria fet sense les trucades d'emergència i les llargues

converses. Pablo, mi compañero de batallas, ha sido un placer poder compartir esta experiencia contigo y podernos ayudar mutuamente. Meli, it was a pleasure to meet you, you changed the energy of the lab! Marta, gracies per tots els moments al lab i per ensenyar-me els trucs del sorting. Melina is was really nice meeting you and you help me a lot with the histology part.

També voldría agrair a tota la resta de companys del IMIM i el PRBB, sense vosaltres la experiencia no hauria set igual. Especialmente a la Thais, mi terapeuta personal, no se que habría hecho yo sin nuestras largas sesiones por las tardes y todo el apoyo que me has mostrado. También querría agradecer a la Patricia por las conversaciones y la ayuda. Y a la resta de companys, sempre ha sigut un plaer trovaros als passadisos i parlar amb vosaltres. También me gustaría darte las gracias a ti, Marisol, especialmente durante esos meses tan duros de cuarentena en las que éramos de las pocas que estábamos por el edificio y discutíamos sobre el mundo. También agradecer a toda la gente del Barccsyn y que conocí en Madrid gracias al Abneural Nets.

También me gustaría agradecer a mi otra familia, los que me conocen des de siempre. Especialmente a vosotras, Mini, Mire, Carmen y

Vicky, que siempre estáis allí y me apoyáis siempre. Gracias por estar siempre allí en todos los momentos jodidos que he tenido que pasar. Siempre tendremos nuestras tardes de cervezas eternas, porque sé que siempre estaréis allí. También a ti Uri, por tomarte tus días de paro para ayudarme a hacer videos de ratones, y también con el Gabal por ser los que siempre han estado y estarán allí. Gracias también a mi familia, especialmente Mama, Papa y Laia, que siempre habéis estado allí para cuidarme y defenderme. Estoy aquí gracias a que vosotros siempre me habéis empujado y guiado a ser la mejor versión de mi misma. Donde he llegado os lo debo a vosotros y siempre seguiré haciendo y buscando lo que me haga feliz.

And finally I wanted to thank you, Amanda, my partner and my best friend. You make me a better person. You are the person that makes me believe in myself. You always are there for me, supporting me and believing in me, even when I can't do it. I would not be here without you. Who would say that you will be that important in my life a few years ago? I am so lucky to have you in my life.

Abstract

Disruption of neural synchrony and spatio-temporal communication in brain circuits involving the prefrontal cortex and the hippocampus has been suggested to be a hallmark characteristic of neuropsychiatric disorders such as schizophrenia. Schizophrenia patients show positive symptoms that can be effectively managed with antipsychotic drugs. However, negative symptoms and cognitive deficits are inadequately treated. Therefore, a better understanding of the prefrontal-hippocampal neural basis of these symptoms is essential for the development of new treatments. In the present thesis, we investigated the alterations of prefrontal-hippocampal circuits in the phencyclidine, acute and subchronic (sPCP), mouse model of schizophrenia and how some of these alterations can be recovered by antipsychotic drugs. We recorded neural activity in the prefrontal cortex and hippocampus of C57BL/6J mice. In the first part of the thesis, we investigated the neural substrates of psychosis-like states induced by acute PCP and the rescuing abilities of antipsychotic drugs or serotonergic agents. In the second part, we investigated the neural substrates of cognitive impairment induced by the sPCP treatment. We also assessed behavioral and neurophysiological

rescue by a 14-day treatment with the atypical antipsychotic drug risperidone. Acute administration of PCP produced hypersynchronization and disrupted communication of prefrontal-hippocampal pathways that were recovered by the atypical antipsychotic drugs risperidone and clozapine, but not typical antipsychotic drug haloperidol, likely due their greater affinity for serotonin receptors. Furthermore, sPCP-treated mice showed brain state alterations in gamma oscillations and theta-gamma cross-frequency coupling. Notably, auditory perception, working memory and long-term memory were profoundly impaired in sPCP-treated mice and were accompanied by disrupted prefrontal-hippocampal functional connectivity within theta (4-12 Hz) and gamma (30-100 Hz) ranges. Finally, the chronic risperidone treatment was able to recover memory deficits by partially restoring some of the neurophysiological biomarkers, but was unable to restore the basal circuit dynamics.

Resumen

Una de las características distintivas de los trastornos psiquiátricos, tal como la esquizofrenia, es la perturbación de la comunicación y sincronicidad de los circuitos cerebrales que incluyen la corteza prefrontal y el hipocampo. Las personas con esquizofrenia presentan síntomas positivos que se pueden tratar con medicación antipsicótica. Sin embargo, los síntomas negativos o los déficits cognitivos no responden a esta medicación. Por lo tanto, un mejor entendimiento de las bases neurales de los circuitos prefrontal-hipocampales durante estos síntomas es esencial para el desarrollo de nuevos tratamientos. En esta tesis, hemos investigado las alteraciones en los circuitos prefrontal-hipocampales en un modelo de esquizofrenia en ratones basado en el tratamiento de fenciclidina, agudo o subcrónico (sPCP), y cómo estas alteraciones pueden ser recuperadas por antipsicóticos. Para poder llevar esto a cabo, hemos registrado actividad neural simultáneamente en la corteza prefrontal y el hipocampo de ratones C57BL/6J. En la primera parte de la tesis, hemos investigado los sustratos neurales de los estados psicóticos inducidos por PCP agudo y como diferentes antipsicóticos o componentes serotoninérgicos los recuperan. En la segunda parte, hemos investigado los sustratos

neurales de los déficits cognitivos producidos por el tratamiento subcrónico de PCP. También hemos evaluado la recuperación del comportamiento y los biomarcadores neurofisiológicos generada por un tratamiento de risperidona de 14 días. La administración aguda de PCP produce híper sincronización y perturba la comunicación de los circuitos prefrontal-hipocampales. Estas alteraciones pueden ser recuperadas por los antipsicóticos atípicos, risperidona y clozapina, pero no típicos, como el haloperidol, probablemente debido a su mayor afinidad por los receptores serotoninérgicos. Además, los ratones tratados con sPCP muestran alteraciones de circuito en las oscilaciones gamma y en el acoplamiento cross-frecuencia theta-gamma. Particularmente, el tratamiento sPCP perjudica la percepción auditiva, la memoria de trabajo y la memoria a largo plazo. Todas estas alteraciones van acompañadas de alteraciones en la conectividad funcional en los rangos theta (4-12 Hz) y gamma (30-100 Hz) de los circuitos prefrontal-hipocampales. Finalmente, el tratamiento crónico de risperidona es capaz de recuperar los déficits de memoria restaurando parcialmente algunos biomarcadores neurofisiológicos, pero es incapaz de restaurar las dinámicas basales del circuito.

Preface or introduction

Cristina Delgado Sallent was supported by a predoctoral fellowship "Grants for the recruitment of new research staff" (FI-2018, 2018 FI_B_00112 to CD-S) awarded by the "Agència de Gestió d'Ajuts Universitaris i de Recerca (AGAUR)" of the Generalitat de Catalunya with the collaboration of the European Social Fund. The work presented in this thesis received financial support from Spanish Agencia Estatal de Investigación (AEI/FEDER, UE; grant numbers SAF2016-80726-R, PID2019-104683RB-I00).

This thesis aimed to understand the neural mechanisms underlying distinct symptomatology in schizophrenia, one of the most devastating neuropsychiatric disorders, from a preclinical point of view. A second major objective has been to gain insight into how the current medication affects pathological neural dynamics within the context of psychosis and cognitive impairment. Understanding how the circuit is disrupted in pathological conditions and how it is affected by the current medication may help develop new therapeutic interventions.

Table of contents

List of figures

Pàg.

List of tables

1. INTRODUCTION

1. INTRODUCTION

1.1. The pathophysiology of schizophrenia

1.1.1 Introduction: symptoms and outcomes

Schizophrenia is a devastating disease inflicting around 50 million people worldwide, with 1.5 million people diagnosed every year, usually between the ages of 18 and 25 years old (Owen et al., 2016). Symptoms of schizophrenia are intricate and vary between patients; however they can be roughly divided into three groups: positive and negative symptoms, and cognitive deficits (Sigurdsson, 2016).

Subtle structural abnormalities have been found in patients with schizophrenia; however they cannot be clearly tied to functional alterations (Hunt et al., 2017a). This may reflect the complex nature of the disease and the heterogeneity of its physiopathology. The lack of specific structural markers has led to hypothesize that schizophrenia and schizophrenia-like symptoms arise from the disruption of the neural development produced by a combination of environmental and genetic factors, which ultimately lead to disruption of neural circuits (Lewis and Levitt, 2002). Neural circuit dysfunction has proved difficult to study in patients, and therefore animal

models of schizophrenia have been vital in understanding the disease in greater depth. Furthermore, animal models are used to investigate the implications of genetic and environmental risk factors, anomalies on neural circuits, pathophysiology and etiology of the disease (Nestler and Hyman, 2010).

Historically, the pathophysiology of schizophrenia has been thought to be explained by two different hypotheses: the dopamine hypothesis and the glutamate hypothesis. The dopamine hypothesis postulates that schizophrenia is caused by the overactivation of dopamine receptors. Alternatively, the glutamate hypothesis theorizes that schizophrenia arises from diminished activation of NMDA (N-methyl-D-aspartate) receptors that lead to hypofunction of glutamatergic signaling resulting in psychotic episodes (Howes et al. 2015). However, as more research has emerged, it appears that the pathophysiology of schizophrenia may be due to a combination of signal dysfunction, specifically alterations in dopaminergic, glutamatergic, serotonergic, cholinergic and gamma-aminobutyric acid (GABA) signaling. Disruption in the collective balance of these neurotransmitter systems is thought to give rise to core symptoms of the disease (Yang and Tsai, 2017). Although such neurochemical anomalies in schizophrenia are beginning to become elucidated, how they

contribute to the pathophysiology of the disease is unclear. Neural circuit abnormalities, specifically changes in oscillatory patterns and circuit connectivity, are most likely the proximal cause for symptoms of schizophrenia in patients and behavioral deficits found in animal models (Sigurdsson, 2016). Therefore, understanding dysfunctional network activity may be the key to understanding the pathophysiological mechanisms that give rise to schizophrenia.

1.1.2. Developmental and neurochemical hypotheses of schizophrenia

Disruption of early neurodevelopment that culminates in neural circuit dysfunction is hypothesized to underlie later onset of schizophrenia and schizophrenic-like symptoms. This disruption in neurodevelopment is likely caused by the combination of genetic susceptibility and environmental factors (Lewis and Levitt, 2002). Therefore, the study of risk factors for schizophrenia are centered around those that affect early brain development, pre- and postnatally. Environmental risk factors include maternal stress, maternal infections, prenatal inflammation and nutritional deficiencies. Risk factors that may affect postnatal development and create a higher risk of developing schizophrenia include traumatic

brain injury, exposure to severe infection, drug abuse and social isolation (Millan et al., 2016; Owen et al., 2016). Genome-wide association studies (GWAS) have given insights into the genetic risk factors and have thus far identified over 100 distinct genetic loci and 11 copy number variants (CNVs) that confer a risk with the onset of schizophrenia. Two major understandings taken from these GWAS studies is that schizophrenia is a highly polygenic disease and genetic risk is quite pleiotropic, and risk variants are shared between many different neuropsychiatric diseases such as bipolar, ADHD and major depressive disorder. These findings imply that there are multiple mechanisms at work that lead to the cause of neuropsychiatric disorders and the clinical definition of each disorder is much more intertwined than previously thought (Owen et al., 2016). Furthermore, environmental interactions with specific risk genes may be the key in understanding which symptoms or neuropsychiatric disorder will arise.

GWAS have predominantly found variants in genes involved in glutamatergic neurotransmission, calcium signaling and broader synaptic functioning (Ripke et al., 2014; Foley et al., 2017). These genes include *GRIN2A,* which encodes the NMDA receptor subunit GluN2B, *GRIN1*, which encodes the AMPA receptor subunit NR1, *CANCA1C*, which

encodes of the ARC complex, and *CNTN4*, which effects hippocampal CA1 synaptic transmission and plasticity (Ripke et al. 2014, Owen et al. 2016, Oguro-Ando et al. 2021). Most of these genes are involved in the fine tuning of glutamatergic transmission.

Genes involving alterations in GABAergic transmission, specifically *GAD1*, have also been identified as schizophrenia risk genes by GWAS (Skene et al., 2018). *GAD1* encodes GAD67, which is an enzyme that metabolizes glutamate to GABA, therefore making it predominantly responsible for the production of most GABA. The expression of the GAD67 mRNA is decreased in parvalbumin-positive interneurons in cortical areas in schizophrenia patients. This decrease coincides with a decrease in the GABA membrane transporter 1, GAT1, which implies that there is impaired GABA reuptake and synthesis in interneurons in patients with schizophrenia (Lewis et al., 2005). GABA-ergic interneurons that express the calcium-binding parvalbumin receive feedforward excitatory inputs from NMDA receptors of the NR2A/NR2B subtype. Consequently these GABAergic cells may be influenced by changes in glutamatergic transmission (Uhlhaas and Singer, 2010). Therefore, the GABA-ergic interneuron dysfunction may be a secondary effect from disrupted glutamatergic transmission.

GWAS have also found variants at the *DRD2* gene that encodes the dopamine D2 receptor (D2R), which is implicated in schizophrenia pathology (Ripke et al., 2014). Dopamine may also impact glutamatergic transmission in schizophrenia by acting on D2Rs found on presynaptic glutamatergic inputs. This modulation occurs through a "convergence effect" onto medium spiny neurons (MSNs) (Gardoni and Bellone, 2015). Specifically, it has been proposed that NMDARs that contain the GluN2B subunit, encoded by *GRIN2A*, mediate synaptic transmission at MSN synapses. Moreover the GluN2B subunits are primarily involved in NMDA responses in D2R cells (Gardoni and Bellone, 2015). In a recent study using single-cell RNA sequencing to genetically identify brain cell types underlying schizophrenia, common genetic variants were found to be predominantly mapped onto MSNs, pyramidal cells and specific interneurons (Skene et al., 2018). *DRD2* was highly expressed in MSNs, and *DRD2* was almost exclusively expressed in MSNs compared to genes. Furthermore, loss-of-function intolerant genes and genes related to dopamine signaling were enriched in MSNs (Skene et al., 2018). These findings suggest that schizophrenia variants resulting in impaired dopaminergic signaling at MSNs expressing D2R can also have a large impact on the fine tuning of glutamatergic transmission. This further

supports that calibration of synaptic transmission, specifically at dopaminergic and glutamatergic synapses, is at the core of the pathophysiology of schizophrenia.

1.1.3. Neural substrates of schizophrenia symptoms

The symptoms of schizophrenia are divided in three categories: positive symptoms, negative symptoms and cognitive deficits. Positive symptoms refer to the presence of abnormal thoughts and behaviors such as hallucinations and delusions. Negative symptoms include lack of normally present responses such as reduced expression of emotion and disorganized speech. Lastly cognitive deficits consist of working and long-term memory impairments, and difficulty with overall executive functioning (Sigurdsson, 2016).

1.1.3.1. Positive symptoms of schizophrenia

The most common positive symptoms of schizophrenia patients are hallucinations, especially auditory hallucinations, and delusions. Hallucinations are abnormal perceptions that can include audible thoughts, voices, thought insertion or withdrawal, among others. On the other hand, delusions are persistent irrational beliefs that do not match with an individual's social or cultural background (Fletcher and Frith, 2009). The

main mechanism that appears to produce hallucinations and delusions is the disrupted basal communication or disconnection of relevant areas for perception and processing (Fletcher and Frith, 2009; Ford et al., 2007) that leads to abnormal connectivity (Mechelli et al., 2007). For instance, hallucinations have been associated with abnormal connectivity and increased neural activity within the hippocampus (HPC) and the thalamus (Amad et al., 2014), whereas the overactivation of the prefrontal cortex (PFC) and diminished deactivation of striatal and thalamic networks are suggested to be essential for delusions (Kesby et al., 2018).

Alterations in the dopaminergic and serotonergic systems have been also linked with the onset of hallucinations (Kumar et al., 2009). Schizophrenia patients present with increased subcortical dopamine which has been strongly associated with positive symptoms (Kesby et al., 2018). Furthermore, serotonin has also been implicated in the generation of hallucinations. This is based on the fact that different drugs that target the serotonin-2A receptor (5-HT2AR) cause hallucinations (Kumar et al., 2009).

Some neurophysiological correlates of hallucinations and delusions have been detected using event-related potentials (ERPs). ERPs are defined as small changes in voltage throughout various brain structures in response to specific stimuli, such as a sound or a light. ERPs present different peaks at different time points that have been linked with different brain processes and, depending on the proximity to the stimuli, they can be divided into early or late components (Sur and Sinha, 2009) (Fig. 1.1.3.1.1). Early components of ERPs have been related with sensory perception and attention while later components have been associated with negative symptoms and cognitive processes. The P50 or P1 is a positive response around 50 ms that represents sensory gating and has been associated with the severity of the hallucinations traits in schizophrenia patients (Galderisi et al., 2014). Furthermore, the N100 or N1 component is a negative peak around 100 ms that is reduced in schizophrenia patients and has also been negatively correlated with positive symptoms. These reductions may be caused by a competition between the auditory sound and hallucinations for auditory resources (Ford et al., 2012).

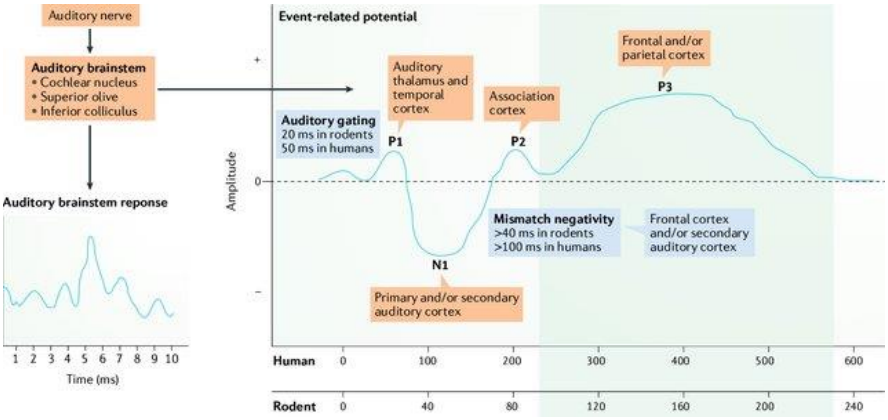

Figure 1.1.3.1.1: Schematic representation of the event-related potential (ERP). The representation shows an example of an auditory evoked potential response in which the relevant peaks are marked. In the left part we can also see an ERP of the auditory brainstem. The areas in which each peak is more prominent are shown next to the peak in orange and the names used to describe different components are shown in blue. Note that the human and rodent time escales of the response are different. (Modi and Sahin, 2017).

1.1.3.2. Negative symptoms of schizophrenia

The most relevant negative symptoms are anhedonia, decreased affect, and difficulties with communication and social functioning. Moreover, these symptoms account for a large part of poor functional outcomes and long-term disability in patients (Correll and Schooler, 2020). Negative symptoms usually appear before the first acute psychotic episode and their development and evolution depend on genetic factors, prenatal events and poor premorbid adjustments (Lyne et al., 2018).

The dopaminergic and glutamatergic systems also play a role in the development of negative symptoms in schizophrenia. Patients with schizophrenia present hypodopaminergic functioning in the frontal lobe and mesolimbic area, where D3 receptors play an important role in the modulation of negative symptoms, mood and cognition. In rodent models, antagonism or partial agonism of D3 receptors produce anti-anhedonic and procognitive effects (Correll and Schooler, 2020; Joyce and Millan, 2005). Moreover, various studies have found that NMDA receptor antagonists, such as ketamine or phencyclidine (PCP), mimic negative symptoms found in patients with schizophrenia, in addition to positive symptoms (Coyle, 2012). Furthermore, different inflammatory biomarkers have been associated with the onset of negative symptoms in schizophrenia through decreases in dopamine release and increased glutamate activity. Moreover, the effects of inflammation in the ventral striatum and other regions of the basal ganglia have been related with decreased activity in these areas in addition to reduced functional connectivity with the PFC. These alterations have been linked with negative symptoms of schizophrenia and other neuropsychiatric disorders, such as major depression or bipolar disorder, which share some of the negative symptoms (Goldsmith and Rapaport, 2020).

1.1.3.3. Cognitive deficits in schizophrenia

Cognitive deficits are one of the core deficits in schizophrenia and include disruptions in various domains of executive functioning, such as working memory, attention and learning. These symptoms usually start before the first psychotic episode and are exacerbated over time, especially memory and abstraction (Fett et al., 2020). Furthermore, cognitive deficits and negative deficits are both linked to the outcome and functionality of patients with schizophrenia (Green et al., 2000).

Different structural and functional alterations may underlie the cognitive deficits in schizophrenia. Reduced cortical thickness within the frontal and temporal regions has been associated with decreased neurocognitive performance (Alkan et al., 2021). For instance, working memory performance in schizophrenia patients correlates with the thickness in the superior temporal gyrus (Ehrlich et al., 2012). Furthermore, alterations in the subcortical dopamine systems such as the associative striatum correlate with executive dysfunctions (Conn et al., 2020), whereas HPC glutamate levels have been linked with episodic memory deficits in schizophrenia patients (Merritt et al., 2013; Valli et al., 2011). These results suggest the involvement of the dopaminergic and the glutamatergic systems in the

cognitive deficits observed in schizophrenia patients.

Cognitive deficits have also been related with different aspects of the ERPs, specially the late components (Fig. 1.1.3.1.1). For instance, the P300 or P3 is an endogenous potential that represents the process of the auditory signals and its amplitude is robustly decreased in schizophrenia patients (Turetsky et al., 2015, 2007). Another relevant component that correlates with sensory encoding, memory and attention is the mismatch negativity (MMN). The MMN is an ERP obtained by the subtraction of the averaged response of a set of standard stimuli from the averaged response of the target stimuli and it primarily reflects preattentive and attention-mediated processing (Hamilton et al., 2018b). It is most commonly studied using an oddball paradigm, in which a sequence of repetitive standard stimuli is interrupted by a deviant stimulus. The MMN is disrupted in schizophrenia patients and has been considered a relevant neurophysiological biomarker of the disorder (Fitzgerald and Todd, 2020; Javitt and Sweet, 2015). In fact, deficits in the MMN precede the illness onset and persist despite the treatment with antipsychotic medication (Javitt and Sweet, 2015).

1.1.4. Abnormal neural oscillations and synchrony in schizophrenia

The pathophysiology of schizophrenia is immensely complex due to its polygenic nature in combination with its susceptibility to environmental stressors, lack of clear structural abnormalities, and varying degrees of symptoms. What is clear regarding the pathophysiology of the disease is that the behavioral abnormalities in schizophrenia are caused by disrupted neural circuitry throughout distinct cortical areas involving a coordinated impairment of various neurotransmitter systems (Phillips and Silverstein, 2003). Consequently, many researchers have sought out to characterize neural circuitry in patients with schizophrenia and animal models of schizophrenia. This line of investigation has led to discoveries such as electrophysiological biomarkers of schizophrenia and has great potential to help further elucidate the pathophysiology of schizophrenia and provide novel interventions to treat the disease. This section will first provide a brief overview of how neural circuitry is studied in the context of neural synchrony and oscillations, and subsequently discuss what circuit alterations are observed in electrophysiological studies of schizophrenia.

Normal brain function depends on neural oscillations to orchestrate coherent and synchronized neuronal activity (Buzsáki and Draguhn, 2004). Neural synchrony is found among local neural populations, otherwise known as local synchrony, and also between neuronal populations in different regions of the brain, known as long-range synchrony. Local synchrony can be measured by the power of oscillations, which comes from the amplitude of oscillations. The amplitude of oscillations in specific neuronal populations is derived from an electrophysiological signal measured by an electroencephalogram (EEG) outside of the brain or an electrode implanted in the brain. This electrophysiological signal is also known as a local field potential (LFP). The oscillations represent a sum of the local network activity and synchronization from the surrounding electrode. Long-range synchrony is measured by looking at how changes in neuronal activity between two different regions are correlated in time (Bastos and Schoffelen, 2015; Sigurdsson, 2016). This can be measured using various computational methods which include coherence, phase-lag index, and phase-slope index. Coherence measures the consistency of phase relationships of oscillations in two different regions over time, phase-lag index estimates how much the phase of an oscillation one regions leads or lags behind the phase of an oscillation in another region and the phase-slope computes the direction of the flow of information

between a signal in one region and another (Sigurdsson and Duvarci, 2016). Oscillations involved in both long-range and local synchrony occur at different frequency bands that have been classically defined: delta (2-6 Hz), theta (4-12 Hz), beta (12-30 Hz), gamma (30-100 Hz) and high frequency oscillations (HFOs) (130-180 Hz) (Sigurdsson, 2016). Oscillations in frequency ranges such as gamma and theta help provide specific spatio-temporal coordination within local cortical networks and lower frequencies, such as delta, help provide such coordination across brain regions spanning longer distances, such as prefrontal-hippocampal (PFC-HPC) networks. Disruption of local and long-range circuit communication mediated by impaired neural oscillatory activity and has been described as a hallmark characteristic of schizophrenia. This disruption of circuit activity has been linked to behavioral impairments associated with schizophrenia such as psychosis, sensory impairment and executive dysfunction (Uhlhaas and Singer, 2010). The following sections will discuss impairments found in delta and gamma in schizophrenia, and how collectively these irregularities lead to a spatio-temporal disruption in brain-wide connectivity.

1.1.4.1. Delta dysfunction in schizophrenia

Brain wide changes in delta oscillation power during wakefulness is commonly found in patients with schizophrenia (Siekmeier and Stufflebeam, 2010). Aberrant delta activity seems to be a direct manifestation of schizophrenia and may be a direct manifestation of the disease, as delta abnormalities are only observed in patients with schizophrenia and not in "at risk", healthy subjects, such as a twin (Hong et al., 2012; Stassen et al., 1999). The expansive changes in delta may be derived from an imbalance in synaptic excitation and inhibition that leads to enhanced thalamo-cortical delta connectivity, which impairs delta mediated cortico-cortical communication. Consequently, a mismatch between delta and higher frequencies is generated within the thalamus and cortex, which subsequently disrupts overall communication between these brain regions and other higher-order structures (Hunt et al., 2017b).

Aberrant delta oscillations have been shown causally related to schizophrenia in the NMDA hypofunction model of the disease and by using optogenetically generated delta oscillations to induce behavioral deficits found in schizophrenia. Aberrant delta oscillations are generated in the thalamus and are dependent on T-type calcium channels. The T-type

calcium channels generate calcium spikes that trigger sodium spike bursts at delta, which allows for the relay nuclei of the thalamus to drive modulation at delta in structures such as the HPC and cortex (Choi et al., 2015). Replicating aberrant delta activity found in schizophrenia by optogenetically entraining delta oscillations in the thalamic nucleus produces a strong impairment in working memory (Duan et al., 2015). This supports the hypothesis that impairment in delta oscillations can produce schizophrenia-like behavioral deficits.

The interhemispheric delta coupling has also been reported during hallucinations (Spencer et al., 2009). Delta oscillations in the cortex arise from intrinsically bursting layer 5 pyramidal cells that are mediated between $GABA_B$ receptor inhibition and recurrent excitation (Hunt et al., 2017b). Therefore, excessive delta power may be a biomarker of disinhibition of pyramidal neurons due to NMDAR hypofunction decreasing the control of PV-positive GABAergic interneurons on pyramidal neurons.

This hypothesis has been supported by a recent study modeling circuit dysfunction based on disruption of ion channels implicated from GWAS of schizophrenia patients. The authors found that altered delta power may

be a consequence of altered expression of ion channels, or calcium transporters, and that the network dynamics that increase delta drive from layer 5 pyramidal cells may underlie the cognitive impairment they observed (Mäki-Marttunen et al., 2019). Collectively, this suggests that selectively targeting aberrant delta activity, or pyramidal neuron excitability, could ameliorate psychosis and cognitive symptoms in schizophrenia.

1.1.4.2 Gamma dysfunction in schizophrenia

Another prominent biomarker for deficits in schizophrenia are abnormalities in gamma oscillations. Gamma dysfunction in schizophrenia was first discovered in patients performing a visual Gestalt task, in which there was a decrease in anterior-posterior connectivity in the gamma frequency (Spencer et al., 2003). Subsequent studies have shown changes in gamma power during cognitive tasks and resting state in patients with schizophrenia, however it is unclear if gamma is increased or decreased (Hunt et al., 2017b). Furthermore, alterations on gamma oscillations amplitude or synchrony between different brain areas have been found to be related with positive symptoms of schizophrenia (Galderisi et al., 2014; Spencer et al., 2009; Uhlhaas and Singer, 2010).

Animal models have been quite useful in elucidating the complex mechanisms of gamma oscillations in schizophrenia. NMDA hypofunction animal models, such as PCP and ketamine administration, show an increase in cortical gamma power that is associated with the NR2A subunit of NMDAR receptors (Hunt et al., 2017). The disruption of this subunit results in an inability to properly excite PV-positive GABA-ergic fast-spiking interneurons. NR2A dysfunction has been implicated in GWAS and post-mortem studies of patients with schizophrenia (Hunt et al., 2017a). Genetic models of schizophrenia have also shown similar changes in gamma oscillatory power, and furthermore have implicated dysfunction in PV interneurons in the generation of aberrant gamma oscillations. Specifically, models in which PV interneurons have reduced excitatory input show an increase in gamma power (Carlén et al., 2012; Sigurdsson, 2016).

Gamma dysfunction is most directly implicated in cognitive impairments in schizophrenia. In an animal model of PV interneuron dysfunction, Dlx5/6(+/-) mice, gamma power is decreased, which in turn leads to cognitive inflexibility, a common behavioral abnormality in schizophrenia. PFC stimulation of gamma oscillations recovers the cognitive deficit in these Dlx5/6(+/-) mice and inhibition of PFC PV

interneurons replicates the inflexibility originally found in the Dlx5/6(+/-) mice (Cho et al., 2015). These findings casually implicate PV interneuron driven gamma abnormalities to cognitive impairments in schizophrenia.

1.1.5. Prefrontal-hippocampal circuits in cognition and schizophrenia

The PFC and the HPC are two relevant areas for the pathophysiology of schizophrenia and they have been specially linked to cognitive impairment (Li and Vlisides, 2016). The PFC is broadly connected with sensory and motor systems and subcortical structures, including the HPC, exerting top-down control of these areas. The PFC is organized in several subregions and it is essential for higher order cognitive processes and emotional regulations (Miller, 2000). These cognitive processes and emotional regulations are disrupted in schizophrenia patients due to anatomical and functional alterations. For instance, post-mortem studies have found abnormalities in PV-expressing interneurons that have been associated with disruptions of gamma oscillations and cognitive impairment (Uhlhaas and Singer, 2010). fMRI studies also have shown a reduced activation of the PFC during cognitive tasks (Minzenberg et al., 2009; Sigurdsson and Duvarci, 2016).

The HPC is a longitudinal structured organization with different subfields, including the CA1, CA3 and the dentate gyrus. Furthermore, the longitudinal organization is divided in dorsal and ventral poles that play relevant roles in spatial information and memory or emotional and motivational behaviors, respectively (Sigurdsson and Duvarci, 2016). However, the HPC is altered in schizophrenia patients and associated with its pathophysiology. The most relevant abnormalities in the HPC of schizophrenia patients are the reduced volume and the hypermetabolism, which have been associated with the symptoms (Heckers and Konradi, 2010).

Furthermore, the PFC and the HPC are two key brain regions implicated in cognition in healthy subjects. especially their local activity or communication via theta and gamma oscillations (Sigurdsson and Duvarci, 2016). For instance, theta oscillations in the PFC cortex prevail during working memory maintenance and long-term memory retrieval in humans (Kaplan et al., 2014; Sauseng et al., 2010), while in rodents they are increased during a spatial task (Negrón-Oyarzo et al., 2018). HPC theta oscillations play a relevant role during spatial navigation and memory

across species (Guderian et al., 2009; Winson, 1978), whereas gamma oscillations are associated with memory encoding and retrieval (Trimper et al., 2017; Zheng et al., 2016). Moreover, PFC gamma oscillations correlate strongly with attention (Fries, 2015). Remarkably, gamma oscillations are modulated by the phase of theta oscillations, both in the PFC and HPC. The depolarizing phases of theta waves promote increases in the amplitude of gamma oscillations (Buzsáki and Chrobak, 1995; Canolty et al., 2006). This increased theta-gamma cross-frequency coupling has been linked with cognitive processes, such as memory and learning (Friese et al., 2013; Tort et al., 2009).

The PFC-HPC communication is also essential for cognitive functions. Both areas are connected anatomically using a directed and indirected pathway, allowing the two structures to interact with each other (Sigurdsson and Duvarci, 2016). The direct pathway is conformed by monosynaptic projections from the ventral HPC to the medial PFC and from the PFC to the dorsal HPC, whereas the indirect pathway consists on indirect routes though the nucleus reuniens of the thalamus and the lateral entorhinal cortex (Condé et al., 1995; Vertes, 2006). In addition, the PFC and the HPC are functionally connected, being theta and gamma

oscillations the preferential routes of communication. Importantly, neurons in the PFC are entrained with theta and gamma oscillations in the HPC during a spatial memory task (Negrón-Oyarzo et al., 2018; Spellman et al., 2015). HPC theta coherence that transfers to the PFC plays a relevant role in spatial working memory (Sigurdsson et al., 2010), and long-term memory consolidation (Brincat and Miller, 2015). Furthermore, PFC-HPC gamma synchrony underlies spatial working memory (Spellman et al., 2015), in which the coupling between HPC theta phase-PFC gamma amplitude is involved (Tamura et al., 2017). However, this communication between the PFC and the HPC is completely disrupted in schizophrenia and associated with cognitive deficits both in humans and rodents (Sigurdsson and Duvarci, 2016).

1.1.6. Animal models of schizophrenia

Animal models are crucial to understand circuit dysfunction in schizophrenia in greater detail than what is possible in human studies. Current technology used to image humans is limited by the lack of spatial and temporal resolution to investigate neural network activity in depth. Animal studies allow for a detailed investigation of the circuit *in vivo* using techniques such as electrophysiology, calcium imaging and optogenetics, allowing for extremely temporal resolute, cell-specific probing. In

studying schizophrenia, this examination into the circuit is generally accompanied by a relationship to a behavioral output, such as working memory performance, that is associated with schizophrenia. The region that is imaged or recorded is based on what circuit underlies a particular behavior one is studying. For example, in investigating memory impairment in schizophrenia, one could probe whether impaired spatial-temporal communication within PFC-HPC circuits underlies cognitive dysfunction (Li and Vlisides, 2016). There are three predominant types of animal models of schizophrenia: genetic, pharmacological and neurodevelopmental models. Genetic models have emerged from the known genetic mutations found in human GWAS studies, such as some of the mutations discussed earlier that confer a large increase in risk of onset of the disease. An alternative approach is to replicate pathophysiological mechanisms found in patients, such as NMDA hypofunction, by using pharmacological agents, for example NMDAR antagonists. Neurodevelopmental models attempt to model environmental stressors that disrupt neural circuitry development, pre-natal or immediately post-natal (Sigurdsson, 2016). All three approaches are important in the study of schizophrenia as they all represent the multiple pathophysiological mechanisms that give rise to the disease in various patients. Here we

discuss the three models of the disease: genetic, pharmacological and developmental models of schizophrenia.

1.1.6.1. Genetic models of schizophrenia

As discussed previously, through GWAS and exome wide association studies schizophrenia has been linked to various genetic risk factors. Many of these genetic variants have been modeled in animals. Two of these genetic models will be discussed in this section, the 22q11.2 microdeletion syndrome mouse model and the *DISC1*, disrupted in schizophrenia-1, mouse model.

Microdeletions on the q11.2 region of chromosome 22, referred to as 22q11.2 deletion syndrome (22Q11DS), are considered as the strongest risk factor currently known for schizophrenia (McDonald-McGinn et al., 2015). 22Q11DS mice show several abnormalities relevant to schizophrenia, most notably specific cognitive deficits such as working memory and sensorimotor gating. These cognitive deficits are accompanied by circuit deficits, specifically impaired PFC-HPC circuitry. During tasks assessing working memory, 22Q11DS mice show disrupted PFC-HPC, long-range, connectivity at theta frequencies, which is accompanied by poor working memory performance (Sigurdsson et al.,

2010). Although theta connectivity was disrupted between the two regions, locally theta production was not disrupted, suggesting that the 22Q11DS mice can maintain some of the local circuitry, however their impairment stems from deficits in connectivity. Furthermore, diminished PFC-HPC synchrony in 22Q11DS mice was correlated with poor spatial memory, in addition to impaired working memory (Sigurdsson et al., 2010). It should be noted that 22Q11DS mouse models show only selective cognitive deficits, for example long-term memory tested in the novel object recognition (NOR) test is not affected, implying that specific genes within the 22q11.2 region are making distinct contributions to specific behavioral deficits.

Consistent with the 22Q11DS model, Disrupted-in-schizophrenia 1 (DISC1) models show impairments in specific cognitive paradigms and also abnormal PFC-HPC circuits. Disc1 mice show deficits in working memory, HPC synaptic plasticity and PFC short-term plasticity (Sigurdsson, 2016). Oscillatory dysfunction along with impaired PFC-HPC synchrony are also apparent in Disc1 models. Awake recordings in Disc1 mice show decreased theta and gamma oscillatory power in the prelimbic cortex that correlate with depressive-like symptoms. The impairment in PFC theta activity was found to be driven by decreased HPC

theta oscillations and the impairment in gamma power corresponded with reduced number of PV interneurons in the PFC that in turn led to reduced inhibitory drive onto pyramidal neurons. Disc1 mice also showed impaired PFC-HPC coherence and signal directionality, which may explain prior studies showing working memory deficits in these mice (Hartung et al., 2016).

1.1.6.2. Pharmacological models of schizophrenia

The most common pharmacological models of schizophrenia involve the administration of NMDAR antagonists, mainly phencyclidine (PCP) and ketamine (Lee and Zhou, 2019). Acute administration of NMDAR antagonists generate psychotic symptoms in healthy subjects and exacerbate symptoms in patients with schizophrenia (Krystal et al., 1994; Lahti et al., 1995).

PCP produces schizophrenia-like behaviors in humans such as hallucinations and subsequently, mechanisms of these PCP-induced behaviors have been investigated as a model of schizophrenia, primarily in rodents (Itil et al., 1967). The effects of different PCP administration protocols -acute, subchronic (sPCP, less than 14 days) and chronic- have been investigated in animals, yielding relevant insights into the

pathophysiology of schizophrenia. Acute administration of PCP induces psychosis-like states in mice while subchronic and chronic PCP produce sustained schizophrenia-like negative and cognitive symptoms allowing for investigation of circuit changes over time (Allen and Young, 1978; Cosgrove and Newell, 1991). More specifically, acute PCP is followed by behavioral alterations such as stereotypic movements and ataxia, which are analogous to behaviors described during psychosis in humans (Sturgeon et al., 1979). Moreover, acute PCP and sPCP produces social withdrawal, mimicking negative symptoms, while anhedonia remains unaffected (Neill et al., 2014). sPCP-induced cognitive impairments have been assessed using behavioral assays such as the NOR task, contextual fear conditioning and the Morris water maze task. These tests evidenced deficits of sPCP-treated mice and executive functions such as recognition memory, cognitive flexibility, and sensorimotor gating (Lee and Zhou, 2019). Furthermore, PCP induces a disbalance in the dopaminergic system, especially in the PFC, where the dopaminergic basal metabolism is decreased (Abdul-Monim et al., 2007). Such changes were accompanied by functional and circuit alterations in the PFC and HPC. For example, sPCP and chronic PCP exposure led to impaired reversal learning and reduced PV-positive GABAergic interneurons in the PFC and the HPC (Abdul-Monim et al., 2007). Some of these results were later confirmed in

postmortem tissue from patients with schizophrenia, where reduced PV-interneuron density in the PFC was found, further validating PCP as a model of schizophrenia (Kaar et al., 2019).

The profound effects that PCP exerts on behavior can be ascribed to changes in neural circuit oscillations and synchronization. An acute dose of PCP decreases low frequency oscillations in the PFC of anesthetized mice, implying an excitatory effect on cortical microcircuits (Lladó-Pelfort et al., 2016). Moreover, acute PCP disrupts theta and gamma oscillations as observed in schizophrenia patients. In contrast, acute PCP also increases HFOs in multiple brain areas of rodents (Hunt et al., 2015) which have not been detected in humans, likely due to the temporal resolution of EEG (Zijlmans et al. 2012). In awake behaving mice, acute PCP causes spatial cognitive impairment that is accompanied by spatio-temporal disruption of theta and gamma oscillations within the HPC that in turn disrupts PFC-HPC connectivity (Kao et al., 2017). These results suggest that PCP produces local circuit dysfunction that perturbs PFC-HPC connectivity, which is associated with cognitive deficits and other behaviors associated with schizophrenia.

Ketamine is also widely used to model schizophrenia. As with PCP, acute and chronic ketamine administration is associated with behavioral phenotypes observed in patients with schizophrenia that are accompanied by changes in neurophysiological biomarkers and neurotransmitter release. Acute and chronic ketamine exposure generates hyperlocomotive activity and stereotypic behaviors that may correspond with psychosis-like behaviors, and cognitive deficits, such as memory and spatial learning impairments (Lee and Zhou, 2019). The hyperlocomotive activity is associated with increases in cortical and striatal dopamine and serotonin. Negative symptoms in the chronic ketamine model are linked to decreased glycine in the cortex, HPC and striatum (Lee and Zhou, 2019).

The changes ketamine produces on behavior and neurotransmitter systems correspond to changes in local circuitry and long-range connectivity within the brain. Acute ketamine increases delta, gamma and HFOs across various brain regions (Flores et al., 2015; Kocsis et al., 2013). Moreover, cognitive impairment following acute and chronic administration of ketamine is accompanied by changes in theta and gamma power in the PFC and the HPC. The change in PFC gamma power may be due to the ketamine-induced increase of the firing rate of PFC pyramidal neurons that in turn decreases interneuron firing rate (Homayoun and Moghaddam, 2007). This

finding corresponds with the increase in glutamatergic transmission found throughout the brain after ketamine exposure (Frohlich and Van Horn, 2014). Acute ketamine has also been shown to desynchronize PFC-HPC circuits by way of enhanced gamma and suppressed theta activity (Moran et al., 2015). This impairment in connectivity most likely results in the cognitive impairment found in ketamine models, however further research is required to elucidate this important issue.

The multidisciplinary studies with PCP and ketamine support the notion that NMDAR hypofunction in PV-interneurons is a key contributor to the psychotomimetic effects of NMDAR antagonists on behavior and circuit dysfunctions. However, further studies are needed to elucidate the exact relationships between NMDAR antagonist-induced neural alterations and schizophrenia-like symptoms, in order to fully understand the pathophysiology of the disorder.

1.1.6.3. Neurodevelopmental models of schizophrenia

Neurodevelopmental models of schizophrenia are based on mimicking the disruption of normal neurodevelopmental processes which may underlie the onset of schizophrenia. The neurodevelopmental disruption occurs years before the onset of the disease and it is produced by genetic and

environmental risk factors (Rapoport et al., 2012). Therefore, the neurodevelopmental models can mimic the delayed onset of the symptoms, capturing alterations in multiple systems associated with schizophrenia. Different risk factors related to schizophrenia, such as maternal stress, infection during pregnancy and extreme stress during childhood have been used to generate several neurodevelopmental models. These models can be grouped based on the type of stressor and the time it is administered into: prenatal stress models, prenatal immune challenge models, perinatal/neonatal stress models and lesion/pharmacologic models (Wilson and Terry, 2010). In this section we will introduce a neurodevelopmental model commonly used that includes prenatal maternal immune activation.

Studies in schizophrenia patients have shown that a maternal infection during pregnancy increases the risk for schizophrenia several fold due to a maternal immune activation (MIA) (Canetta and Brown, 2012). Consistent with this, MIA is generated by injecting pregnant mice with Poly I:C, a synthetic strand of RNA, producing structural and behavioral deficits in their offspring. These behavioral alterations include deficits in social interaction, learning and object recognition (Wilson and Terry, 2010). Furthermore, the MIA model presents impaired PFC-HPC coherence and

phase-locking from PFC firing rate to HPC theta oscillations that correlates with prepulse inhibition deficits (Dickerson and Bilkey, 2013).

1.2 Antipsychotic medication in schizophrenia

Antipsychotic drugs or neuroleptics are the most commonly prescribed drugs for schizophrenia patients. They target mainly dopamine and serotonin receptors, but can also bind to other pharmacological targets such as noradrenaline and histamine receptors (Meltzer and Huang, 2008). The primary objectives of antipsychotic drugs are to decrease frequency and severity of psychotic episodes, ameliorate the negative and cognitive deficits and improve the functional outcomes and quality of life of the patients (Bruijnzeel et al., 2014). The pharmacological property that all antipsychotic drugs share is the direct or indirect blockade of dopamine D2R. The differences between antipsychotic drug actions depend on the percentage of D2R occupancy, which has implications for the clinical outcomes. For instance, 60% occupancy is needed for antipsychotic action, whereas 80% occupancy is associated with the emergence of extrapyramidal effects (EPS) (Tandon and MD, 2011). EPS are drug-induced movement disorders that include dyskinesias, Parkinsonism, akinesia and neuroleptic malignant syndrome. EPS are considered one of

the main undesired side effects of antipsychotic drugs (Blair and Dauner, 1992). In preclinical studies, the severity of catalepsy is used to predict EPS (Hoffman and Donovan, 1995). Therefore, depending on the propensity to generate EPS and their affinity for D2R or serotonergic receptors (5-HTR), antipsychotic drugs have been categorized in two types: the first generation or typical antipsychotic drugs and the second generation or atypical antipsychotic drugs. Chronic treatment with antipsychotic drugs is necessary for a better prognosis of the disorder. For example, cumulative exposure to antipsychotic drugs is associated with increased gray matter in the cingulate gyrus for typical antipsychotic drugs and in the thalamus for atypical antipsychotic drugs (Tomelleri et al., 2009).

1.2.1. Typical antipsychotic medication

Typical antipsychotic drugs (or classical neuroleptics) were the first effective treatment that reduced psychotic symptoms in schizophrenia patients. Neuroleptics such as haloperidol or chlorpromazine are effective in reducing positive symptoms, but they barely have any effect on negative symptoms or cognitive deficits in humans or animal models (Bruijnzeel et al., 2014; Meltzer and Huang, 2008). As previously described, their efficacy is based on their ability to block limbic and cortical D2R.

However, the same D2R blockade and their slow dissociation with D2R in the striatum or the prolactin-secreting cells in the pituitary gland produces EPS effects and elevated prolactin, respectively. Prolactin is a hormone in which its elevated levels are associated with abnormalities in the reproductive, endocrine and metabolic systems (Bostwick et al., 2009). These side effects are the most important reason for not compliance and a worst outcome of the disorder (Meltzer, 2012). In preclinical studies, typical antipsychotic drugs are able to restore hyperlocomotive behaviors but they are unable to restore cognitive deficits of schizophrenia mouse models, highlighting their ability to recover positive symptoms but not cognitive deficits (Lee and Zhou, 2019; Meltzer and Huang, 2008).

Haloperidol is the prototypal classical neuroleptic and it is prescribed to treat positive symptoms (Tandon and MD, 2011). Haloperidol has strong affinity for D2R, barely having any effect on the other systems (Siafis et al., 2018). We have also shown that haloperidol suppresses PFC and HPC spiking activity, theta and gamma oscillations, while amplifying delta oscillations in healthy rodents (Gener et al., 2019).

1.2.2. Atypical antipsychotic medication

Atypical antipsychotic drugs are as effective as typical antipsychotic drugs in reducing the positive symptoms of schizophrenia patients but they produce less EPS. This is due to their higher affinity for 5-HT2ARs than D2R (Meltzer and Huang, 2008). Furthermore, atypical antipsychotic drugs show a modest amelioration of negative symptoms and improvement of certain domains of cognitive impairment. Their efficacy for negative and cognitive symptoms appears to depend on the reduction in the positive symptoms and the lack of EPS (Tandon and MD, 2011). In rodents, atypical antipsychotic drugs can attenuate some of the behavioral effects induced by ketamine or PCP, including sPCP-induced cognitive deficits (Grayson et al., 2007).

Atypical antipsychotic drugs enhance dopamine efflux in the cortex and the HPC, affecting less the limbic system, whereas classical neuroleptics have the opposite effect. These actions are mediated by the affinity of atypical antipsychotic drugs for serotonin receptors, especially the 1A (5-HT1AR) and the 2A (5-HT2AR) subtypes, which have a widespread expression in the brain and modulate the dopaminergic, serotonergic, glutamatergic and GABAergic systems. The increased dopamine efflux

may contribute to the improved cognitive performance observed in sPCP-treated monkeys and rodents following the administration of atypical antipsychotic drugs (Meltzer and Huang, 2008). However, chronic antipsychotic treatment changes the composition of NMDARs and decreases their activity in the HPC and thalamus, which produces effects on the cortical-limbo-thalamic circuit. All these effects may negatively impact the cognitive function of schizophrenia patients and explain the incomplete recovery of cognitive deficits by atypical antipsychotic drugs (Krzystanek and Pałasz, 2019). Therefore, further studies are needed to fully understand the neural substrates of the behavioral effects of chronic atypical antipsychotic drugs.

Clozapine was the first atypical antipsychotic drug to be developed and the first that does not produce EPS. Clozapine is also effective for addressing treatment-refractory schizophrenia. However, clozapine is not often prescribed because of another adverse effect, the agranulocytosis which is a serious side effect that may cause the death of the patient. Therefore, it is only prescribed to schizophrenia patients that are resistant to other treatments (Tandon and MD, 2011). Clozapine has a greater affinity for 5-HTR receptors, especially 5-HT2AR and 5-HT1AR, than for D2R. These

greater affinity may be involved in the cognitive recovery of sPCP animal models (Meltzer, 2012).

Risperidone is one of the most commonly prescribed atypical antipsychotic drugs. It targets D2R and 5-HTRs, especially 5-HT2AR. Risperidone is effective at treating the positive symptoms but it only modestly ameliorates negative and cognitive symptoms in humans and rodents (Grayson et al., 2007; Houthoofd et al., 2008; Marder and Meibach, 1994; Meltzer, 2012). In a previous study of our lab, we have shown that a medium-high dose of risperidone strongly reduces PFC-HPC activity, decreasing spiking activity, theta, beta and gamma oscillations and increasing delta oscillations, in healthy mice. These actions are accompanied with suppressed locomotion activity associated with sedative states (Gener et al., 2019). Moreover, risperidone can also reduce P3 latencies in schizophrenia patients while not affecting MMN (Umbricht et al., 1999).

1.2.3. Contribution of serotonergic activities to antipsychotic actions

As previously mentioned, 5-HT1ARs and 5-HT2ARs receptors are major targets for atypical antipsychotic drugs such as risperidone or clozapine.

The PFC and HPC densely express both serotonin receptors (Berumen et al., 2012; Pau Celada et al., 2013; Puig and Gener, 2015; Puig and Gulledge, 2011), whereas D2R are moderately present (Puighermanal et al., 2015; Santana et al., 2009). Therefore, atypical antipsychotic drugs binding to these receptors are expected to have major effects on PFC-HPC neural dynamics. Furthermore, 5-HT1AR agonism and 5-HT2AR antagonism ameliorate NMDAR antagonist induced effects on locomotion and memory. Other 5-HTRs, such as the 5-HT6R or the 5-HT7R, also restore the acute and subchronic NMDAR antagonist induced effects (Meltzer et al., 2011). For instance, the atypical antipsychotic drug lurasidone, which is a 5-HT1R partial agonist and a 5-HT7R antagonist, as well as a D2R and 5-HT2AR antagonist, can reverse the sPCP reversal learning deficits (Rajagopal et al., 2016a).

We have recently shown that risperidone alone reduces local and cross-regional synchronization of PFC-HPC circuits in freely moving mice, with 5-HT1AR, 5-HT2AR and D2R shaping delta, beta and gamma bands. This study shows an important role of 5-HT1AR agonism and 5-HT2AR antagonism in risperidone-induced alterations of delta, beta and gamma oscillations, while D2R antagonism may contribute to risperidone-

mediated changes in delta oscillations (Gener et al., 2019). However, these results were obtained in healthy rodents and the observations may differ from those obtained in schizophrenia-like mouse models. Therefore, a major aim of this thesis has been to understand the effects of antipsychotic medication on PFC-HPC neural dynamics, and the selective contribution of serotonin receptors, under the psychotomimetic conditions produced by the NMDAR antagonist PCP.

2. HYPOTHESIS AND OBJECTIVES

2. HYPOTHESIS AND OBJECTIVES

2.1. Significance

The main aim of this thesis was to unravel the neural dynamics of PFC-HPC circuits under the psychotomimetic conditions induced by PCP in mice and to evaluate the rescuing effects of antipsychotic medication. We investigated the neural substrates of two hallmarks of schizophrenia phenotypes: psychosis-like states and cognitive deficits. We also investigated the effects of highly prescribed classical and atypical antipsychotic medication on the neural substrates of these symptoms. We addressed these questions in two separate projects:

1. Project 1: We investigated the neural substrates of psychotic-like states within PFC-HPC circuits induced by acute PCP administration and the rescuing abilities of three antipsychotic drugs and two serotonin compounds.
2. Project 2: We investigated the neural correlates of the cognitive impairment induced by sPCP treatment and subsequent rescuing abilities of a chronic risperidone treatment in the PFC-HPC circuits.

2.2. Hypotheses

Project 1:

1. Psychotic-like states induced by acute PCP produce major alterations on PFC-HPC neural activity and synchrony.
2. Antipsychotic drugs ameliorate psychosis-induced aberrant neural activity in PFC-HPC circuits.
3. The affinity of atypical antipsychotic drugs for serotonin receptors may be relevant for the rescue of abnormal PFC-HPC neural dynamics.

Project 2:

1. The subchronic phencyclidine (sPCP) treatment causes alterations of PFC-HPC neural dynamics and this contributes to memory and attentional impairment.
2. sPCP-induced alterations in PFC-HPC circuits underlie disruptions in working memory and long-term memory.
3. The sPCP treatment produces anomalous auditory perception and processing, similar to those observed in schizophrenia patients.
4. The chronic risperidone treatment ameliorates sPCP-induced PFC-HPC circuit alterations improving memory performance and

auditory perception and processing.

2.3. Objectives

Project 1:

1. To identify the contribution of PFC-HPC neural activity patterns to psychosis-like behaviors induced by acute PCP.
2. To decipher the differential neural mechanisms of typical and atypical antipsychotic medication during psychosis-like states induced by acute PCP.
3. To unravel the contribution of 5-HT1AR and 5-HT2AR to the effects of atypical antipsychotic drugs during psychosis-like states induced by acute PCP.

Project 2:

1. To identify aberrant PFC-HPC neural activity patterns induced by sPCP treatment during different brain states.
2. To unravel PFC-HPC neurophysiological biomarkers of working memory, memory acquisition and retrieval, and determine the effects of sPCP.
3. To identify neurophysiological biomarkers of auditory perception

and processing in PFC-HPC circuits and determine the effects of sPCP.

4. To elucidate whether a chronic risperidone treatment ameliorates memory via PFC-HPC neural mechanisms.

3. MATERIALS AND METHODS

3. MATERIALS AND METHODS

3.1. Animals

Thirty and twenty-nine adult male C57BL/6 mice 2 to 3 months old, obtained from the PRBB inner colony, were used for the first project and second project, respectively. All procedures were conducted in compliance with EU directive 2010/63/EU and Spanish guidelines (Laws 32/2007, 6/2013 and Real Decreto 53/2013) and were authorized by the PRBB Animal Research Ethics Committee.

3.2. In vivo electrophysiology in freely moving mice

3.2.1. Surgery

Stereotrodes (two-wire electrodes) were used for the recording of neural activity. These electrodes were custom made with two twisted strands of tungsten wire 25 μm wide (Advent Research Materials, UK) and were held together using heat insulation with a heat gun and tips were welded to golden pins. The golden pins connected to the electrode wires were pinned to an adaptor to facilitate their connection to the recording system. Mice were induced with a mixture of ketamine/xylazine and placed in a

stereotaxic apparatus. Anesthesia was maintained with continuous 0.5-4% isoflurane. Small craniotomies were drilled above the medial PFC and HPC. Four micro-screws were screwed into the skull to stabilize the implant, and the one on top of the cerebellum was used as a general ground. Three tungsten electrodes, one stereotrode and one single electrode (only one of the electrodes of the stereotrode was used), were positioned stereotaxically in the prelimbic region of the medial PFC (AP: 1.5, 2.1 mm; ML: ± 0.6, 0.25 mm; DV: -1.7 mm from bregma), and one stereotrode more was implanted in CA1 of the HPC (AP: -1.8, -2.5 mm; ML: -1.3, -2.3 mm; DV: -1.15, -1.25 mm). The electrodes were placed 0.6 mm apart and equally distributed in both the PFC and HPC, respectively. In addition, three reference electrodes were implanted in the corpus callosum and lateral ventricles (AP: 1, 0.2, -1; ML: 1, 0.8, 1.7; DV: -1.25, -1.4, -1.5, respectively). The recorded hemisphere was chosen randomly. At the time of implantation the electrodes had an impedance from 100 to 400 kOhm and were implanted unilaterally with dental cement. After surgery animals were allowed at least one week to recover during which they were extensively monitored and received both analgesia and anti-inflammatory treatments. Additionally, animals were handled and familiarized with the implant connected to the recording cable. To avoid the implant to be

damaged, mice were individualized in their home cages from the day of the surgery.

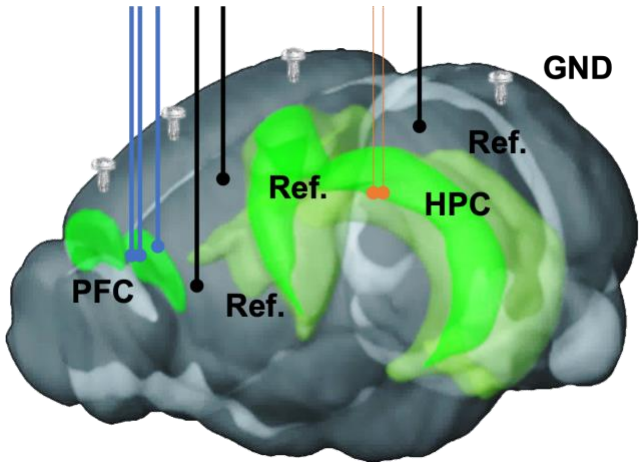

Figure 3.2.1: Diagram of stereotrode implantation in the PFC and the HPC of the mouse brain.

3.2.2. Electrophysiological recordings

All the recordings were carried out with the multi-channel Open Ephys system at 0.1-6000 Hz and a sampling rate of 30 kHz, recording local field potentials (LFPs) and multi unit activity (MUA) in freely moving mice. Intan RHD2132 amplifiers equipped with an accelerometer were used. Accelerometer signals in the X, Y and Z axis were used to monitor mobility. We quantified the variance of the instantaneous acceleration module (Acc; variance (Root square[X2, Y2, Z2])) that was maximum

during exploration and decreased as the animals were in quiet alertness. In fact we selected low mobility epochs of quiet wakefulness (10 or 3 seconds duration) by defining a threshold in the accelerometer's output. To obtain LFPs, recorded signals were detrended, notch-filtered and decimated to 1kHz offline. The frequency bands considered for the band-specific analyses included: delta (2-5 Hz), fast delta or slow theta (4-8 Hz), theta (8-12 Hz), alpha (10-14 Hz), beta (18-25 Hz), low gamma (30-48 Hz), high gamma (52-100 Hz), and HFO (100-200 Hz). MUA represents an aggregate signal and was obtained by filtering the signals between 450-6000 Hz and thresholded at -3 sigma standard deviations. Action potentials from different neurons were quantified during the time windows and provided as spikes per 10 milliseconds. Noisy windows or artifacts were removed from the analyses. Artifacts were discarded if the LFP voltage was outside the range (PFC: 1000 to -1000 mV, HPC: 1500 to -1500 mV) or if the maximum point of the power spectral analyses was above 3 standard deviations from the averaged maximum point of the recording. All these analyses were carried out using custom Python scripts.

3.3. Behavioral and cognitive assessment

3.3.1. Locomotion, ataxia and stereotypic behaviors assessment

Changes in locomotion, stereotypic behaviors and ataxia caused by the drugs were investigated using video recordings with a PointGrey Camera. Freely moving mice were recorded in their home cages (369 × 165 × 132 mm with standard bedding) for these quantifications. Quantifications of these measures were done on 10 minutes consecutive windows before and after the phencyclidine administration. Locomotion was calculated using the MouseActivity software (Zhang et al., 2020). Stereotypic behaviors and ataxia were rates using a custom scale from 0 to 5 after the PCP injection based on (Sturgeon et al., 1979). Scales were adapted to the electrophysiological recordings taking into account the influence of the cable and implant (Table 1).

Rates	0	1	2	3	4	5
Stereotypic Behaviors	Non-repetitive activity	Small rate of weaving, more locomotion, sniffing and grooming	Moderate weaving, non-directed movements and rearing	Fast and frequent weaving and intermittent turning	Rapid rate and continuous turning and weaving	Dyskinetic extension and flexion of the limbs
Ataxia	Coordinated movement	Small rate of unusual movement and loss of balance during rearing	Moderate rate of unusual movements and falling. May support weight on the abdomen while moving.	Constant rearing with loss of balance and falling. Moderate support of weight in the abdomen while moving	Can't move from a restricted area and support weight on the abdomen while not moving	Unable to move or convulsive movements

Table 1: Adapted scale for measuring stereotypic behaviors and ataxia.

3.3.2. Quiet wakefulness in freely moving mice

A defined threshold in the accelerometer signal was used for detecting epochs of low mobility or quiet wakefulness of the mice in their home cage or the open field exploration box. Analyses of LFPs signals during quiet wakefulness were performed averaging epochs of different duration depending on the place the animal was recorded (home cage: 10 seconds; open field box: 3 seconds; as one continuous epoch). Epochs were chosen based on the stability of the accelerometer output and LFP signal.

3.3.3. Memory assessment with the novel object recognition task (NOR)

Working memory and long-term recognition memory were tested using a

well-established non-operant task that relies on mice' innate instinct to explore novel objects in the environment (Leger et al., 2013; Meltzer et al., 2011). We used a custom designed T-maze made of 3 mm aluminum painted in black with wider and higher arms than the standard mazes (8 cm wide x 30 cm long x 20 high). The maze was shielded and grounded for electrophysiological recordings and was placed on an aluminum platform. The novel and familiar object pairs were previously validated as in (Gulinello et al., 2019) and mice were always tested with different pairs of objects in different experiments. The arm of the maze where the novel object was placed was randomly chosen across experiments. The test was implemented in four phases: habituation, familiarization and working memory test, 3 minutes after the familiarization (during the first day) and long-term memory test, 24 hours after familiarization. Mice were first habituated to an empty maze for 10 min. Five minutes later, mice were placed again in the maze where they could explore two identical objects located at the end of the two lateral arms for 10 min. Three minutes later, in the first test phase, mice were presented with one familiar and one novel object for 10 min. Twenty-four hours later, in the second test phase, mice were presented with one familiar (from the familiarization phase) and another novel object for 10 min. Each session was videotaped via a video

camera located on top of the maze. Any investigative behavior of objects, including head orientation towards the objects or sniffing at a distance below or equal to 2 cm or when the mice touched the objects with the nose, was considered object exploration. Exploratory events were identified online by looking at the video using a custom-designed joystick with a right and left button that were pressed continuously during the time of explorations. Button presses were automatically aligned to the electrophysiological file by sending TTL pulses to the acquisition system so that two more event channels were added to the recording files. Object recognition memory was defined by the discrimination index (DI) for the novel object using the difference in exploration time for the familiar object divided by the total amount of exploration of both objects (DI = [Novel Object Exploration Time-Familiar Object Exploration Time]/Total Exploration Time). DIs vary between +1 and -1, where a positive score indicates more time spent with the novel object, a negative score indicates more time spent with the familiar object, and a zero score indicates a null preference (Leger et al., 2013). The tests were only considered if they had a minimum of 10 valid seconds of total exploration on each phase of the NOR and minimum of 3 seconds per each object in the case of the tests. In the case of the analyses of the neural substrates of memory in baseline mice

only NORs with a good performance, DI over 0.2, were selected. LFP measures associated with memory acquisition, working memory and retrieval were obtained by averaging one-second non-overlapping windows triggered by the button presses on the joystick. Each one-second window was only considered if the mouse explored the object over 600 ms. This allowed us to have identical size windows to compare between objects and mice. Windows that contained artifacts were filtered out applying an automatic electrophysiologic artifact rejection offline based on two criteria: if the voltage of local field potentials is outside a range (PFC: 1000 to -1000 mV, HPC: 1500 to -1500 mV) and if the maximum peak of power spectral analysis is above 3 standard deviations of the median peak of the total windows. Memory acquisition was investigated during the familiarization phase when the two objects were identical. We ordered the explorations of the two objects in time and compared neural activity during the first 5 vs. the last 5 seconds of exploration (i.e., 5 early vs. 5 late one-second windows). Working memory and long-term memory retrieval were analysed during the 3 minute and 24-hour memory tests, respectively, by comparing neural signals during the first 5 seconds of exploration of familiar versus novel objects (Fig 3.3.3.1).

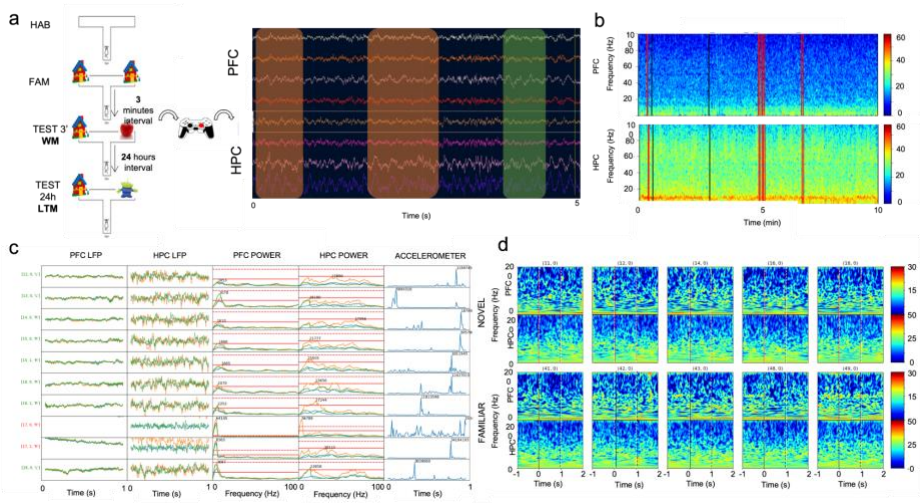

Figure 3.3.3.1: Novel object recognition (NOR) protocol and analysis process. (a) Different phases of the NOR (left) and a representation of how the explorations of the objects are aligned with the electrophysiological recording using a joystick in the open ephys software. (b) Representative spectrograms of the PFC (top) and HPC (upper) during a 24 hour session of a baseline mouse. Black and red lines indicate the explorations of the familiar and novel object, respectively, aligned with the electrophysiological data. (c) Example of the automatic artifact discard plot. The PFC and HPC LFP and power and the variance of the accelerometer are shown in different 1 second windows of explorations. Continuous red lines in the power represent the median power of the maximum peak and the dashed lines represent 3 standard deviations above that median. On the left side, windows discarded are shown in red while windows accepted are shown in green. (d) Representative spectrograms showing between one second before the exploration and one second after the exploration of the novel (top) and familiar (bottom) explorations.

3.3.4. Auditory perception and attentional assessment with the auditory evoked potential, the auditory state-steady response (ASSR) and the oddball paradigm task

We tested auditory perception and hearing sensitivity using three paradigms: auditory evoked potential, auditory state-steady response (ASSR) and the oddball paradigm to test mismatch negativity (MMN). Recordings of these tests were performed in freely moving mice in their homecage placed inside a soundproof box with the sound system inside (Fig. 3.3.4.1). We used the Python library simpleaudio for the sounds, using custom python scripts, that synchronized the sound with the electrophysiological recording using an EIB board.

3.3.4.1. Auditory evoked potential

Mice were habituated to the box and the cage for 5 minutes. Next, 100 consecutive clicks separated by 10 seconds were presented to the mice for a total of 8 minutes. A click consisted of a 15 ms white noise sound ('15ms_whitenoise.wav', from the *simpleaudio* library) (Fig 3.3.4.1). During the whole protocol animals were being electrophysiologically recorded.

3.3.4.2. Auditory state-steady response (ASSR)

The recordings were performed in the same cage and box than the auditory evoked potential. The ASSR protocol consisted of 50 periodic 40 Hz white noise clicks that lasted for 500 ms ('500ms_40Hz_1msclick.wav', from the *simpleaudio* library) with intervals of 20 seconds between trains (Fig 3.3.4.1). The whole protocol lasted for approximately 5 minutes. For the analyses of the ASSR we used the stockwell power and the inter-trial coherence (see Methods below).

3.3.4.3. The oddball paradigm: mismatch negativity (MMN)

An auditory oddball paradigm was used to measure the MMN. In the same conditions of the other auditory tasks mice were presented with a series of standard tones (6 or 8 kHz) in which a target tone (6 or 8 kHz) was presented randomly with a 75-25 % proportion, respectively. The frequencies of the standard and the target tone were switched after 500 trials in a flip-flop design (Hamilton et al., 2018a). The length of the tone was 10 ms and it was separated with 0.5 s of intertrial interval. The protocol lastet around 10 minutes and finished when the 1000 tones were presented.

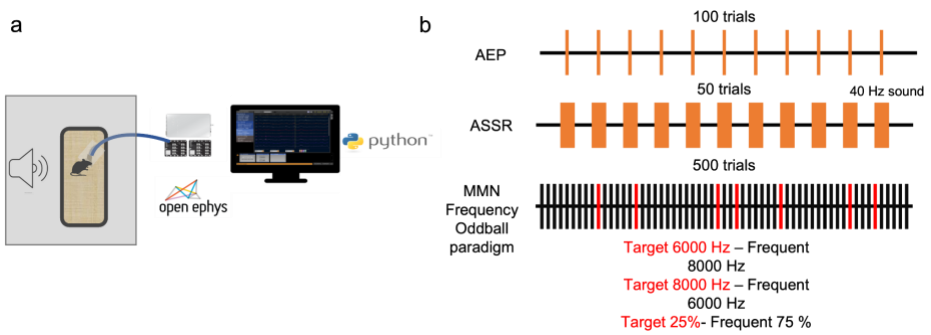

Figure 3.3.4.1: Protocol of the three auditory tasks. (a) Recordings during the auditory task were carried out in the home cage inside a soundproof box. (b) Representation of the three auditory protocols.

3.4. Pharmacology

3.4.1 Acute treatments

The doses used were: phencyclidine (PCP) 10 mg/kg; risperidone (RIS) 0.5 mg/kg; clozapine (CLZ) 1 mg/kg; haloperidol (HAL) 0.5 mg/kg; M100907 1 mg/kg; 8-OH-DPAT 1 mg/kg (Gener et al., 2019). PCP was administered subcutaneously (SC) and the rest of the drugs were administered intraperitoneally (IP). All drugs were dissolved in saline with the pH adjusted to 6.5-7.0. Twenty-four animals were used in two experiments and six mice were used in three experiments. We left at least one week between experiments for proper washout of the drugs.

3.4.2. Subchronic phencyclidine, risperidone or saline treatment

PCP (10 mg/kg) or saline were administered to the mice for 10 days subcutaneously (s.c) (daily on days 1-5, 8-12) as described in (Castañé et al., 2015; Hashimoto et al., 2005). Risperidone (0.5 mg/kg) or saline were administered for 14 consecutive days intraperitoneally (i.p.) (McKibben et al., 2010). Both drugs were dissolved in saline and the pH was adjusted 6.5-7.

3.5. Data analyses

3.5.1. Power spectral analyses

Power spectral density results were calculated using the multi-taper method (time frequency bandwidth; TW = 5 and K = 9 tapers; 1-200Hz range, non-overlapping sliding windows of 1 minute for spectrograms and power spectrum of the acute injection experiments, 3 seconds for the resting state conditions and 1 second for object explorations). The stockwell method from the mne library (Gramfort et al., 2013) was used for spectrograms of less than 1 second window during NOR explorations and the ASSR task. Spectrograms were constructed using consecutive

Fourier transforms. Some spectrogram results were provided as z-scores with respect to baseline statistics (i.e., data is demeaned by the baseline mean and then normalized by the baseline standard deviation).

3.5.2 Phase-amplitude coupling

We used two different functions for the analyses of the phase amplitude coupling depending on the size of the window to analyze. We used the modulation index (MI) described on (Tort et al., 2008) for windows of one minute or more. Moreover, we used the Canolty method as implemented on (Onslow et al., 2011) for shorter windows. First, low frequency (delta and theta) phases were divided into 18º bins (i.e., each cycle is divided into 20 bins) and gamma (low, high gamma) and HFOs amplitudes were calculated for each phase bin. MI measures the divergence of the phase amplitude distribution and is higher as further away is from the uniform distribution (i.e., no modulation) (Fig. 3.5.1). In order to choose specific frequency band pairs for the MI quantification we represented overall MI in two-dimensional pseudocolor comodulation maps. A warmer color indicates coupling between the phase of the low frequency band (x axis) and the amplitude of the high frequency band (y axis) while blue depicts absence of coupling.

3.5.3. Functional connectivity analyses

To quantify functional connectivity between the PFC and the HPC we used two different approaches. Non-directed phase coherence was assessed using weighted phase lag index (wPLI) whereas signal directionality was measured using phase slope index (PSI).

3.5.3.1. Weighted phase lag index (wPLI)

PFC-HPC phase coherence was estimated via the weighted phase-lag index (wPLI, Butterworth filter of order 3), a measure of phase synchronization between areas aimed at removing the contribution of common source zero-lag effects that allowed us to estimate the synchronization between the PFC and the HPC mitigating source signals affecting multiple regions simultaneously (Gener et al., 2019; Hardmeier et al., 2014; Stam et al., 2007; Vinck et al., 2011). First, we used Hilbert transformation to obtain instantaneous phases from LFP. wPLI measures the asymmetry in the distribution of phase differences for each frequency band between the two time series resulting in values ranging between 0 and 1, being a higher value a high asymmetric distribution as a consequence of a consistent phase-lag between signals in the two areas. wPLI reduces the probability of detecting false positive connectivity in the

case of volume conducted noise sources with near zero phase lag and shows higher sensitivity in detecting real phase synchronization. wPLI color plots were built applying the previous function multiple times with a 1 Hz sliding frequency window (using Butterworth bandpass filters of order 3), and PLI quantifications were generated applying the PLI spectra function over a 60s sliding window (without overlap). wPLI color plot results were provided as z-scores with respect to baseline statistics (i.e., data is demeaned by the baseline mean and then normalized by the baseline standard deviation).

3.5.3.2. Phase slope index

Signal directionality between areas was calculated with the phase slope index (PSI) with a Python translation of MATLAB's data2psi.m (epleng = 60s, segleng = 1s) as in reference (Nolte et al., 2008). PSI is a robust measure based on the conceptual temporal argument supporting that the driver is earlier than the recipient and contains information about the future of the recipient. It quantifies the consistency of the direction of the change in the phase difference across frequencies. Given a specific bandwidth parameter, it computes for each frequency bin the change in the phase difference between close frequency bins, weighted with the coherence.

Then, when phase difference changes consistently across frequencies, and there is coherence, PSI deviates from zero (Bastos and Schoffelen, 2015). Positive slope reflects an PFC-to-HPC flow of information in a specific frequency range while a negative slope reflects HPC-to-PFC signal directionality. PSI color plots and quantifications were constructed with the same strategy as wPLI plots but using a 2 Hz sliding frequency window.

3.5.3.3. Surrogates analyses of connectivity

In order to establish the significance level of the wPLI and PSI analyses, the surrogate method of randomization was used (Lancaster et al., 2018; Puig and Miller, 2015). The surrogate analyses were performed by randomizing the data of two pairs of channels, one PFC and one HPC, using all the combinations of different pairs of channels. The data was shuffled across time series and across the pair of channels for 1000 times before obtaining the correspondent wPLI and PSI analyses. Next, the randomized data wass averaged and subtracted from the not randomized results, in order to remove the chance effects from the data. Statistical analyses on the subtracted data and comparing the surrogates data with the results were performed to establish significance.

3.5.4. Event-related potential (ERPs) analyses

To analyse the ERPs, the LFP data (30.0000 Hz, without downsampling) recorded in the PFC electrodes was used. The windows to analyze the ERP started 5 ms before the start of the stimulus (baseline) and finished 400 ms after the stimulus starts. Windows that presented artifacts were discarded for the analyses. Furthermore, only trials that presented an ERP were selected for comparison and the response rate was computed by dividing the responsive trials among the total trials. Each window was normalized by subtracting the baseline signal before averaging.

3.5.5. Intertrial coherence analyses (ITC)

The ITC analyses were used to compare the evoked gamma generated after the ASSR protocol over trials. The ITC is a measure of the consistency of an oscillatory phase across trials. The ITC was examined 0.1-0.5 ms after the sound between 38-42 Hz. We used the itc output of the stockwell function inthe mne library (Gramfort et al., 2013).

3.5.6. Mismatch negativity (MMN)

The MMN was defined according to previous rodent and human studies (Rissling and Light, 2010; Schuelert et al., 2018). It was obtained by

subtracting the averaged response of a set of standard stimuli from the averaged response of the target stimuli. Only the standard stimuli before the target stimuli were selected, in order to have an equal number. The analyses of the 6 KHz and 8 KHz tones were performed separately, always comparing the standard and target tone of the same frequency. In order to compare the negative deflection between the two tones, the MMN was obtained using the area under the curve of the peak containing a 50 ms window (25 ms before and 25 ms after) as described in (Schuelert et al., 2018).

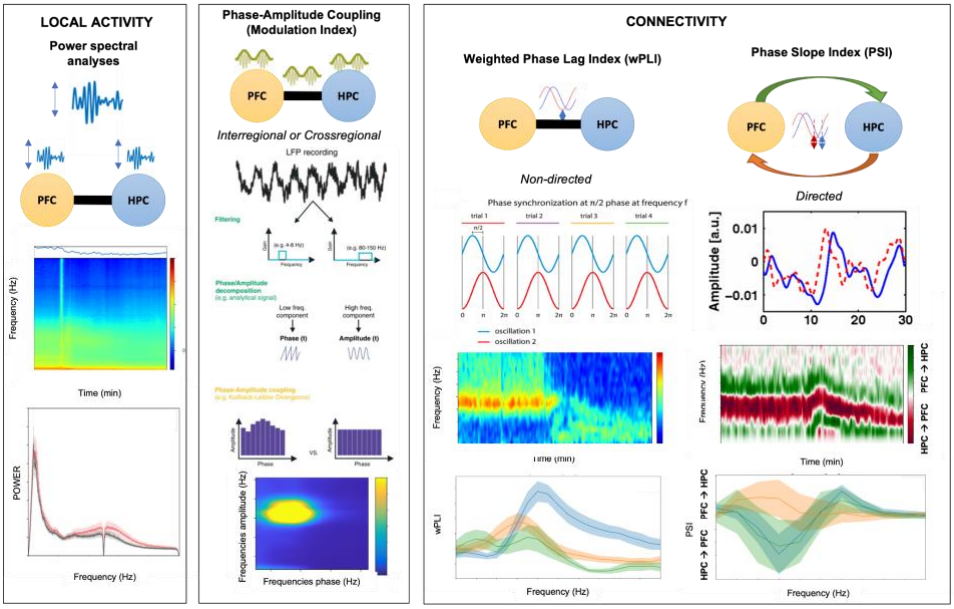

Figure 3.5.1: Classification of local field potential analyses. Power spectral analyses are performed to analyse the amplitude of the local field potentials in the PFC or the HPC locally. Phase amplitude coupling is performed locally or inter-regionally using the (Onslow et al., 2011; Tort et al., 2008, p. 2) methods for short or long windows, respectively. First we performed a band-pass filtering and extraction of phase and amplitude and then assessed correlations between amplitude and phase to quantify deviations of the uniform distribution from the amplitude vs phase histogram (Aru et al., 2015). The non-directed phase coherence analyses were performed using the weighted phase lag index using a sum of the cross-spectral densities of different trials, while the directed connectivity measure was the phase slope index, measuring the consistency of the direction of the change in the phase difference across frequencies (Bastos and Schoffelen, 2015). Spectrograms, comodulograms and quantifications will be used to present these analyses.

3.6. Statistical analysis

All the statistical analyses described below were performed for acc, power, PAC, wPLI, PSI, ERPs, ITC and MMN. Paired T-student analyses were used to compare object explorations between the same group of animals during one treatment condition (novel vs familiar) or treatment conditions in the same animals over time (baseline vs sPCP/saline), whereas unpaired T-student was used to compare different group of animals at different treatments (sPCP vs saline). One-way repeated measures ANOVA was used to test for statistical significance with time as within subject factor (first project: baseline, saline, PCP and drug; second project: baseline, sPCP/saline, risperidone/saline). Additionally, in the first project two-way repeated measures ANOVA was used to test for statistical significance with treatment as between factor (PCP+saline vs. saline controls and PCP+saline vs. PCP+drug) and time as within subject factor (baseline, saline, PCP and drug). In the second project, two-way repeated measures ANOVA were used differently depending if animals were the same across different treatment conditions over time or if we were comparing treatment at the same time but in different groups of animals. In the first condition, two-way repeated measures ANOVA had as within factors the treatment condition and the type of object exploration (treatment: baseline vs

sPCP/saline vs risperidone/saline; object: novel vs familiar), whereas in the second case the treatment was considered the between factor (sPCP vs saline or risperidone vs sPCP-saline vs saline) and the type of object exploration was considered as a within factor (novel vs familiar). Sidak and Bonferroni post-hocs were used for Multiple Comparisons between the ANOVAs. Statistical analyses were conducted using raw data in Python with the Pingouin statistical package (Vallat, 2018). Furthermore, to determine significant correlations between neurophysiological measures and DIs or other neurophysiological measures, Pearson or Spearman correlations were used for parametric and non-parametric distributions, respectively.

3.7. Histology

On the last day of electrophysiological recordings, small electrolytic lesions of the recording sites were carried out via electrical stimulation of the electrodes (100 Hz, 0.1 mA for 2 s) under anaesthesia. Then, mice were sacrificed and their brains extracted and preserved in 2-methylbutane. Brains were sliced into 30 Pm sections with a cryostat. Electrode placements were confirmed histologically by staining the brain slices using

the Nissl method. Electrodes with tips outside the targeted areas were discarded from data analyses.

3.8. Protocols

We have designed two different protocols two address the two objectives of the thesis (Fig 3.8.1). The first was designed for investigating the psychotic-like states induced by acute PCP administration and the rescuing effects of antipsychotic drugs. The second one was used to assess the cognitive impairment induced by sPCP treatment and subsequent cognitive amelioration by a chronic risperidone treatment.

3.8.1. Protocol to investigate the psychotic-like states and the effects of antipsychotic drugs

Surgeries (see Methods) were performed in adult, 8-12 weeks of age, C57BL6 mice. The mice recovered for a week after the surgery. Electrophysiological recordings were carried out in the home cage which was shielded with aluminum fold and grounded to the electrophysiological recording system. Two different protocols were designed. First, the protocol to mimic the psychotic-like conditions induced by acute PCP, in which 15 minutes of the freely moving mice in the home cage (baseline)

were recorded. After that, the acute PCP was injected (10 mg/kg) and recorded for another hour. The second protocol was used to assess the rescuing effects of antipsychotic drugs or serotonergic compounds after the acute PCP treatment. The baseline state was recorded for 30 minutes followed by an internal control of a saline injection that was recorded for another 30 minutes. After the first hour acute PCP (10 mg/kg) was injected. 15 minutes later we injected the antipsychotic drug (atypical antipsychotic drugs: CLZ or RIS; classical antipsychotic drug: HAL), the serotonergic compound (M100907 or DPAT) or saline (control) and recorded for another hour.

3.8.2. Protocol to investigate the cognitive deficits induced by sPCP and the amelioration of a chronic risperidone treatment

Surgeries (see Methods) were performed in adult, 8-12 weeks of age, C57BL6 mice. The mice recovered for a week after the surgery. The battery of tests used for the characterization of the mice were: open field exploration, NOR task and three auditory tasks (auditory evoked potential, ASSR and the oddball paradigm to assess MMN). All tests were electrophysiologically recorded. Mice were randomly divided in three

different groups according to the treatments received: sPCP-risperidone (mice that received the sPCP treatment followed by the chronic risperidone treatment), sPCP-saline (mice that received the sPCP treatment followed by a chronic saline treatment) and saline-saline (mice that received two saline treatments, one subchronic (10 days s.c) and one chronic (14 days i.p.) saline treatments). The first characterization was done during the baseline state of the mice one week after the surgery. Once this characterization was done the mice started the sPCP (10 mg/kg) or saline treatment for 10 non-consecutive days (5 days treatment + 2 days off + 5 days treatment s.c.). Starting 3 days after finishing the treatment another full characterization was done. Finally, a chronic risperidone (0.5 mg/kg) or saline treatment (14 consecutive days, i.p.) was done followed by another full characterization.

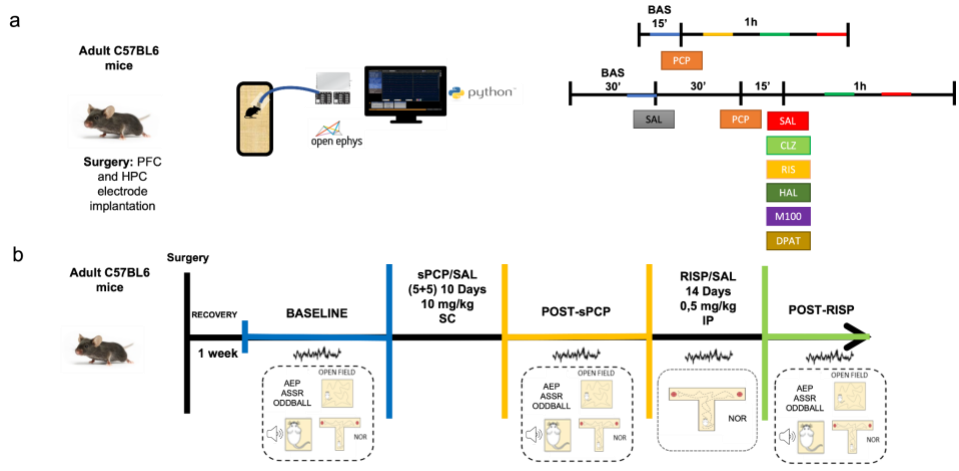

Figure 3.8.1: Protocols of the two main objectives of the project. (a) Protocol to

investigate the psychotic-like states and the effects of antipsychotic drugs. First animals are implanted using the surgery mentioned before (see Methods). Next, animals were recorded in their home cage using the open ephys system. The protocol used for studying the psychotic is on the top, while the protocol used for analysing the effects of antipsychotic drugs is on the bottom. Color lines in the protocol represent the moments of quantification. (b) Protocol to investigate the cognitive deficits induced by sPCP and the amelioration by chronic risperidone. The color lines in the arrow represent the different treatment conditions: baseline was represented in blue, sPCP or saline were represented in orange and risperidone or saline were represented in green.

4. CHAPTER I.NEURAL SUBSTRATES OF PSYCHOSIS-LIKE STATES INDUCED BY ACUTE PHENCYCLIDINE AND RESCUING EFFECTS OF ANTIPSYCHOTIC MEDICATION

4. CHAPTER I. NEURAL SUBSTRATES OF PSYCHOSIS-LIKE STATES INDUCED BY ACUTE PHENCYCLIDINE AND RESCUING EFFECTS OF ANTIPSYCHOTIC MEDICATION

In this chapter we explore the neural dynamics of PFC-HPC circuits during psychosis-like states produced by an acute dose of PCP. We further explore the ability of the antipsychotic drugs risperidone, clozapine and haloperidol, the 5-HT_{2A}R antagonist M100907 and the 5-HT_{1A}R agonist 8-OH-DPAT to rescue the circuit dysfunction produced by PCP.

4.1. Prefrontal-hippocampal circuit alterations induced by acute phencyclidine

We investigated how acute NMDAR antagonism influences behavior and neural activity in the prelimbic PFC and the CA1 region of the HPC. To elicit psychotomimetic conditions we administered PCP acutely (10 mg/kg, SC) in freely moving mice. This dose of PCP induces strong psychotic-like behaviors in mice, such as hyperlocomotion, stereotypies and ataxia, that can be mostly treated with antipsychotic drugs (Castañé et al., 2015; Lee et al., 2017; Sturgeon et al., 1979). We first aimed to validate

this PCP model of psychosis in our experimental conditions where mice were connected to an electrophysiological data acquisition system via an electrical cable. Mice received PCP followed by saline or risperidone (RIS, 0.5 mg/kg, IP) fifteen minutes post PCP administration. Mice were given one week of wash out between each experimental condition. As expected, PCP increased locomotor activity (distance traveled) and stereotypies that were greatly reduced by risperidone (n = 4 mice; [Time*Treatment: Locomotion, stereotypies]: $F_{7,42}$ = 10.35, 2.59, $p < 0.0005$, 0.03; two-way ANOVA with time as within factor and drug combination as between factor) (Fig. 4.1.1.a,b). In contrast, PCP-mediated ataxia was exacerbated by risperidone in an initial phase ([time with no interaction]: $F_{7,42}$ = 23.16, $p < 0.005$) and then followed PCP´s pattern (Fig. 4.1.1.b). The PCP-induced and risperidone-induced behaviors were reflected as partial and large reductions of accelerometer rates, respectively, that were recorded via the accelerometer integrated within the headstages of the electrophysiological system ([time with no interaction]: $F_{8,64}$ = 6.73, $p < 0.0005$; Fig. 4.1.1.c). We harnessed these changes in accelerometer rates to assess PCP-induced and antipsychotic drug-induced behaviors over time in the subsequent pharmacological experiments described below.

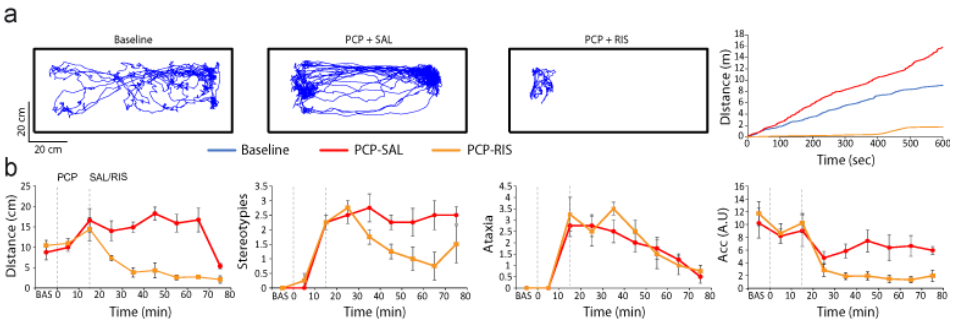

Figure 4.1.1: Acute PCP (10 mg/kg, SC) induced psychotic-like behavioral effects in mice. (a) Representative examples of 10 minute traces during baseline (left), after the administration of PCP + SAL (middle) and after the administration of PCP + RIS (0.5 mg/kg, IP; right) in one mouse. Quantification of distance traveled is shown on the right of baseline (blue), PCP + SAL (red) and PCP+RIS (orange). (b) Quantification of distance traveled, stereotypes, ataxia and accelerometer during 10 minutes epoch after the PCP injection. The groups quantified are PCP + SAL (n = 4 mice, red) and PCP + RIS (n = 4 mice, orange).

In a different cohort of animals, we examined the time course of PCP´s effects on PFC-HPC neural dynamics at 15, 30 and 60 minutes after PCP administration (n = 9 mice) compared to saline administration (n = 10 mice; Fig. 4.1.3 and 4.1.2.). Again, PCP induced hyperlocomotion, stereotypies and ataxia partially reduced the accelerometer rates ([Time*Treatment]: $F_{1,8}$ = 16.73, p <0.0005). The atypical behaviors induced by PCP were accompanied by substantial alterations in neural oscillations, particularly in the PFC, that could be readily seen in the

unprocessed local field potentials (Fig. 4.1.3.b). Several aberrant bands emerged in the PFC after injection of PCP: a wide band from 1 to 8 Hz that included the standard "slow" delta (2-5 Hz) and a "fast" delta (4-8 Hz, peak at 6.4 ± 0.2 Hz), an alpha band (10-14 Hz, peak at 10.2 ± 0.06), a narrow band within the high gamma range (40-75 Hz, peak at 60.3 ± 1.1 Hz), and broadly increased HFOs (100-200 Hz) that included a prominent band between 140-180 Hz (peak at 160.5 ± 2.54 Hz; $F_{1,8}$ = 21.4, 22.73, 13.67, 17.31 and 17.93, respectively; $p < 0.0005$; one-way ANOVA; significant differences with saline controls; Fig. 4.1.3.c,d). These bands appeared *de novo* and revealed strong hypersynchronization of PFC microcircuits by PCP. In the HPC, the power changes were modest and mostly differed from the PFC, except for the delta band that closely followed the pattern found in the PFC ($F_{1,8}$ = 20.07, $p < 0.0005$). PCP decreased the power of HPC theta oscillations (8-12 Hz) with respect to baseline ($F_{1,8}$ = 14.6, p = 0.002) and increased high gamma oscillations in a band that appeared earlier and was shorter than in the PFC (the first 15 min only; $F_{1,8}$ = 18.2, $p < 0.0005$; Fig. 4.1.3.c).

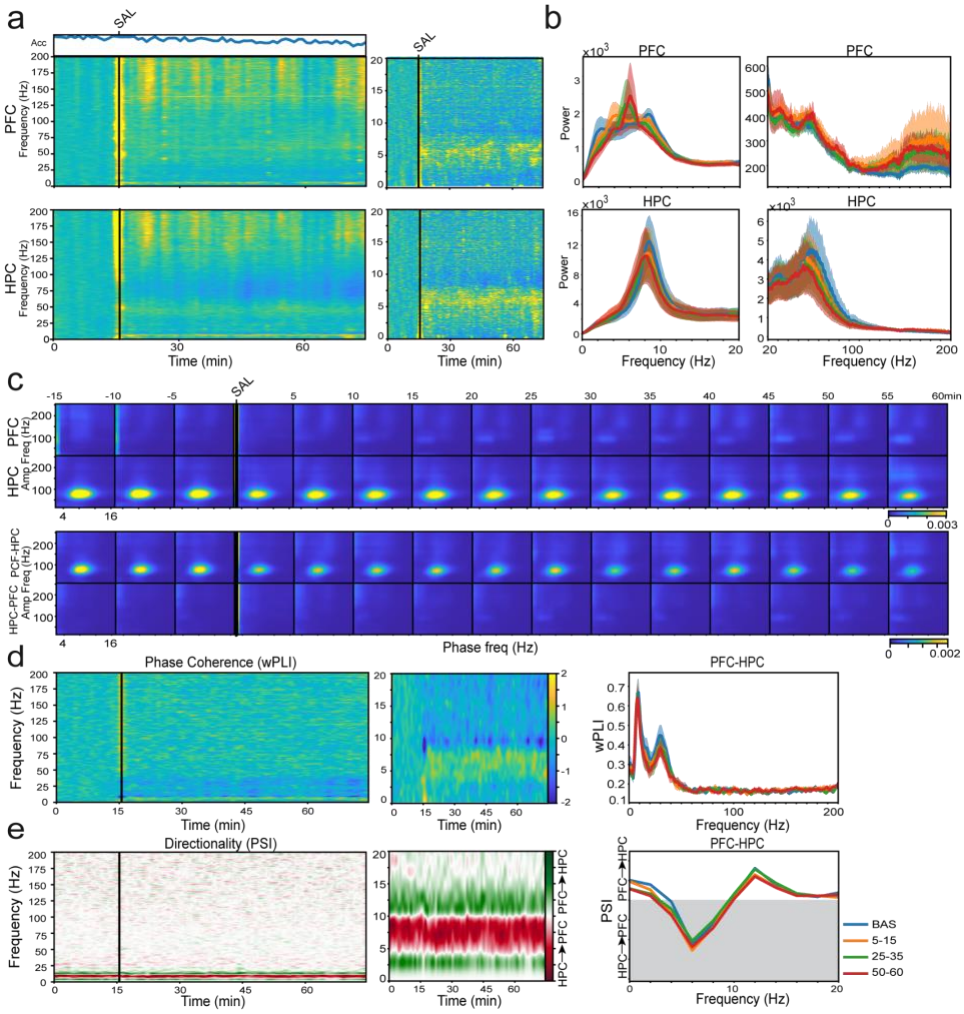

Figure 4.1.2. Saline (SAL, SC; n = 10 mice) had minor effects on PFC-HPC neural dynamics. It induced a modest mobility reduction (Acc, $F_{1,8}$ = 5.08, p = 0.006) that likely affected theta oscillations in both areas and theta-gamma l-PAC and ir-PAC ($F_{1,8}$ = 7.45, 7.58, 6.6, 6.83 p = 0.011, 0.001, 0.002, 0.002). However, the circuit connectivity was overall not affected, only showing a significant decrease in low gamma phase coherence ($F_{1,6}$ = 4.39, p = 0.032). (a) Normalized spectrograms (z-scores) of signals in the PFC (upper panels) and HPC (lower panels). The corresponding quantification of the animals' mobility (Acc) is also shown. (b) Power spectra of PFC and HPC signals. The plots have

been divided into 0-20 Hz and 20-200 Hz to facilitate visualization. (c) Comodulation maps quantifying local and inter-regional cross-frequency coupling in consecutive non-overlapping 5-min epochs. (d) Normalized (z-scores) time course of changes in wPLI (phase coherence) and corresponding quantification. (e) Normalized (z-scores) time course of changes in PSI (circuit signal directionality) and corresponding quantification. The shaded area represents HPC-to-PFC signal directionality and the line indicates zero PSI. Group colors: baseline (blue), 5 to 15 min (orange), 25 to 35 min (green) and 50 to 60 min (red) after the administration of saline.

To further assess local and circuit synchronization we quantified cross-frequency phase-amplitude coupling (PAC) between slow rhythms (2-16 Hz) and faster oscillations (50-250 Hz) (Jensen and Colgin, 2007; Scheffer-Teixeira and Tort, 2017). PAC was investigated both within the PFC and the HPC (local PAC or l-PAC: PFC_{phase}-PFC_{amp} and HPC_{phase}-HPC_{amp}) and at the circuit level via coupling of HPC phase with PFC amplitude and vice versa (inter-regional PAC or ir-PAC: HPC_{phase}-PFC_{amp} and PFC_{phase}-HPC_{amp}). As reported previously (Colgin, 2015; Hentschke et al., 2007; Scheffer-Teixeira and Tort, 2017), theta-gamma l-PAC within the CA1 region was present during baseline periods, with phases varying from 5 to 12 Hz and amplitude frequencies varying from 50 to 100 Hz (Fig. 4.1.3.e). After PCP, this theta-gamma coordination rapidly subsided and delta-HFO coupling emerged ([decrease theta-gamma, increase delta-HFO

l-PAC] $F_{1,8}$ = 23.13, 14.6, p < 0.0005, 0.002; Fig. 4.1.43.e). At a circuit level, we found that the phase of PFC theta modulated the amplitude of CA1 high gamma (PFC_{phase}-HPC_{amp}), as reported recently (Nandi et al., 2019; Tavares and Tort, 2020; Zhang et al., 2016). Again, PCP weakened this circuit coupling while upregulating delta-HFO ir-PAC ([decrease theta-gamma, increase delta-HFOs PAC] $F_{1,8}$ = 17.4, 16.6, p = 0.0006, 0.0008; Fig. 4.1.3.e), as observed in the HPC. Furthermore, PCP promoted fast delta-HFO l-PAC in the PFC and HPC_{phase}-PFC_{amp} ir-PAC ($F_{1,8}$ = 21, 18.77, p < 0.0005, 0.002; Fig. 4.1.3.e).

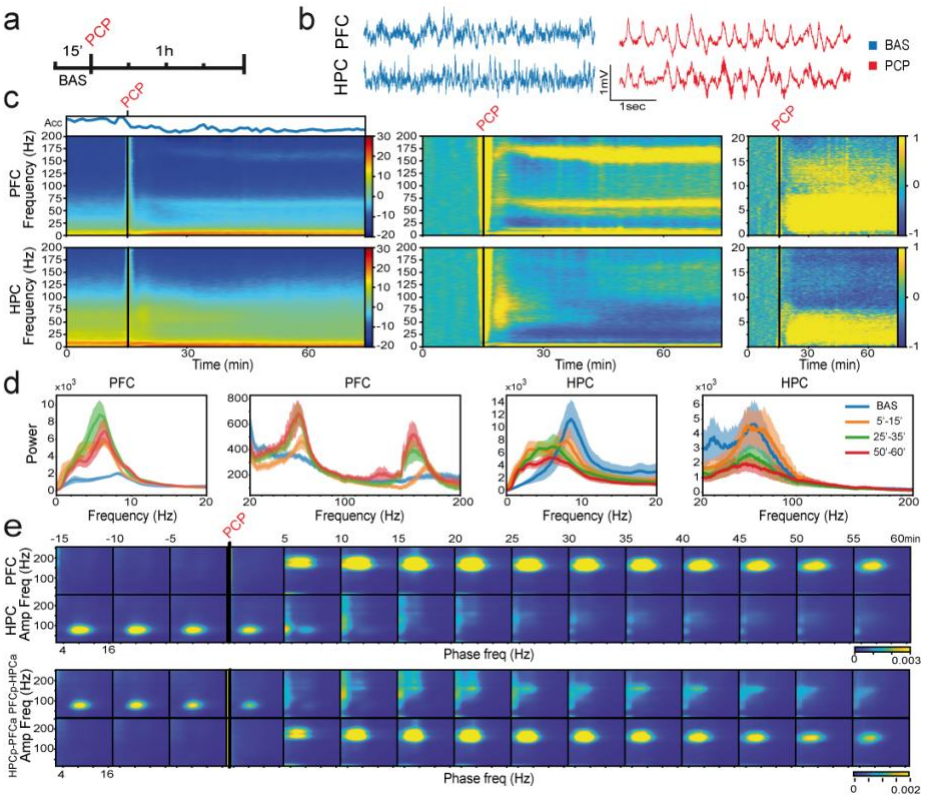

Figure 4.1.3: Acute administration of PCP boosts the synchronization of prefrontal and hippocampal microcircuits. (a) Experimental protocol. Recording LFP signals in freely moving mice during baseline conditions (BAS) for 15 minutes and for 1 hour following the administration of PCP (SC, 10 mg/kg; n = 10 mice). (b) Representative examples of 5 second LFP traces recorded in the PFC and the HPC during baseline (blue) and after the administration of PCP (red) in one mouse. (c) Averaged spectrograms of signals in the PFC (upper panels) and the HPC (lower panels). Left panels represent the raw data with the corresponding quantification of the animals' mobility (Acc, variance of signals from the accelerometer); middle and right panels represent the z-scores relative to baseline. Note the different frequencies on the y-axis between spectrograms. (d) Power spectra of PFC (left panels) and HPC (right panels) signals during baseline (blue), 5 to 15

min (orange), 25 to 35 min (green) and 50 to 60 minutes (red) after the administration of PCP. The plots have been divided into 0-20 Hz and 20-200 Hz to facilitate the comparison. (e) Comodulation maps quantifying cross-frequency coupling in consecutive non-overlapping 5-min epochs. The x-axis represents phase frequencies (2-16 Hz) and the y-axis represent amplitude frequencies (10-250 Hz). Numbers on top of the panels indicate the minute after PCP administration. (Top) Local modulation index in the PFC and the HPC. (Bottom) Cross-regional modulation index between the PFC phase and the HPC amplitude (upper panels) and between the HPC phase and the PFC amplitude (bottom panels). PCP administration is marked in red.

We subsequently investigated PCP-induced alterations in the functional connectivity of the circuit. We first examined PFC-HPC phase coherence via the weighted phase-lag index (wPLI), a measure of phase synchronization between LFP signals that minimizes the effects of volume-conduction, noise and sample size (Hardmeier et al., 2014; Vinck et al., 2011). PCP generated circuit hypersynchronization at fast frequencies ([HFO wPLI]: $F_{1,8} = 12.87$, $p = 0.005$; milder increases at low and high gamma) while desynchronizing the middle frequencies ([theta, alpha and beta wPLI]: $F_{1,8} = 21, 8.07, 14.47$, $p < 0.0005, 0.044$ and 0.002, respectively; significant differences with saline controls). In fact, theta coherence shifted to fast delta (peak from 8.45 ± 0.15 to 6.36 ± 0.43) for at least 45 min after PCP injection (Fig. 4.1.4.a). We also quantified the signal directionality between the PFC and the HPC via the phase slope

index (PSI) (Nolte et al., 2008). During baseline, a strong flow of information at theta originated in the HPC and traveled to the PFC. In accordance with changes in phase coherence, PCP disrupted theta signal directionality ($F_{1,8}$ = 4.04, p = 0.018) and generated an aberrant flow of information between 3 and 6 Hz (delta) from the PFC to the HPC ($F_{1,8}$ = 3.4, p = 0.034; 4.1.4.b).

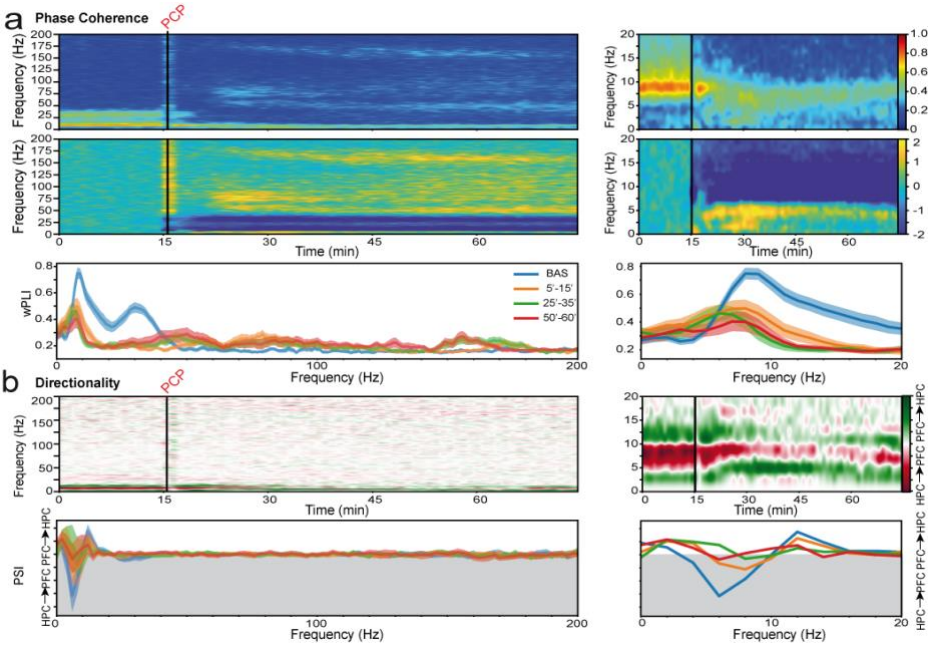

Figure 4.1.4: Acute administration of PCP disrupts PFC-HPC phase coherence and signal directionality. (a) Time course of changes in weighted phase lag index (wPLI, phase coherence) and corresponding z-scores. Quantification of wPLI is shown below. (b) Time course of changes in phase slope index (PSI, circuit signal directionality). HPC-to-PFC signal directionality is represented in red and PFC-to-HPC signal directionality in green. A simplified representation of PSI is shown below where the shaded areas indicate

HPC-to-PFC signal directionality (the line marks zero). 0-20 Hz magnifications are shown on the right. Average signals during baseline are shown in blue and signals during the 5-15, 25-35, and 50-60 min after PCP administration are represented in orange, green and red, respectively.

4.2 Effects of antipsychotic drugs on phencyclidine-induced prefrontal-hippocampal alterations

We next investigated the individual fingerprints of antipsychotic action on PCP-induced neurophysiological alterations by the atypical antipsychotic drugs risperidone and clozapine and the classical antipsychotic drug haloperidol. Fifteen minutes after the administration of PCP one of the three antipsychotic drugs was administered. We compared the neural signals recorded at 15 and 45 min after antipsychotic drug injection (30 and 60 min after PCP injection) with a control group that only received saline (PCP+SAL, n = 6 mice, Fig 4.2.1.a, 4.2.2.a, 4.2.4.a). In these experiments, additional control injections with saline were performed before the administration of PCP.

We first examined the actions of the three antipsychotics on the power of PCP-induced abnormal neural oscillations in the PFC and the HPC. Risperidone (RIS, 0.5 mg/kg; n = 7 mice) reduced the hyperlocomotion

and stereotypies produced by PCP and left the mice in a sedative state that generated high immobility ([Acc]: $F_{1,6}$ = 23.82, p <0.0005, one-way ANOVA; [PCP+SAL vs. PCP+RIS] $F_{2,22}$ = 4.33, p = 0.026, two-way ANOVA; Fig. 4.1.1) and a strong inhibition of neural activity, as we reported previously (Gener et al., 2019). More specifically, risperidone decreased PCP-associated increases in power at theta, high gamma and HFO in the PFC (two-way ANOVA with time and treatment [PCP+SAL vs. PCP+RIS] as factors; [Time*Treatment] $F_{2,22}$ = 3.64, 9.99, 5.75, p = 0.043, 0.0008, 0.01, respectively) (Fig. 4.2.1.b) and reduced theta oscillations in the HPC ($F_{2,22}$ = 4.55, p = 0.056). In contrast, risperidone exacerbated PFC slow delta power ($F_{2,22}$ = 8.55, p = 0.002) shifting its main frequency from fast to slower ranges in both brain regions (PFC: peak from 6.4 Hz to 3.7 Hz; HPC: peak from 6.01 Hz to 3.67 Hz; Fig. 4.2.1.b). Intriguingly, narrow bands in the high gamma and HFO domains continued in the PFC, steadily decreasing their frequency over time (Fig. 4.2.1.b). We next investigated the actions of clozapine (CLZ, 1 mg/kg; n = 6 mice) on PCP-mediated effects. Clozapine reduced PCP-induced behavioral alterations and power increases, however caused fewer suppressive effects than risperidone. First, clozapine decreased general mobility of mice ($F_{1,5}$ = 6.82, p = 0.004, one-way ANOVA; [PCP+SAL vs. PCP+CLZ] $F_{2.20}$ =

4.93, p = 0.051, two-way ANOVA), but less than risperidone ([PCP+CLZ vs PCP+RIS] $F_{2.22} = 6.28$, p = 0.005). It slightly decreased amplified high gamma in the PFC ($F_{2,22} = 4.46$, p = 0.066; two-way ANOVA) (Fig. 4.2.1.c) but, unlike risperidone, it was unable to rescue increased HFOs. In addition, fast delta partially shifted to slow delta: two peaks at 5.05 Hz and 3.14 Hz were observed in the power spectrum (Fig. 4.2.1.c; insignificant changes in slow and fast delta power). We subsequently examined the effects of the classical antipsychotic drug, haloperidol (HAL, 0.5 mg/kg; n = 5 mice), on PCP-induced alterations. The general mobility of the mice after the administration of haloperidol was similar to the control group ([PCP+SAL vs. PCP+HAL] $F_{2,18} = 0.26$, p = 0.77, two-way ANOVA), and above that of the risperidone group ([PCP+HAL vs. PCP+RIS] $F_{2,18}= 7.31$, p = 0.004). This suggests that the administration of haloperidol did not induce major sedative effects. Notably, haloperidol was unable to block the aberrant fast delta, high gamma and HFO bands elicited by PCP in the PFC (Fig. 4.2.1.d).

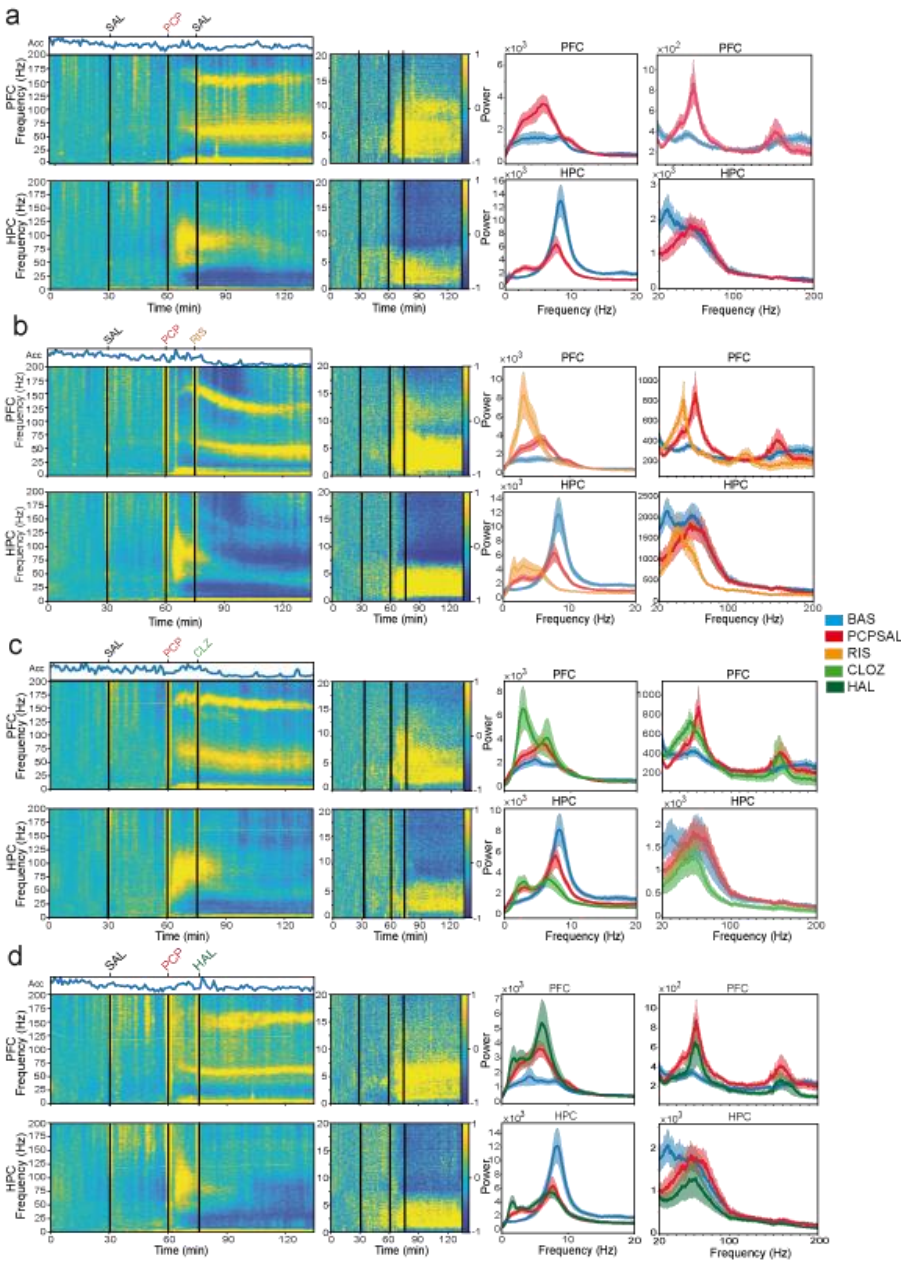

Figure 4.2.1: Comparison of antipsychotic effects on local PFC and HPC power after the PCP acute injections. All panels present normalized spectrograms (z-scores) of signals in the PFC (upper panels) and HPC (lower panels). The corresponding

quantification of the animals' mobility (Acc) is also shown. The Acc results are presented as a ratio to the highest value in the baseline condition. (b) The power spectra of PFC and HPC signals during 10 min of baseline are depicted in blue and signals from min 35 to 45 after antipsychotic administration (50-60 min after PCP) are shown in red (saline; shown as control in all the panels), orange (risperidone), light green (clozapine) and dark green (haloperidol). The figure presents the different effects of antipsychotics in the local power 15 minutes after the PCP injection: saline(a), risperidone (b), clozapine (c) and haloperidol (d).

Subsequently, we assessed the effects of the antipsychotic drugs on PCP-induced changes in phase-amplitude coupling (PAC). Risperidone markedly reduced the anomalous fast delta-HFO l-PAC and ir-PAC ($F_{2,22}$ = 5.73, 5.14, p = 0.001, 0.014) (Fig. 4.2.1.b), but it did not restore the intrinsic local or interregional theta-gamma coupling. On the other hand, clozapine shifted the aberrant fast delta-HFO to slow delta-HFO coupling consistent with the power effects (Fig. 4.2.1.c). Interestingly, baseline HPC and inter-regional theta-gamma coupling was partially reinstated (Fig. 4.2.2.c). Also consistent with the power results, haloperidol did not reduce fast delta-HFO l-PAC and ir-PAC (Fig. 4.2.2.d). Moreover, HPC theta power and theta-gamma coupling remained very low.

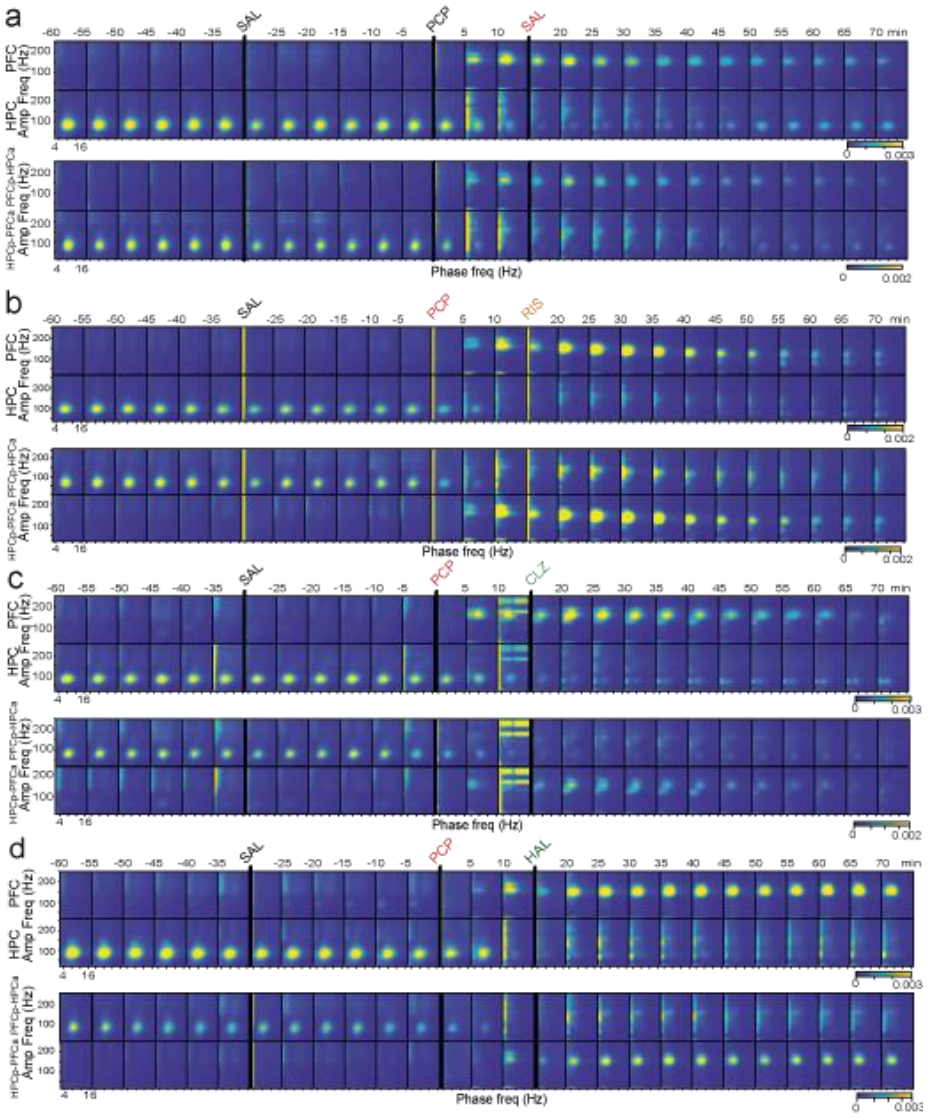

Figure 4.2.2: Comparison of antipsychotic effects on local and interregional phase amplitude coupling after the PCP acute injections. All panels present comodulation maps quantifying local and inter-regional cross-frequency coupling in consecutive non-overlapping 5-min epochs.The numbers on top of the panels indicate time after PCP administration. The upper panels show the local, PFC and HPC, course of changes in the modulation index, while the lower panels show the interregional, PFC-phase HPC-

amplitude and HPC-phase and PFC-amplitude. The figure presents the different effects of antipsychotics 15 minutes after the PCP injection: saline(a), risperidone (b), clozapine (c) and haloperidol (d).

The inability of atypical antipsychotics to reinstate theta oscillations and theta-gamma coupling in the HPC could be influenced by their sedative properties that cause immobility of mice (Fig. 4.1.1, 4.2.1). To provide insight into the influence of immobility in neurophysiological biomarkers, we compared neural activity during periods of typical mobility and periods of immobility naturally occurring during quiet wakefulness. We found that theta oscillations and theta-gamma coupling in the HPC were disrupted during quiet wakefulness episodes (Fig. 4.2.3). Therefore, reduced HPC theta oscillations and theta-gamma coupling after the administration of the atypical antipsychotic drugs could be attributed to the immobility associated with sedation. However, considering that the mice maintained the PCP-induced activity after haloperidol, this likely reflects the lack of effect of the antipsychotic drug on PCP-mediated disruption of hippocampal synchronization.

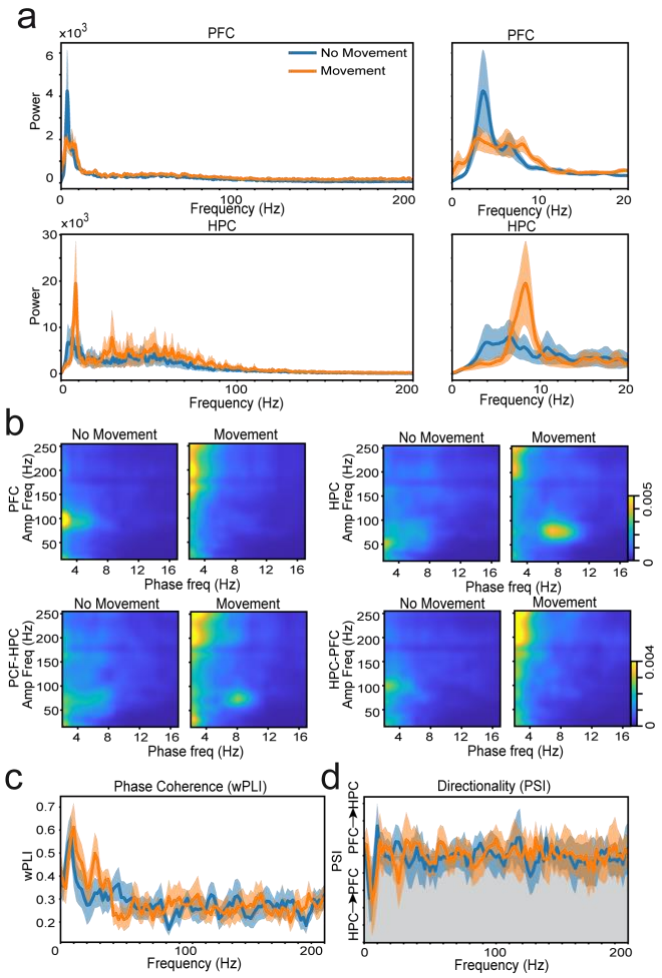

Figure 4.2.3: Little influence of mouse mobility in PFC-HPC neural dynamics. We analyzed periods of low mobility and compared them to periods of normal mobility during baseline (n = 8 mice, 10 consecutive second epochs). Low mobility was determined by a defined threshold in the output of the accelerometer signals and normal movement was defined as above that threshold. (a) Power spectra of PFC and HPC signals while animals rest or move. PFC power was in fact sensitive to movement changes in baseline, specifically showing increased power during epochs of mobility compared to low mobility at theta, beta and gamma frequencies ($F_{1,7}$ = 2.84, 3.62, 7.82, p = 0.025, 0.009,

<0.0005). Moreover, as observed in the previous literature, theta oscillations increased within the CA1 region during movement ($F_{1,6}$ = 2.36, p = 0.057). (b) Averaged comodulation maps of local and inter-regional modulation index in the two groups. Theta-gamma coupling tended to increase within the CA1 region during movement ($F_{1,6}$ = 2.18, p = 0.072). In addition, during periods of low mobility there was a minor increase in delta-gamma coupling in CA1 that was statistically insignificant ($F_{1,7}$ = 2.08, p = 0.083). (c) The circuit phase synchronization was overall not affected by the movement, only showing a significant increase in high gamma phase coherence ($F_{1,6}$ = 2.84, p = 0.029). (d) The circuit signal directionality was not affected by the movement. The shaded area represents HPC-to-PFC signal directionality and the line indicates zero PSI.

We next investigated the effects of the antipsychotic drugs on phase coherence and signal directionality within PFC-HPC circuits. Risperidone was able to restore circuit hypersynchronization at high frequencies HFOs that emerged after PCP ($F_{2,22}$ = 4.25, p = 0.027) but was unable to rescue phase coherence at lower frequencies and had no major effects on the aberrant PFC-to-HPC delta signals compared to the PCP+SAL group (Fig. 4.2.4.a and b). However, connectivity alterations elicited by PCP were partially corrected by clozapine. First, clozapine blocked PCP-induced enhanced phase coherence at fast delta ($F_{2.22}$ = 5.62, p = 0.039) and reduced the high gamma and HFOs hypersynchronization. However, increased theta coherence was not recovered and remained very low (Fig. 4.2.4.b).

Notably, clozapine prevented the emergence of PFC-to-HPC delta signals ($F_{1,16} = 5.2$, $p = 0.045$) and the flow of information within the circuit highly resembled that observed during baseline (Fig. 4.2.2.4c). Overall, clozapine was effective in rescuing abnormal circuit signal directionality after administration of PCP but had limited efficacy on recovering local hypersynchronization within PFC and HPC microcircuits. Furthermore, haloperidol did not correct augmented coherence at delta, high gamma and HFOs, which remained similar to saline controls (Fig. 4.2.4.a and d). Finally, the abnormal PFC-to-HPC delta drive was in fact exacerbated by haloperidol with respect to the control group ([PCP+SAL vs. PCP+HAL] $F_{1,9} = 8.42$, $p = 0.018$; Fig. 4.2.4.a and d). We note that the dose of haloperidol used was medium to high (Hashimoto et al., 2005; Horiguchi et al., 2012), thus the dose is not the main cause of its limited efficacy. We conclude that the main antipsychotic effects of haloperidol do not rely on PFC-HPC neural activities.

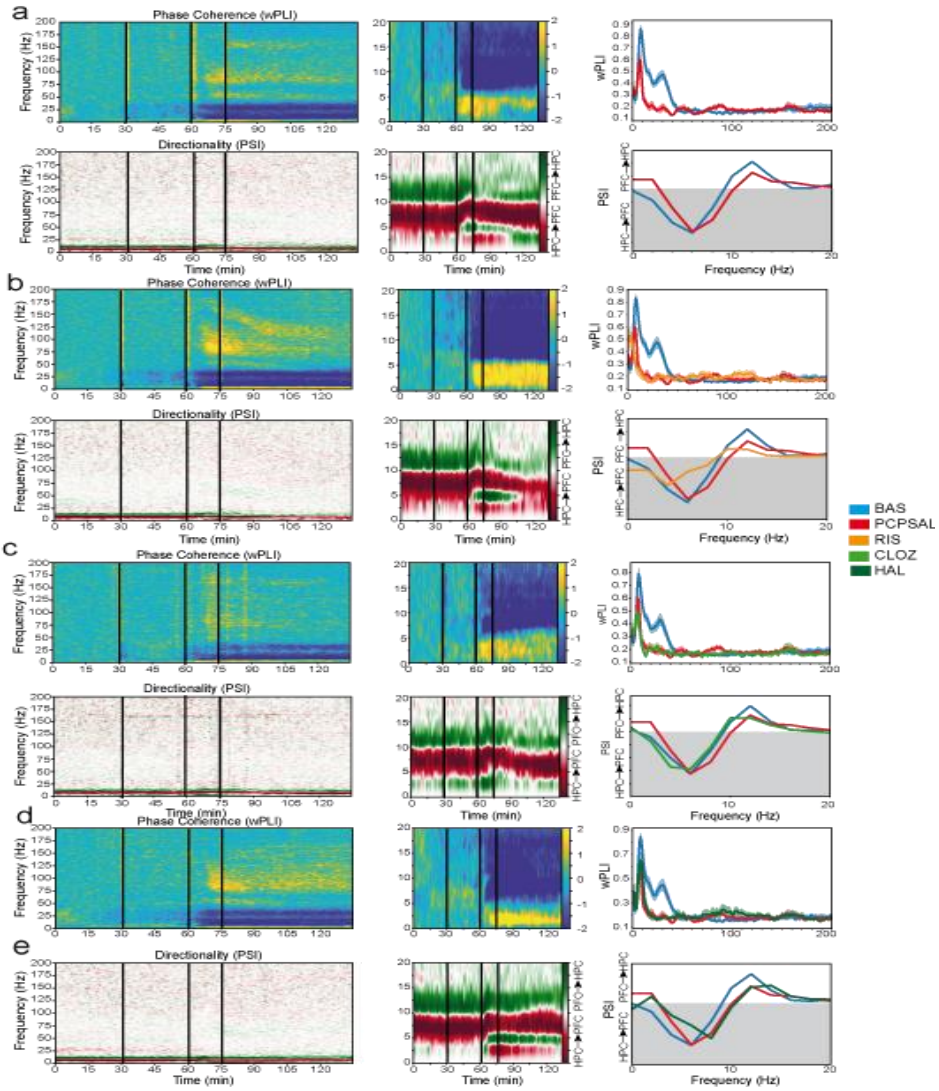

Figure 4.2.4: Comparison of antipsychotic effects on PFC-HPC connectivity after the acute PCP injections. All panels present a normalized (z-scores) time course of changes in wPLI (phase coherence) and corresponding quantification (top panels). The lower panels show the time course of changes in PSI (circuit signal directionality) and corresponding quantification. The shaded area represents HPC-to-PFC signal directionality, the line denoting zero PSI. The figure presents the different effects of

antipsychotics 15 minutes after the PCP injection. saline represented in red (a), risperidone represented in orange (b), clozapine represented in light green (c) and haloperidol represented in dark green (d).

Altogether, the two atypical antipsychotic drugs, risperidone and clozapine, but not the typical antipsychotic drug, haloperidol, partially reduced PCP-induced increased local PFC power, phase-amplitude coupling, circuit hypersynchronization and disrupted circuit communication. However, antipsychotic drugs were unable to restore the normal circuit dynamics, probably due to the sedative effects they produce. Figure 4.2.5 presents a schematic summary of the main effects of acute PCP on PFC-HPC neural circuits and the impact of risperidone, clozapine and haloperidol.

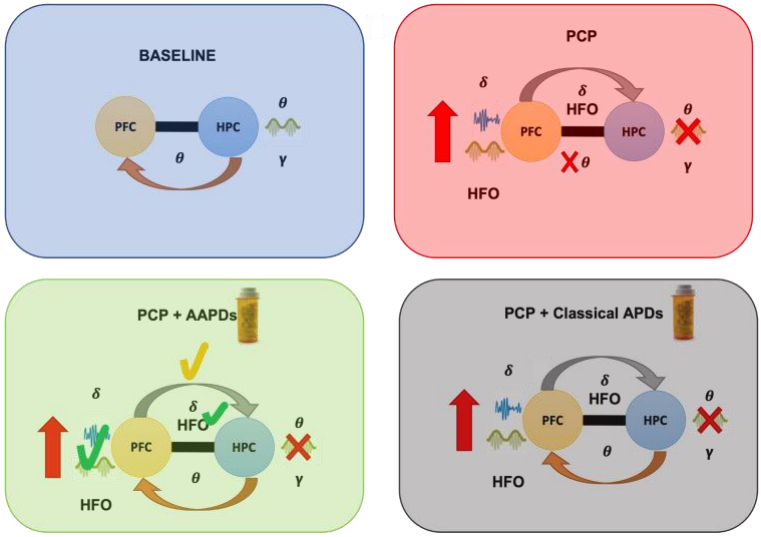

Figure 4.2.5: Summary of PFC-HPC circuit alterations induced by acute PCP and the effects of antipsychotic medication. Baseline state, shown in the top left panel in blue, is characterized by theta-gamma oscillations in the HPC and a HPC-to-PFC theta signal directionality. The effects of acute PCP in the circuit are shown in the top right panel in red. The effects of atypical antipsychotic drugs and typical antipsychotic drugs on the acute PCP-induced circuit are shown in the left and right bottom panels, respectively. Acronyms: AAPDs (atypical antipsychotic drugs), **δ** (delta), **θ** (theta), ***γ*** (gamma), HFO (high frequency oscillations), red cross or arrow (PCP-effect) green tick (risperidone recovery) and yellow tick (clozapine recovery).

4.3. Contribution of serotonin receptors 5-HT_{2A} and 5-HT_{1A} on phencyclidine-induced prefrontal-hippocampal circuit alterations

Risperidone and clozapine block 5-HT_{2A}Rs directly and stimulate 5-HT_{1A}Rs indirectly (P. Celada et al., 2013; Meltzer and Massey, 2011). We examined the abilities of a 5-HT_{2A}R antagonist and a 5-HT_{1A}R agonist to rescue PCP-induced effects to gain further insight into the serotonergic actions of the two atypical antipsychotic drugs. The selective 5-HT_{2A}R antagonist M100907 (1 mg/kg; n = 6 mice) produced strong sedative effects that caused the animals to be immobile ([Acc]: $F_{1,5}$ = 57.47, p <0.0005, one-way ANOVA; $F_{2,20}$= 10.2, p = 0.01, two-way ANOVA) and reduced PCP-generated bands in the PFC ([theta, alpha, high gamma, HFOs]: $F_{2,20}$ = 6.39, 5, 12.06, 9.98, p = 0.007, 0.017, 0.0003, 0.01; two-way ANOVA) (Fig. 4.3.1. a and b). Notably, narrow bands in the gamma and HFO domains remained in both structures, following similar temporal patterns than risperidone. Also concurrent with risperidone, M100907 shifted the power of fast delta and fast delta-HFO l-PAC and ir-PAC towards slower frequencies. Notably, the intrinsic theta-gamma coupling in the HPC shifted to delta-high gamma ([2-5 to 50-80 Hz]; $F_{2,18}$ = 9.17, 10.74, p = 0.009, 0.006; Fig. 4.3.1.c), a type of coupling that could be

caused by the large decrease in mobility after M100907 (Fig. 4.2.3.b). M100907 also normalized circuit phase hypersynchronization at gamma and HFOs ($F_{2,18}$ = 10.34 6, p = 0.0010, 0.036; Fig. 4.3.1.d), however the reduction of theta coherence was further exacerbated ($F_{1,9}$ = 17.8, p = 0.002). Moreover, M100907 shifted fast delta to slow delta phase synchronization, closely following the changes observed in delta power in the PFC. Finally, the intrinsic HPC-to-PFC theta signal directionality was not restored and the PFC-to-HPC fast delta band not prevented by M100907 (Fig. 4.3.1.e).

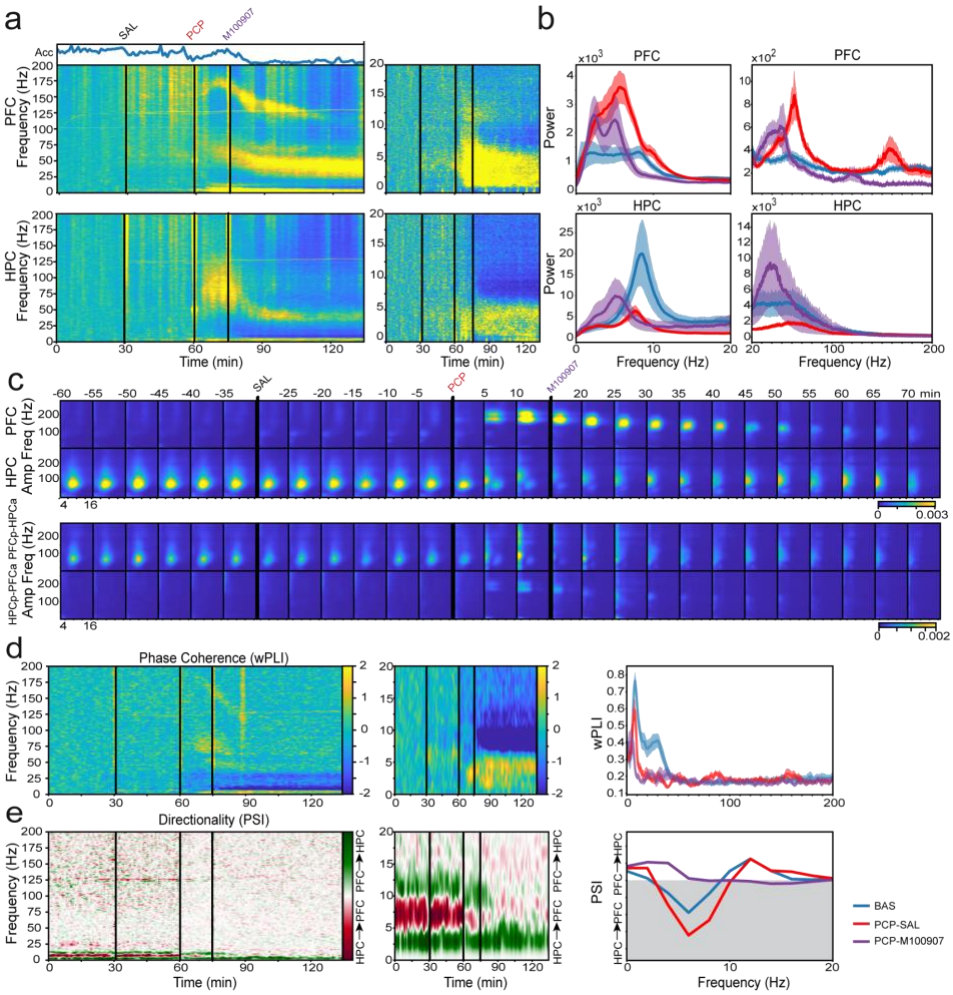

Figure 4.3.1: M100907 (5-HT2AR antagonist; 1 mg/kg, IP; n = 6 mice) reduced many PCP-induced alterations of PFC-HPC neural dynamics but not the circuit connectivity. (a) Normalized spectrograms (z-scores) of signals in the PFC (upper panels) and HPC (lower panels). The corresponding quantification of the animals' mobility (Acc) is also shown. The Acc results are presented as a ratio to the highest value in the baseline condition. (b) The power spectra of PFC and HPC signals during 10 min of baseline are represented in blue and signals from min 35 to 45 after M100907 (50-60 min after PCP) are illustrated in purple. Power spectra of signals recorded from min 35 to 45 after saline

administration (50-60 min after PCP) are shown in red for comparison. (c) Comodulation maps quantifying local and inter-regional cross-frequency coupling in consecutive non-overlapping 5-min epochs. The numbers on top of the panels indicate time after PCP administration. (d) Normalized (z-scores) time course of changes in wPLI (phase coherence) and corresponding quantification. (e) Normalized (z-scores) time course of changes in PSI (circuit signal directionality) and corresponding quantification. As above, the shaded area represents HPC-to-PFC signal directionality, the line denoting zero PSI.

Lastly, we investigated the effects of the selective 5-HT_{1A}R agonist DPAT (1 mg/kg; n = 6 mice). Mice mobility was reduced less by DPAT than by M100907 ($F_{1,5}$ = 4.38, p = 0.021, one-way ANOVA; $F_{2,26}$ = 0.83, p = 0.44, two-way ANOVA; [PCP+DPAT vs PCP+M100907] $F_{2,20}$ = 5.66, p = 0.011, two-way ANOVA), suggesting less sedative effects. DPAT rescued aberrant power in both brain regions, although it had less influence on PFC neural activities than M100907 (Fig. 4.3.2.a and 4.3.1.a). More specifically, DPAT decreased the power of high gamma and HFOs in the PFC ($F_{2,26}$ = 7.79, p = 0.002). In addition, there was a partial transition from fast to slow delta power. DPAT rescued increased fast delta-HFO coupling ([l-PAC, ir-PAC]:$F_{2,26}$ = 2.68, 4.57, p = 0.087, 0.002) but baseline theta-gamma coupling was not restored (Fig.4.3.2.c). Finally, 5-HT_{1A}R

agonism had little effect on phase coherence and circuit signal directionality (Fig 4.3.2.d).

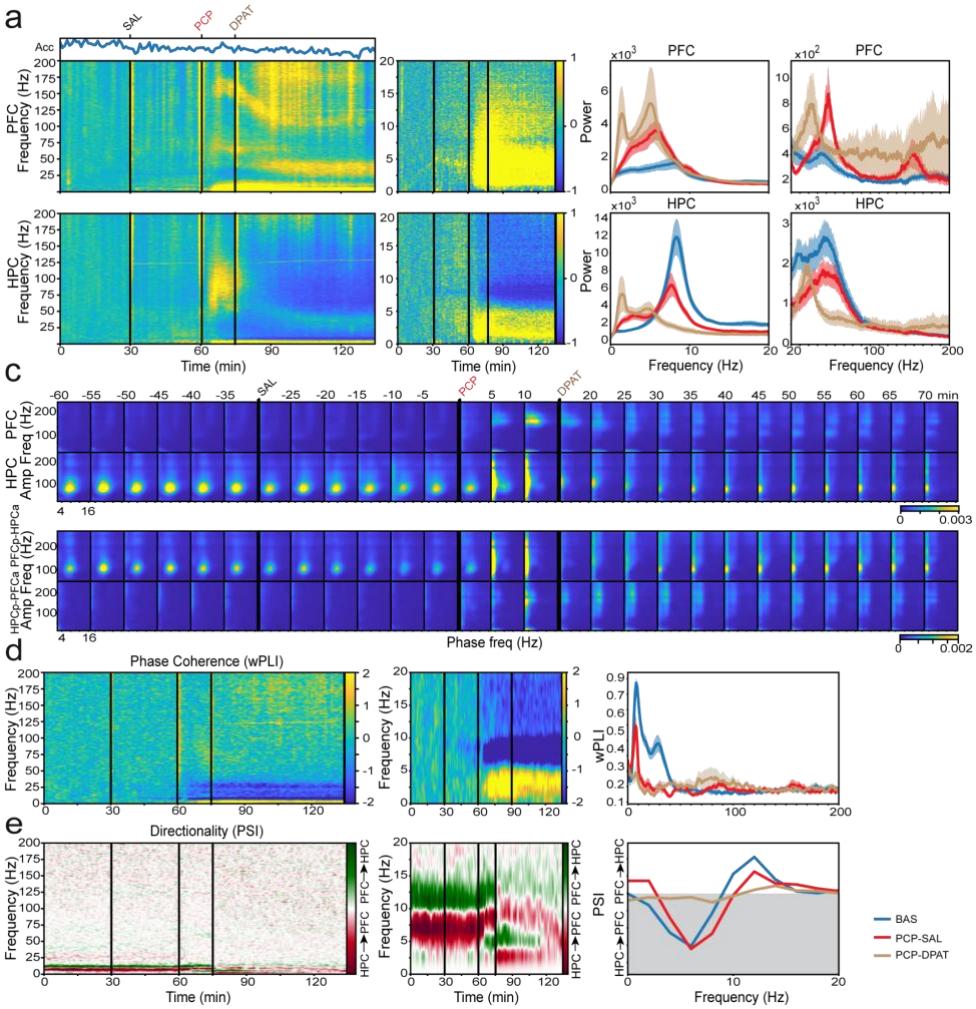

Figure 4.3.2: 8-OH-DPAT (DPAT, 5-HT$_{1A}$R agonist; 1 mg/kg, IP; n = 6 mice) reverses some PCP-induced alterations of PFC-HPC neural dynamics but not the circuit connectivity. (a). Normalized spectrograms (z-scores) of signals in the PFC (upper panels) and HPC (lower panels). The corresponding quantification of the animals' mobility (Acc) is also shown. The Acc results are presented as a ratio to the highest value

in the baseline condition. (b) The power spectra of PFC and HPC signals during 10 min of baseline are represented in blue and signals from min 35 to 45 DPAT administration (50-60 min after PCP) are illustrated in tan, respectively. Consistent with the figure above, an additional group with power spectra of signals recorded 50-60 minutes after the administration of PCPSAL are shown in red for comparison. (c) Comodulation maps quantifying local and inter-regional cross-frequency coupling in consecutive non-overlapping 5-min epochs. The numbers on top of the panels indicate time after PCP administration. (d) Normalized (z-scores) time course of changes in wPLI (phase coherence) and corresponding quantification. (e) Normalized (z-scores) time course of changes in PSI (circuit signal directionality) and corresponding quantification. The shaded area represents HPC-to-PFC signal directionality, the line denoting zero PSI.

5. CHAPTER II. NEURAL SUBSTRATES OF THE SUBCHRONIC PHENCYCLIDINE MOUSE MODEL OF SCHIZOPHRENIA

5. CHAPTER II. NEURAL SUBSTRATES OF THE SUBCHRONIC PHENCYCLIDINE MOUSE MODEL OF SCHIZOPHRENIA

In this chapter we explore the alterations induced by sPCP in PFC-HPC neural networks to unravel the neural correlates of memory impairment. We recorded neural activity from the mPFC and HPC of mice during distinct brain states: quiet wakefulness, memory acquisition, working memory and long-term memory. In addition, we evaluated three auditory tasks: auditory evoked potentials, ASSR and the oddball paradigm. The animals' behavior and neural activity were fully characterized before (baseline condition) and after the sPCP or saline treatments (sPCP or SAL, respectively).

5.1. Prefrontal-hippocampal circuit alterations during quiet wakefulness

We first investigated the alterations produced by sPCP (10 day treatment) on PFC-HPC neural dynamics during baseline conditions. To note, sPCP treatment can induce hyperlocomotion (Castañé et al., 2015; Mouri et al., 2012). To control for any confound related to differences in locomotion between baseline and sPCP, we selected 3 second epochs with low

accelerometer rates during the open field exploration task, which we define as quiet wakefulness (see Methods).

During quiet wakefulness, sPCP mice showed an increased-decreased pattern of high gamma oscillations in the PFC and the HPC, respectively (n = 21 mice; [baseline vs sPCP: increased PFC high gamma, decreased HPC high gamma], p = 0.047, 0.004, paired T test) that was not observed in the saline controls (n = 7 mice; [baseline vs saline: PFC high gamma, HPC high gamma]; p = 0.11, 0.53, respectively). Furthermore, low gamma oscillations in the HPC were also reduced (p = 0.016, not significant in the controls: p = 0.56), indicating a reduction of the whole gamma range in the HPC (Fig. 5.1.1).

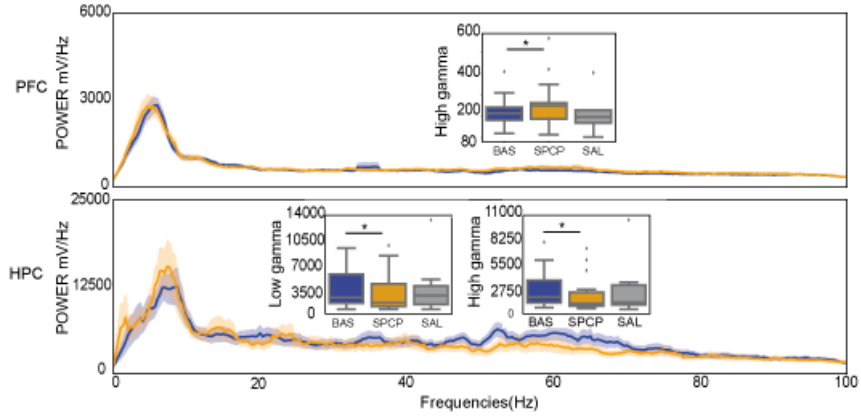

Figure 5.1.1: Mean oscillatory power in the PFC and the HPC of baseline (blue) and sPCP-treated (orange) mice. The insets represent quantifications of low gamma (HPC) and high gamma (PFC and HPC) power. Baseline is represented in blue, sPCP-treated animals in orange and saline treated in grey. Significant differences are found in low gamma (HPC) and high gamma (PFC and HPC) power between baseline mice and sPCP mice.

To further assess the effects of sPCP on the circuit we compared the l-PAC and the ir-PAC during baseline and sPCP conditions. As previously mentioned, intrinsic theta-gamma coupling was present in CA1 and also within the circuit (PFC_{phase}-HPC_{amp}) during baseline conditions. sPCP markedly decreased local and inter-regional theta-gamma coupling ([lPAC HPC, ir-PAC PFC_{phase}-HPC_{amp}]: $p = 0.008, 0.001$; baseline not significantly different than the saline controls; $p = 0.22, 0.22$) (Fig. 5.1.2).

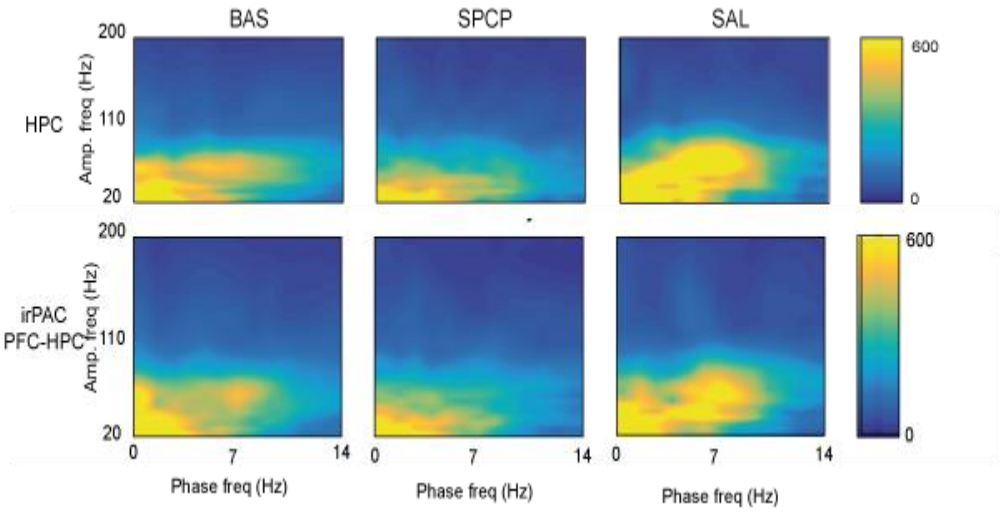

Figure 5.1.2: Local Hippocampus and interregional PFC (phase) - HPC (amplitude) phase-amplitude comodulograms in baseline, sPCP-treated and saline treated conditions during quiet wakefulness. Theta-gamma (phase: 6-10, amplitude: 40-60 Hz) reduction on sPCP-treated (middle panels) compared to baseline (left panels) and saline treated (right panels) on local HPC PAC (upper panels) and interregional PFC_{phase}-HPC_{amp} (lower panels).

Next, we investigated the relevance of HPC gamma oscillations in the local and circuit theta-gamma modulation. HPC high gamma power correlated positively with theta-gamma coupling both in the HPC and at the circuit level during the baseline (correlations: [lPAC HPC: High-gamma HPC-theta-gamma coupling, ir-PAC PFC_{phase}-HPC_{amp} High-gamma HPC- theta-gamma coupling]; R = 0.73, 0.69, $p < 0.0005$, 0.0005) and in sPCP mice (R = 0.81, 0.76, $p < 0.0005$), suggesting that sPCP-induced reductions of

HPC high gamma power and theta-gamma coupling were associated and likely caused by the same neural mechanism (Fig. 5.1.3).

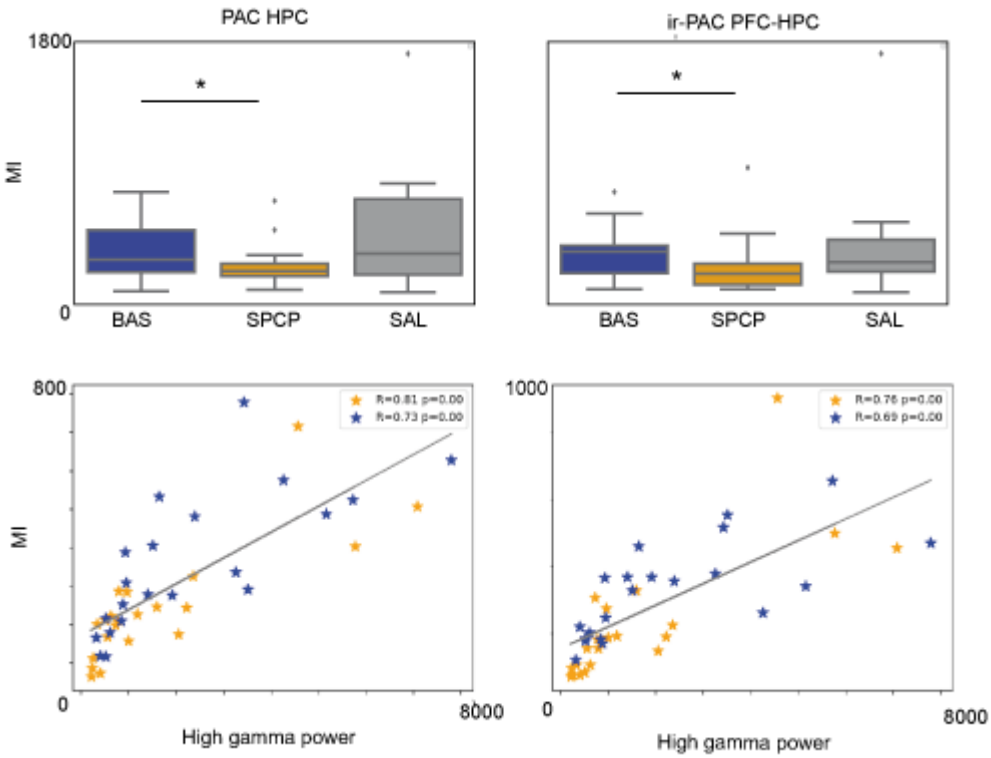

Figure 5.1.3: Correlations between hippocampal high gamma power and the modulation index (MI) of l-PAC and ir-PAC. The upper panels show quantifications of the modulation index locally in the HPC (left) and inter-regional PFC_{phase}-HPC_{amp} (right). Baseline is shown in blue, sPCP is shown in orange and saline is shown in grey. Correlations between the modulation index and the HPC high gamma activity. The grey line represents linear regression of data from baseline (blue dots) and sPCP (orange dots) from the l-PAC (left) and ir-PAC (right).

We next investigated the circuit neural dynamics using the wPLI and PSI measures comparing baseline and sPCP conditions. As shown in Fig 5.1.4, no major significant changes were found between baseline and sPCP conditions, only a slight decrease of slow theta phase synchronization ($p = 0.082$), confirmed by surrogate controls).

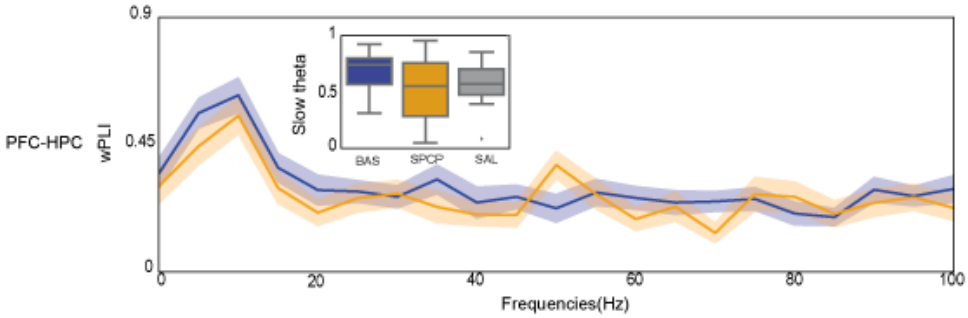

Figure 5.1.4: Phase synchronization of PFC-HPC circuits during baseline and sPCP conditions in quiet wakefulness. Mean weighted phase-lag index (wPLI) between PFC and the HPC of baseline (blue) and sPCP-treated (orange) mice. The inset shows the quantification of slow theta wPLI in which saline is represented in grey.

5.2 Prefrontal-hippocampal circuit alterations during memory acquisition and retrieval in subchronic phencyclidine mice

We subsequently investigated the memory abilities using the NOR task, which is a well validated test for assessing object recognition memory in rodents. This task has been proposed as a valid animal model of human declarative memory, which is frequently impaired in schizophrenia patients (Winters et al., 2010; Young et al., 2009). The NOR task is a non-operant, non-rewarded test based on the rodents' natural preference to explore more novel objects than familiar objects. Memory acquisition and retrieval processes involved in the NOR task depend on the activity of the PFC and the HPC (Warburton and Brown, 2015). Importantly, working memory and long-term memory performance are impaired after treatment with sPCP and recovered by atypical antipsychotic drugs (Castañé et al., 2015; Meltzer and Massey, 2011).

The protocol consisted of four phases of 10 minutes each: 1) habituation to the maze without objects, 2) familiarization to two identical objects placed at the end of the two arms, 3) test 3 minutes after the familiarization phase to assess working memory and 4) test 24 hours after the

familiarization phase to assess long-term memory. In both tests, one of the familiar objects, randomly selected, was replaced by a novel object, and different objects were used in each test. We used a custom designed T-maze adapted for electrophysiological recordings (see Methods). We used the T-maze design to reduce the anxiety generated by the animals' exposure in an open field arena (Cruz et al., 2020). The alignment of the object explorations with the electrophysiological recordings was implemented online using a custom built joystick in which we pressed the right or the left button for the duration of object explorations. This system helped us automatize and align neural activity and behavior. At an analytical level, we discarded object explorations offline with an automated electrophysiological artifact rejection script that was based on two criteria: large voltage of local field potentials and abnormal power spectra of the signals (see in Methods) (Fig 3.3.3.1). All of these procedures allowed us to have precise and clean electrophysiological data that was aligned with the behavior. Finally, animals that explored both objects less than 10 seconds or each object less than 3 seconds were discarded for the analyses.

5.2.1. Working memory and long-term memory impairment in the subchronic phencyclidine mouse model

The index used to quantify recognition memory is the discrimination index (DI), a meaure that compares the time exploring the novel object with respect to the familiar object and divides it with the total time of exploration (DI = (time exploring the novel object - time exploring the familiar object) / total exploration time). A good DI is typically positive and above 0.2, that is, at least 20% more time exploring the novel object than the familiar object.

Consistent with standard results in the field, during the working memory test in baseline conditions mice explored more the novel object than the familiar object (n = 7 mice; mean DI = 0.35 +- 0.05). By contrast, sPCP-treated mice explored novel and familiar objects for similar amounts of time in the same test (n = 7 mice; mean DIs = 0.01 +- 0.06), and this was not observed in the saline controls (n = 4 mice; mean DIs = 0.52 +- 0.11) (Fig. 5.2.1.1). These results indicated impaired working memory in sPCP-treated mice, which showed smaller DIs than during baseline and saline controls ([DI: baseline vs. SPCP, baseline vs. saline], $p < 0.0005$, 0.1, paired T test). We next aimed to gain deeper insight into the causes of the

reduced DIs observed after the sPCP treatment by analysing the total time of the visits to the objects, the number of visits and the mean time of individual visits to each object. sPCP-treated mice explored familiar objects for longer periods of time than baseline mice ([time exploring the familiar object:]: $p > 0.005$) which produced a slight increase in total exploration time ([total time of exploration baseline vs sPCP]: $p = 0.045$), while this phenomenon was not observed in the saline controls ([time exploring the familiar object]: $p = 0.14$). During baseline and saline conditions, the mice visited more times the novel object than the familiar object ([number of visits familiar vs novel object: baseline, saline]: $p = 0.019, < 0.005$) and explored it for longer periods of time in each visit ([mean duration of individual exploration familiar vs novel objects: baseline, saline]: $p < 0.005, 0.1$). However, sPCP-treated mice visited both objects similar number of times, increasing the number of total visits, ([number of explorations baseline vs sPCP: familiar, total]: $p = 0.011, 0.016$) despite they still explored longer periods of time the novel object than the familiar object ([mean duration of individual visits familiar vs novel in sPCP-treated mice]: $p = 0.005$).

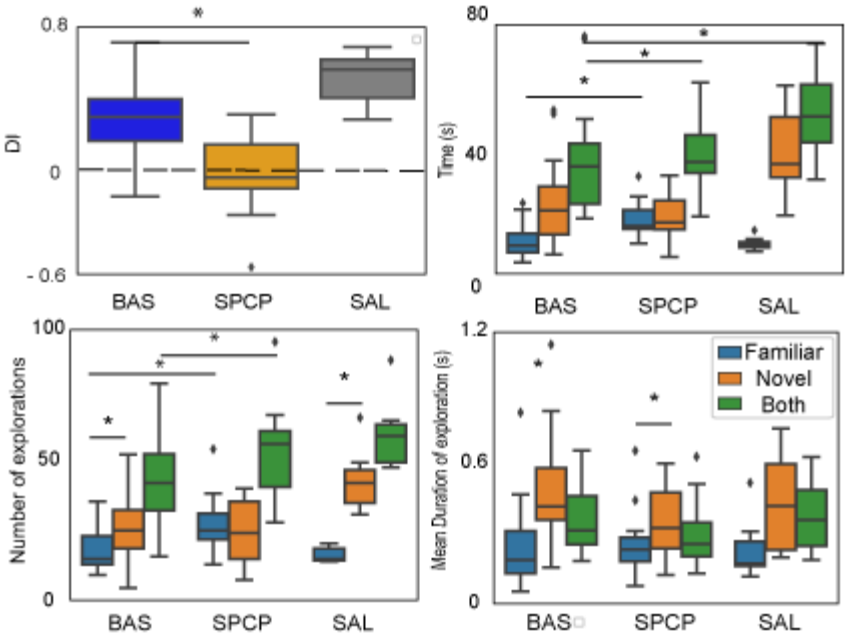

Figure 5.2.1.1: Working memory performance during baseline, sPCP and saline controls. Discriminations indexes (DIs) (top left panel) during baseline (blue), sPCP (orange) and saline (grey); total duration of object explorations (top right panel), number of explorations (lower left panel) and mean duration of individual explorations (lower right panel) of familiar objects (blue), novel objects (red) and the combination of both (green).

To further characterize the animals' behavior in this task, we analysed the mean duration of each visit across time (Fig 5.2.1.2). Overall, the average time of each visit decreased over time as the mice became less interested in the objects, ($F_{2,26}$ = 3.52, p = 0.005; repeated measures ANOVA with time as factor), and this occurred both during baseline and after the sPCP

treatment. During baseline, mice explored the novel object longer periods of time than the familiar object and this pattern was more evident on the first 5 visits ($F_{2,26}$ = 36.03, p < 0.0005; repeated measures ANOVA with time as the within factor and novel and familiar objects as the between factor). These differences were also observed after the sPCP treatment due to the first visit with the novel object ($F_{2,26}$ = 10.4, p = 0.003). However, the patterns of familiar object explorations were different between baseline and sPCP-treated conditions ($F_{1,13}$ = 15.12, p = 0.002; repeated measures two-way ANOVA with time as the within factor and baseline and sPCP groups as the between factor during the visits to the familiar object), sin which PCP-treated mice explored longer periods of time the familiar object.

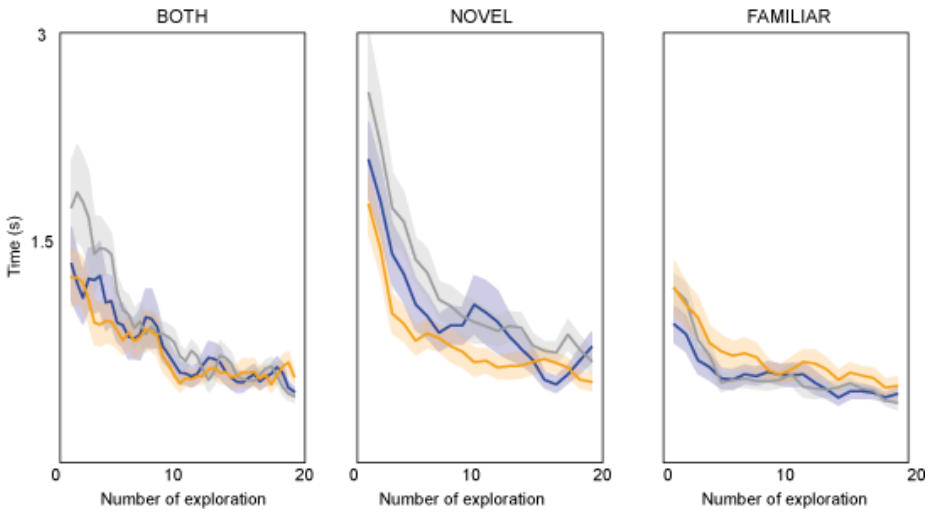

Figure 5.2.1.2: Mean duration of individual visits to novel and familiar objects over

time during the working memory test. The first 20 explorations are shown for both objects combined (left), the novel object (middle) and the familiar object (left). Data from baseline is shown in blue, data from sPCP-treated is shown in orange and data from saline controls is shown in grey.

Poor memory performance was also detected in sPCP-treated mice (n = 8 mice, DI = -0.06 +- 0.06) during the long-term memory test compared to the baseline assessment (n = 8 mice, DI = 0.29 +- 0.04) and the saline controls (n = 4 mice, DI = 0.31 +- 0.07) ([baseline vs sPCP, baseline vs the saline group]: $p < 0.0005$, 0.152, paired T test) (Fig. 5.2.1.3). Similar to the working memory test, mice visited more frequently and for longer periods of time the novel objects than the familiar objects during baseline conditions ([familiar vs novel: number of explorations, mean time of exploration]: $p = 0.003$, 0.023). But again, these behaviors were disrupted by sPCP. First, we again observed an increased number of visits to the familiar objects with respect to baseline ($p = 0.016$). During the 24 hour test, there was also a steady decrease in the duration of individual visits over time during baseline and sPCP conditions ($F_{2,26} = 3.53$, $p = 0.006$), again likely due to the loss of interest in the objects (Fig. 5.2.1.4). Baseline mice explored the novel object for longer periods of time each visit and again this pattern was more evident during the first 5 visits ($F_{2,32} = 11.57$,

p = 0.002). However, sPCP-treated mice explored similar periods of time the novel and familiar objects during each visit ([novel vs familiar time of exploration in sPCP-treated, time of familiar explorations baseline vs sPCP]; $F_{2,32}$ = 4.41, 5.2 p = 0.045, 0.037).

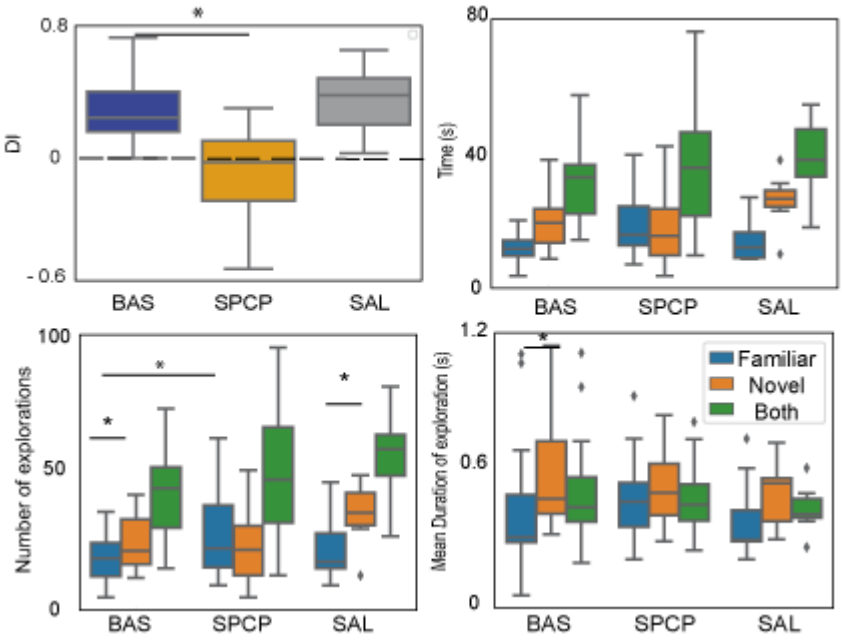

Figure 5.2.1.3: Long-term memory performance during baseline, sPCP and saline controls. Discriminations indexes (DIs) (top left panel) during baseline (blue), sPCP (orange) and saline (grey); total duration of object explorations (top right panel), number of explorations (lower left panel) and mean duration of individual explorations (lower right panel) of familiar objects (blue), novel objects (red) and the combination of both (green).

Overall, similar behavioral observations were obtained during working memory and long-term memory tests. During baseline, the mice explored more frequently and for longer periods the novel object than the familiar object, particularly during the first interactions. Following the sPCP treatment, there was an increase in the number of visits to the familiar objects, thus sPCP mice explored familiar and novel objects equally, indicating poor recognition memory for the familiar object.

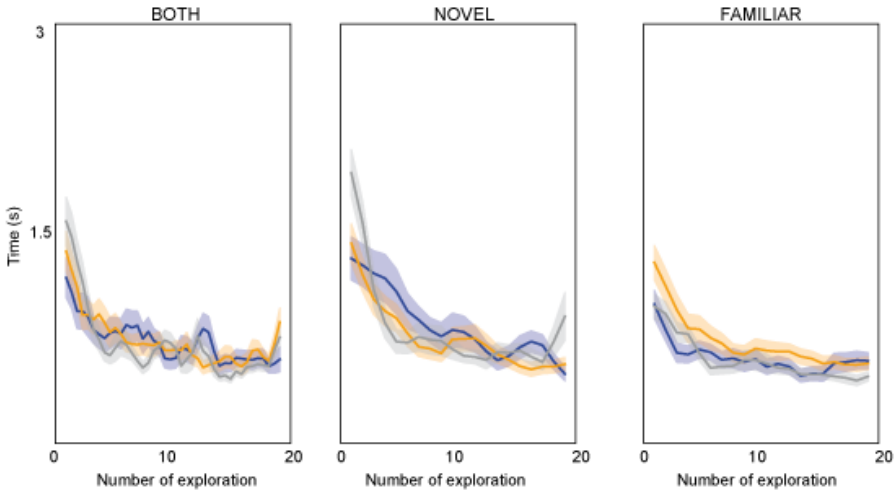

Figure 5.2.1.4: Mean duration of individual visits to novel and familiar objects over time during the long-term memory test. The first 20 explorations are shown for both objects combined (left), the novel object (middle) and the familiar object (left). Data from baseline is shown in blue, data from sPCP-treated is shown in orange and data from saline controls is shown in grey.

5.2.2. Neural substrates of memory acquisition, working memory and long-term memory retrieval in healthy mice

First, we assessed the PFC-HPC neural substrates of memory acquisition, working memory and long-term memory in C57/BL6 mice during the baseline conditions. We analyzed individual explorations in one-second non-overlaping windows in which only windows longer than 600 ms seconds were included (see Methods). Memory acquisition was investigated during the familiarization phase. As mentioned above, working memory and long-term memory were investigated in the 3 minutes and 24 hour test following the familiarization phase, respectively. The analyses were carried out comparing the first 5 seconds of familiar object explorations (memory retrieval) with the first 5 seconds of novel object explorations (novelty/memory acquisition).

5.2.2.1. Memory acquisition

To understand the neural substrates of memory acquisition, we compared the neurophysiological signals within PFC-HPC circuits during the first five seconds of exploration, the initial interactions with the new objects, with the last 5 seconds of exploration, when the animals had already acquired the memory about the object (i.e., first 5 vs last 5 one-second

windows) (Fig. 5.2.2.1.1). Five seconds were chosen for each group because 10 seconds of interaction were the minimum criterion to consider a successful familiarization (see Methods). Selecting 5 seconds also allowed a direct comparison of neural signals with the 5-second explorations of familiar and novel objects during the working and long-term memory tests. Interestingly, theta power presented a different pattern between both areas during memory acquisition: it increased in the PFC and decreased in the HPC (baseline: n = 9 mice; [early vs late explorations: PFC theta power increase, HPC theta power decrease]; p = 0.012, 0.024, paired T test). Moreover, the ir-PAC HPC_{phase}-PFC_{amp} at delta-low gamma was reduced over time (p = 0.032). We also noticed that phase synchronization (wPLI) of theta oscillations was enhanced during the early explorations compared with the late ones (p = 0.029). Finally, we also observed changes in the signal directionality between the early and the late explorations in different frequency bands: slow theta, theta and high gamma. First, early explorations presented a PFC-to-HPC slow theta and theta signal directionality that were shifted to HPC-to-PFC during the late explorations ([slow theta, theta]: p = 0.004, 0.066). The signal directionality was the opposite in the case of high gamma that showed a

partial HPC-to-PFC in the early explorations that shifted to PFC-to-HPC in the late explorations.

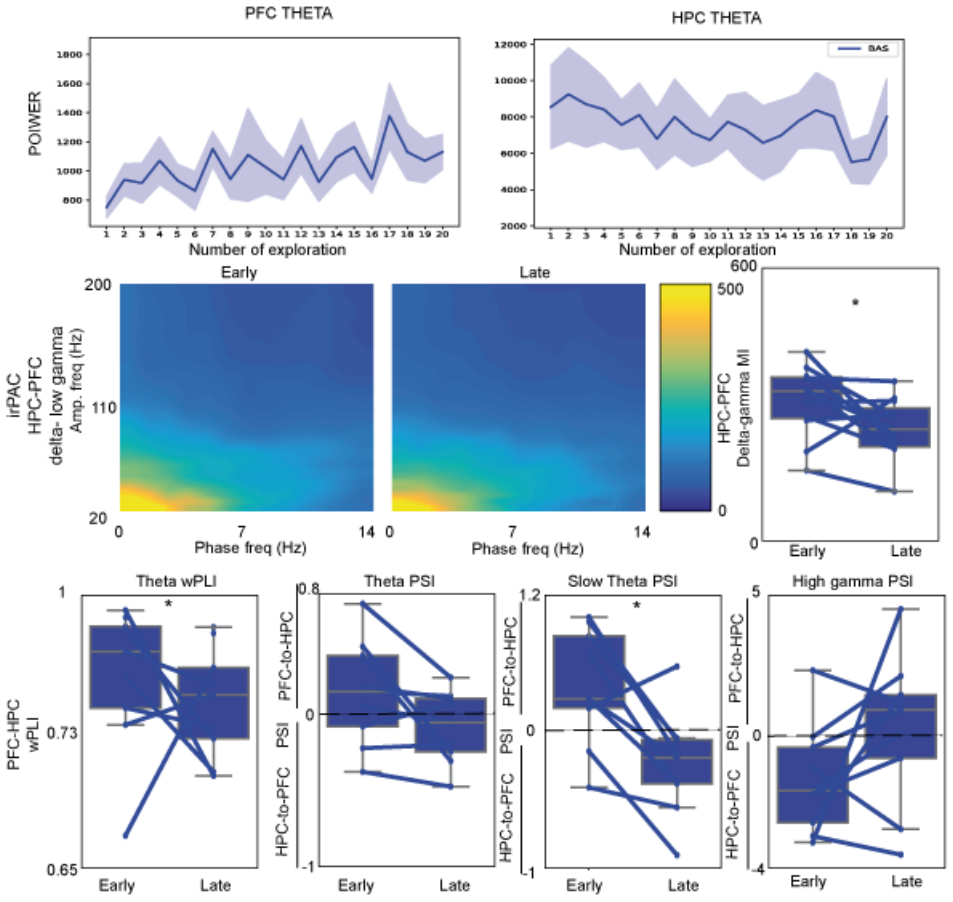

Figure 5.2.2.1.1: Neural substrates of memory acquisition within PFC-HPC circuits during baseline. The upper panels show the increase in PFC theta power (left) and decrease in HPC theta power (right) over the number of explorations. The middle panels present the HPC_{phase}-PFC_{amp} ir-PAC of delta- low gamma (phase:2-5 Hz, amplitude: 20-40 Hz). The lower panels present the changes between early and late interactions of theta wPLI (left), theta PSI (middle left), slow theta PSI (middle right) and high gamma PSI

(right). The dashed line represents the 0 or change of the signal directionality. Positive numbers present PFC-to-HPC signal directionality and negative numbers present HPC-to-PFC signal directionality. Each line corresponds to one mouse.

5.2.2.2. Working memory

To investigate the neural substrates of working memory, we compared the differential neurophysiological signals between the first 5 seconds of exploration of the novel and the familiar objects during the 3 minute test. We analysed the first 5 seconds of exploration to be able to compare the same time between both objects and those of memory acquisition. Furthermore, the duration of the visits was significantly reduced after the first 5 explorations (Fig. 5.2.2.2.1). To have a better understanding of the neural substrates, only animals with a DI over 0.2 were chosen for the analyses (n = 7 mice). The most relevant differences between novel and familiar explorations during the working memory test were found analysing the directionality of the flow of information at slow theta and high gamma ranges (Fig. 5.2.2.2.1). Similar to the late interactions during memory acquisition, we observed a flow of information from the HPC to the PFC at slow theta and from the PFC to the HPC at high gamma during the visits to the familiar objects that tended to flow in the opposite direction

during the visits to the novel objects ([slow theta, high gamma]; p = 0.041, 0,014).

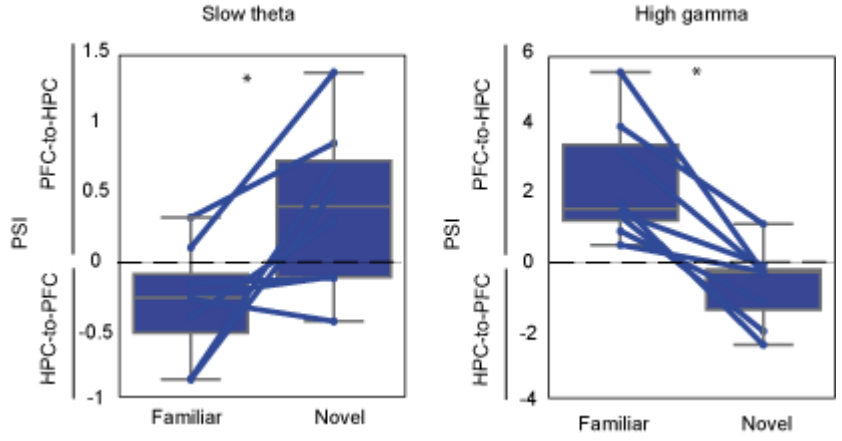

Figure 5.2.2.2.1: Neural substrates of working memory within PFC-HPC circuits during baseline. Shown are changes in flow of information within the circuit during familiar and novel explorations at slow theta (left) and high gamma (right) frequencies. The dashed line represents no change of signal directionality. Positive numbers depict PFC-to-HPC signals whereas negative numbers depict HPC-to-PFC signals. Each line corresponds to one mouse.

5.2.2.3. Long-term memory retrieval

To understand the PFC-HPC neural implications in long-term memory retrieval, we analyzed the 24-hour memory test using the same methods of analysis as performed for the working memory task. That is, we compared the neural signals during the 5 first seconds of the visits to the familiar and the novel objects (Fig. 5.2.2.3.1). First, we observed that HPC theta-

gamma coupling tended to augment during the visits to the familiar objects compared to the novel objects (n = 8 mice, p = 0.075). We also observed a partial reduction of phase synchronization at low gamma and an increase at HFO during the familiar explorations ([low gamma wPLI, HFO wPLI]: p = 0.067, 0.014). Moreover, relevant neural activities were identified during the visits to the objects that corresponded to the ones observed during memory acquisition. More specifically, the HPC-to-PFC theta signals observed during the visits to the familiar objects resembled those observed 24 hours prior during the last explorations of the familiarization phase. Conversely, novel explorations were associated with PFC-to-HPC theta signals, which resembled those observed during early explorations of the familiarization phase ([theta PSI]: p = 0.0007). Overall, these results unraveled a contribution of theta signals within PFC-HPC circuits for memory retrieval and object recognition processes.

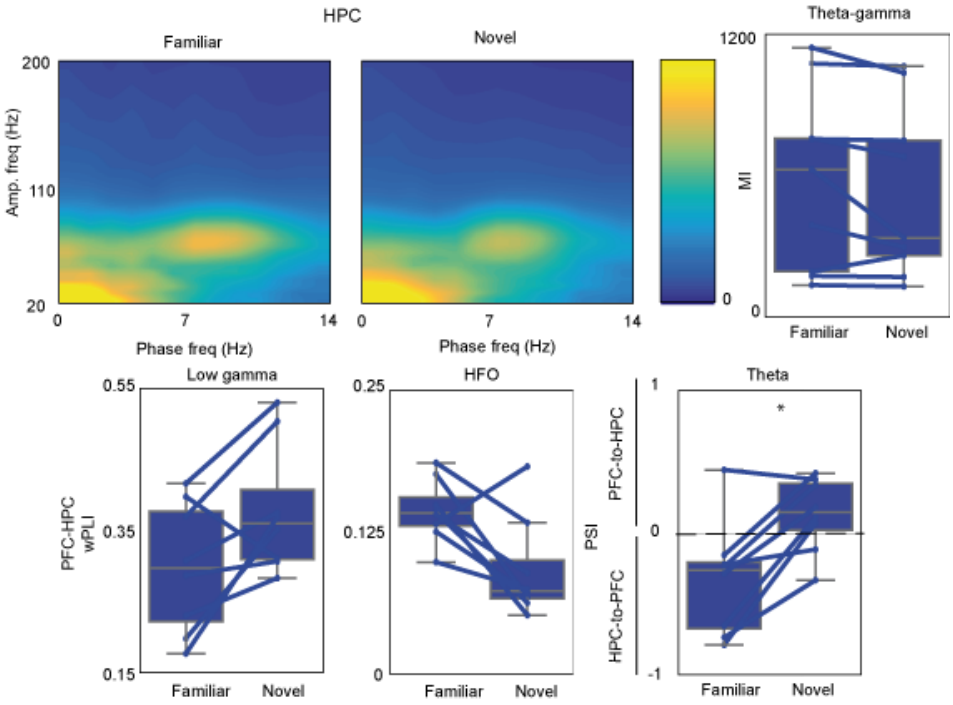

Figure 5.2.2.3.1: Neural substrates of long-term memory within PFC-HPC circuits during baseline. The upper panels depict HPC l-PAC where clear theta-gamma coupling can be observed (phase: 7-10 Hz, amplitude: 60-80 Hz) during the visits to familiar and novel objects. The lower panels show changes in phase synchronization (left and middle) and signal directionality (right) between familiar and novel object interactions. Dashed lines represent no change in signal directionality. Each line corresponds to one mouse.

5.2.3. Abnormal neural activities during memory acquisition, working memory and long-term memory in sPCP-treated mice

We next investigated neural activities within PFC-HPC circuits during the NOR task after the subchronic treatment with PCP (Fig. 5.2.3.1). Most of the neurophysiological biomarkers of normal memory acquisition, working memory and long-term memory retrieval were disrupted by sPCP. Similar to quiet wakefulness, in the HPC high gamma power was reduced by sPCP in all behavioral tests ([familiarization, working memory, long-term memory]; $F_{1,12}$ = 9.59, 8.37, 15.33, p = 0.011, 0.023, 0.006, repeated measures ANOVA with time (early vs late) or object (familiar vs novel) as within factors and animal group (baseline vs sPCP) as between factor; significant differences with saline controls: $F_{1,20}$ = 3.55, 6.44, 5.28, p = 0.075, 0.022, 0.021, mixed two-way ANOVA with time and object as factors). Consistently, both local ([$F_{1,12}$ = 37.68, 10.36, 15.96, p < 0.0005, 0.009, 0.003; significant differences with the saline controls: $F_{1,22}$ = 6.31, 19.13, 6.31, p = 0.02, < 0.0005, 0.02) and inter-regional theta-gamma coupling ($F_{1,12}$ = 41.09, 16.38, 33.19, p < 0.0005, 0.002, < 0.0005; significant differences with the saline controls: $F_{1,22}$ = 4.62, 17.5, 5.97, p = 0.024, < 0.0005, 0.02) were reduced in all the memory tests. Importantly,

these abnormal neural activities were not observed in the controls where saline was administered instead of PCP (Figure 5.2.3.1).

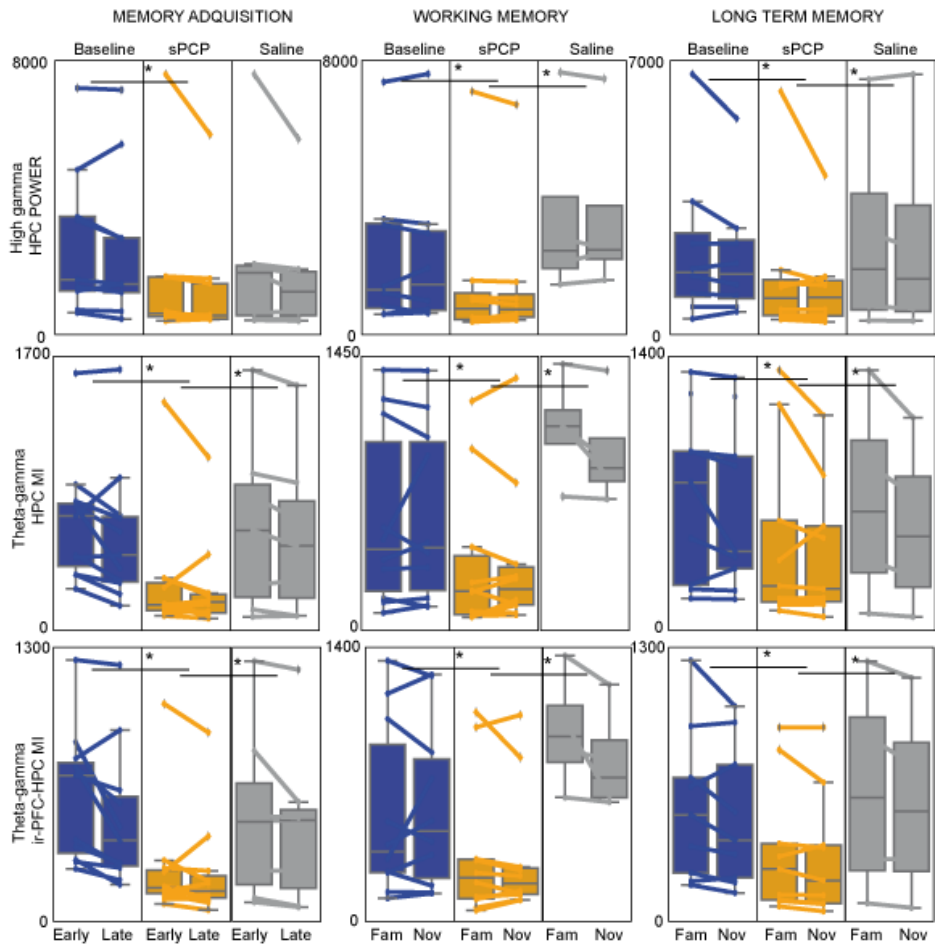

Figure 5.2.3.1: sPCP-induced PFC-HPC circuit deficits during memory acquisition, working memory and long-term memory. Baseline biomarkers are depicted in blue, sPCP-biomarkers in orange and saline controls in grey. Each line corresponds to one mouse.

In the PFC, we observed a non-specific increase of theta power during memory acquisition in the familiarization phase ($F_{1,10}$ = 7.46, p = 0.021), which interfered with the progressive increase in theta power observed during normal memory acquisition (n = 9 mice for the baseline and sPCP groups, n = 7 mice for the saline group) (Fig. 5.2.3.2). Similarly, HPC theta power followed the same decrease found in memory acquisition during baseline ([time]: $F_{1,10}$ = 4.81 p = 0.053). Moreover, HPC_{phase}-PFC_{amp} delta-gamma ir-PAC was increased in sPCP-treated mice, although the early-to-late decreases previously observed during baseline were still present ([time, condition]: $F_{1,10}$ = 7.72, 5.6, p = 0.017, 0.036). Furthermore, sPCP-treated mice did conserve the early-to-late reduction in theta coherence found in baseline conditions ([condition, time]: $F_{1,10}$ = 11.25, 11,71, p = 0.007, 0.007). Lastly, the baseline shifts in the signal directionality, that is PFC-to-HPC in the early explorations and HPC-to-PFC in the late explorations at slow theta and theta frequencies, were partially disrupted by sPCP ([condition: slow theta, theta]: $F_{1,10}$ = 3.28, 3.56, p = 0.095, 0.089). The disruption was most notable in PFC-to-HPC signals during early explorations ([slow theta PSI, theta PSI]: p = 0.062, 0.068), where the parameters became close to zero, indicating no flow of information between brain regions. In addition, the early-to-late HPC-to-PFC and PFC-

to-HPC high gamma signals were partially shifted ([time*condition]: $F_{1,10}$ = 3.6, p = 0.087), particularly during the early explorations HPC-to-PFC signals were strengthened compared to baseline (p = 0.013).

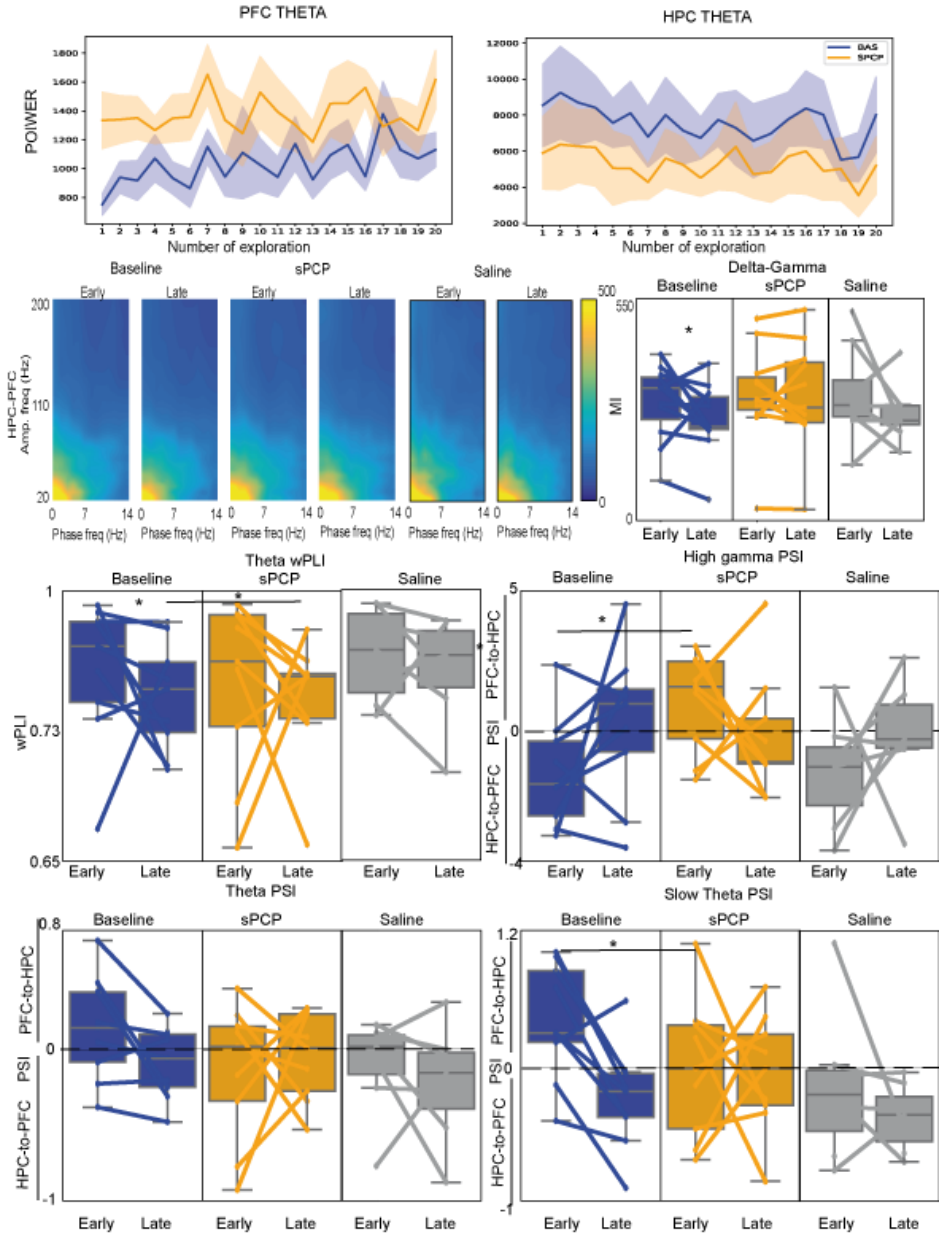

Figure 5.2.3.2: PFC-HPC neural activity associated with memory acquisition during baseline, and after sPCP and saline treatments. The upper panels show changes in PFC theta power (left) and HPC theta power (right) with increasing number of explorations. The middle panels depict HPC_{phase}-PFC_{amp} ir-PAC of delta-low gamma (phase: 2-5 Hz, amplitude: 20-40 Hz). The lower panels show changes between early and late interactions of theta wPLI (upper left), theta PSI (lower left), slow theta PSI (lower right) and high gamma PSI (upper right). Note the color used: blue for baseline, orange for sPCP and grey for saline. Dashed lines represent no change in signal directionality. Each line corresponds to one mouse.

In the working memory task, PFC theta power was also increased during object explorations in sPCP-treated mice, most notably during the visits to the familiar objects (n = 7 mice for baseline and sPCP, n = 4 mice for saline; [condition]: $F_{1,7}$ = 5.91, p = 0.04). sPCP-treated mice mostly conserved the normal patterns of slow theta directionality ([object], $F_{1,7}$ = 5.53, p = 0.051), particularly PFC-to-HPC signals during novel object explorations. However, the signal directionality became close to zero during familiar object explorations (p = 0.049). Moreover, high gamma directionality was completely disrupted by sPCP ([condition, object*condition]: $F_{1,7}$ = 6.4, 35.83, p = 0.039, 0.001), especially PFC-to-HPC signals during familiar object interactions (p = 0.001).

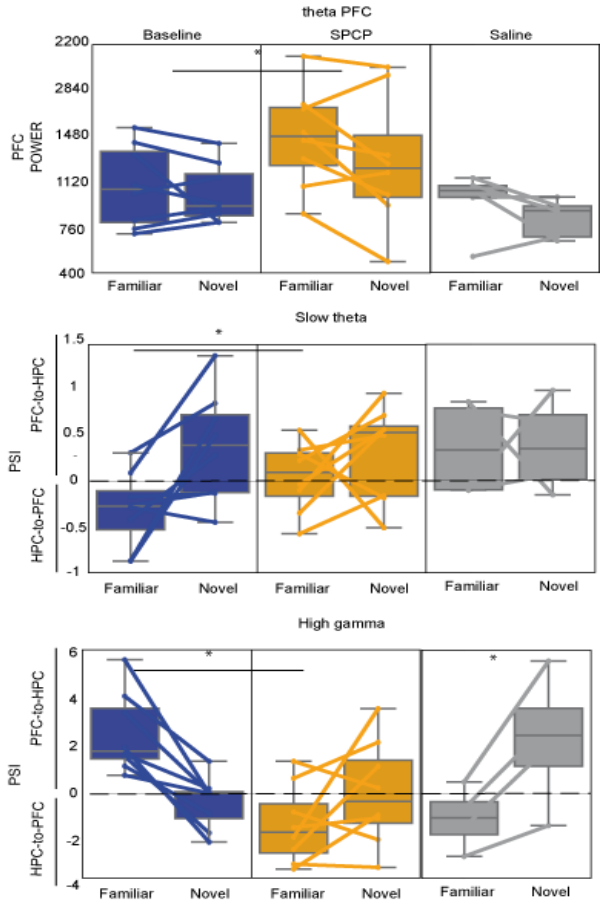

Figure 5.2.3.3: PFC-HPC neural activity associated with working memory during baseline, and after sPCP and saline treatments. The panels present the changes between familiar and novel explorations of PFC theta power (upper), slow theta PSI (middle) and high gamma PSI (lower). Note the color used: blue for baseline, orange for sPCP and grey for saline. Dashed lines represent no change in signal directionality. Each line corresponds to one mouse.

Also during the long-term memory task, several neural biomarkers for memory retrieval were disrupted in sPCP-treated mice (Fig. 5.2.3.4). First,

the familiar-novel HPC theta-gamma dynamics were disrupted due to the sPCP-induced HPC theta-gamma reduction (n = 8 mice for baseline and sPCP, n = 4 mice for saline, [condition]: $F_{1,9} = 15.96$, $p = 0.003$, significant changes with saline group which followed the baseline pattern: [object*condition, condition]: $F_{1,21} = 8.95, 6.3$, $p = 0.007, 0.02$). sPCP treatment also reduced the HFO phase synchrony during familiar object explorations, which made HFO phase synchrony in the familiar explorations similar to HFO phase synchrony found in the novel object explorations ([object*condition]: $F_{1,9} = 4.11$, $p = 0.082$). Low gamma phase synchronization and theta signal directionality followed the baseline patterns ([object: low gamma wPLI, theta PSI]: $F_{1,9} = 9.64, 7.04$, $p = 0.017, 0.033$), however they were not significantly different between novel and familiar explorations ($p = 0.35, 0.31$). Furthermore, gamma HPC-to-PFC signal directionality found in familiar object explorations in baseline conditions was partially disrupted by the sPCP treatment ([condition]: $F_{1,9} = 4.49$, $p = 0.071$).

It should be noted that despite the good memory performance, animals treated with saline instead of sPCP exhibited alterations in some of abovementioned biomarkers. There may be two reasons for this: first, the

smaller number of mice used in the saline group compared with the baseline and sPCP-treated groups ([familiarization, working memory test, long-term memory test]: n = 7, 4, 4 mice) and second, the stress caused by the injections that could have influenced the neural activities.

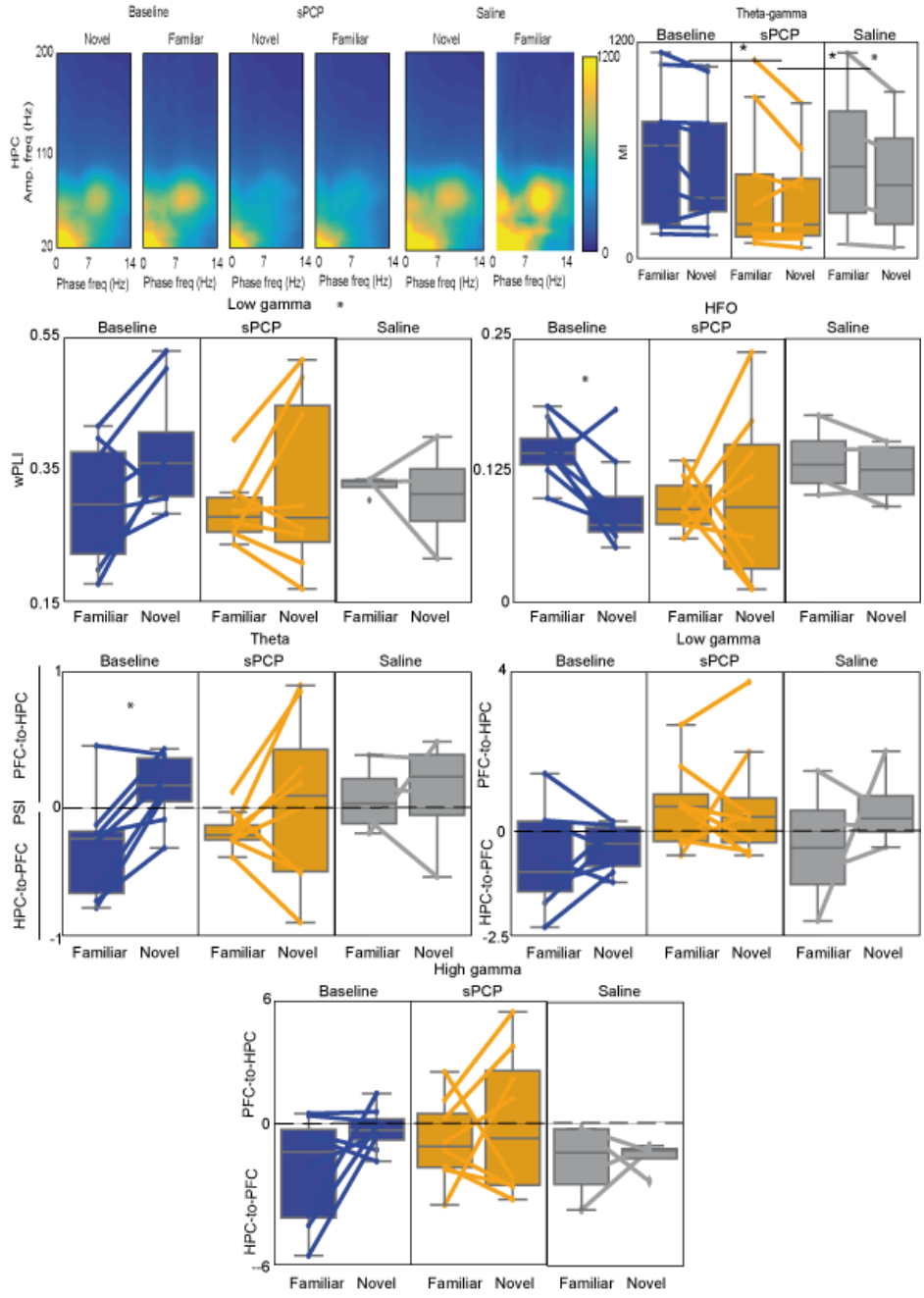

Figure 5.2.3.4: PFC-HPC neural activity associated with long-term memory during baseline, and after sPCP and saline treatments. The upper panels show the HPC of theta-gamma l-PAC (phase: 7-10 Hz, amplitude: 60-80 Hz) of novel and familiar objects

during baseline (left), sPCP (middle) and saline (right) conditions. The lower panels present the changes between familiar and novel object interactions of low gamma wPLI (upper left), HFO wPLI (upper right), theta PSI (middle left), low gamma PSI (middle right) and high gamma PSI (lower). Note the color used: blue for baseline, orange for sPCP and grey for saline. Dashed lines represent no change in signal directionality. Each line corresponds to one mouse.

5.2.4. Prefrontal-hippocampal neurophysiological biomarkers of memory performance

Next, we analysed the relationships between healthy and pathological PFC-HPC neurophysiological biomarkers and the memory performances assessed by the NOR task. We looked for significant correlations between various neural biomarkers and the DIs of the working memory and long-term memory tests. It should be noted that some of the neural biomarkers were collected in different brain states and during separate sessions (e.g., quiet wakefulness and working memory recordings).

First, we examined whether sPCP-induced abnormal neural activities recorded during quiet wakefulness predicted the memory deficits observed during working memory and long-term memory tests (Fig. 5.2.4.1). In addition, PFC theta power and phase synchrony in sPCP-treated mice

correlated negatively with long-term memory performance ([PFC theta, theta phase synchrony]: R = -0.55, -0.56, p = 0.015, 0.012), possibly indicating that they were pathological oscillatory rhythms. Interestingly, these correlations were not present in the group that received saline instead of sPCP. Another potential biomarker that could predict long-term memory performance was inter-regional high gamma flow of information during quiet wakefulness, in which more robust HPC-to-PFC signals correlated with better memory performance in baseline, an association not observed in sPCP-treated mice ([baseline, sPCP]: R = -0.51, -0.43, p = 0.02, 0.065). We did not find any relationships between memory performance and sPCP-induced non-specific circuit alterations, such as abnormal high gamma power or theta-gamma coupling.

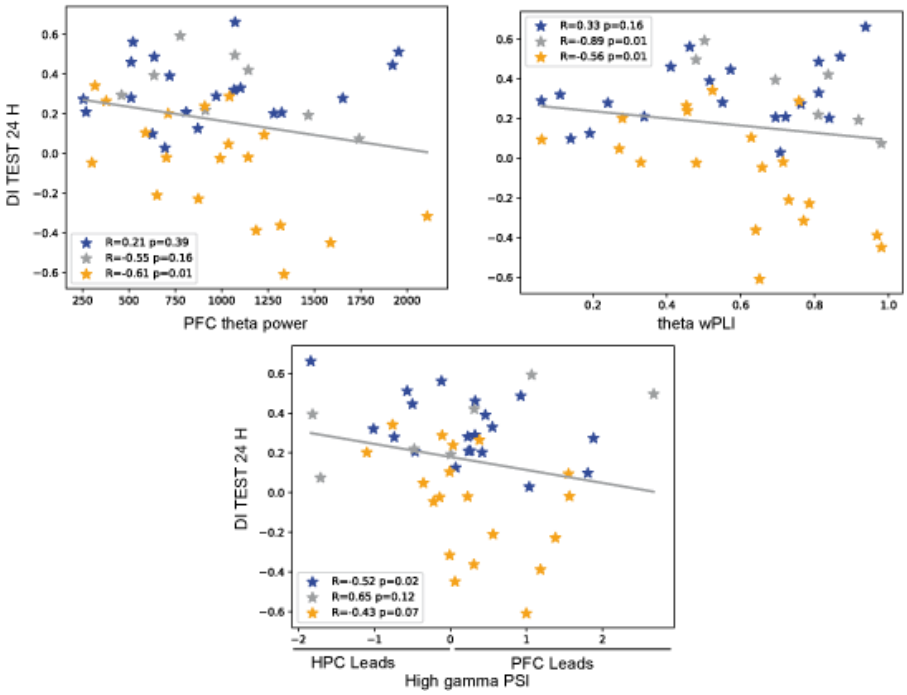

Figure 5.2.4.1: Correlations between long-term memory performances and PFC-HPC neurophysiological biomarkers during quiet wakefulness in baseline, sPCP and saline groups. Relevant correlations of PFC theta power (upper left), theta wPLI (upper right) and high gamma PSI (lower), with long-term memory performance are shown.

Subsequently, we investigated whether the neurophysiological biomarkers recorded during memory acquisition correlated with working and long-term memory performances (Fig. 5.2.4.2). We used the differences between measures recorded during the late object interactions and the early object interactions during the familiarization phase. A greater difference in

theta phase synchronization during memory acquisition correlated with better working memory performance during baseline, and this correlation was not observed in the same animals after the sPCP treatment ([baseline, sPCP]: R = 0.61, 0.39, p = 0.035, 0.21). This implies that the circuit synchronization at theta frequencies may reflect neural mechanisms relevant for the acquisition of new memories.

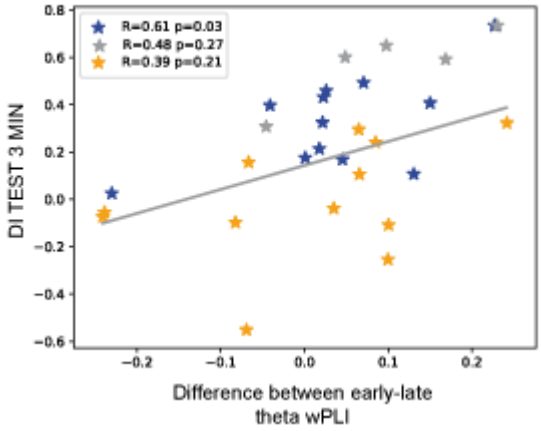

Figure 5.2.4.2: Correlation between accumulated theta phase coherence (wPLI) during memory acquisition and working memory performance in the baseline, sPCP and saline groups.

Next, we investigated whether the neurophysiological biomarkers recorded during the working memory task correlated with working memory performance (Fig. 5.2.4.3). We also used the differences between measures recorded during visits to familiar and novel objects. As above,

the directionality measures could be positive (PFC-to-HPC) or negative (HPC-to-PFC). During baseline, PFC-to-HPC high gamma signals identified during familiar object explorations correlated positively with working memory performance. Furthermore, a greater difference of this parameter with respect to novel object explorations, also correlated with superior performance ([familiar object high gamma PSI, difference familiar vs novel PSI]: R = 0.69, 0.69, p = 0.01, 0.001). These correlations were not observed in sPCP-treated mice.

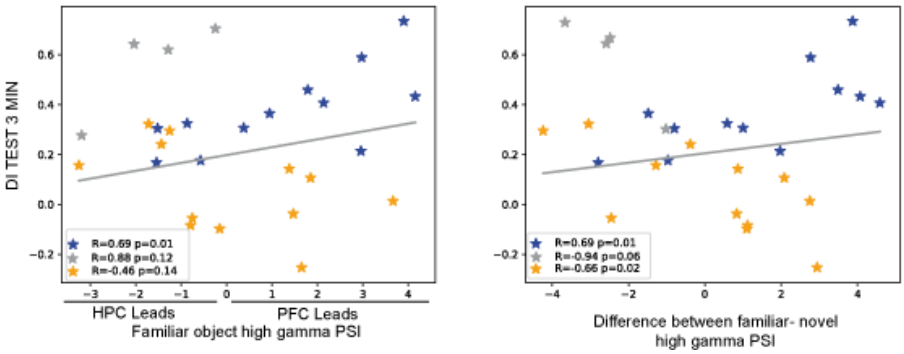

Figure 5.2.4.3: Correlations between PFC-HPC neurophysiological biomarkers and DIs during working memory performance in baseline, sPCP and saline groups. Correlations between familiar object high gamma PSI (left) and the difference of familiar object signal directionality and the novel object signal directionality (right) with the working memory performance.

Finally, we examined the correlations between the neurophysiological biomarkers recorded during the long-term memory test and long-term

memory performance (Fig. 5.2.4.4). During baseline, HPC-to-PFC theta directionality during familiar object explorations and the difference in signal directionality between familiar and novel object explorations correlated with a superior long-term memory performance ([familiar object signal directionality, difference familiar vs novel]: R = -0.63, -0.75, p = 0.02, 0.003). These correlations did not occur after sPCP. Similarly, baseline HPC-to-PFC low gamma and high gamma directionality during familiar object explorations correlated with better memory performance and these correlations were reduced after sPCP ([low gamma: baseline, sPCP, saline]: R = -0.5, -0.42, -0.04, p = 0.07, 0.14, 0.94; [high gamma: baseline, sPCP, saline]: R = -0.5, 0.21, -0.8, p = 0.08, 0.49, 0.11). Altogether, these relationships suggested that precise flows of information at theta and gamma frequencies within PFC-HPC circuits played a role in long-term memory retrieval.

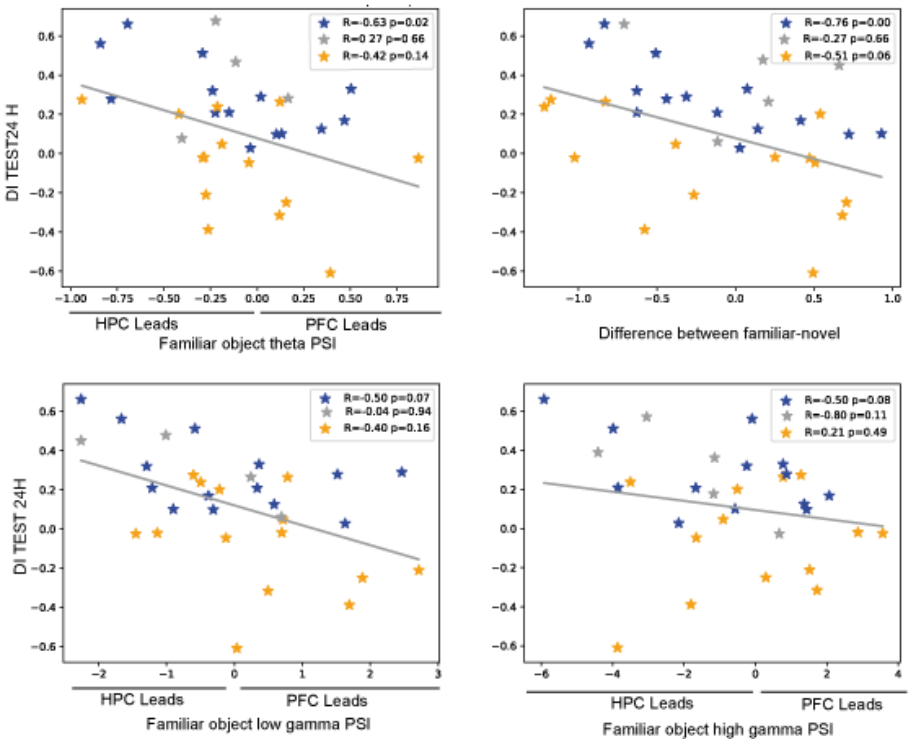

Figure 5.2.4.4: Correlations between PFC-HPC neurophysiological biomarkers and the DI during the long-term memory test in baseline, sPCP and saline groups. Correlations between familiar object theta PSI (upper left), low gamma PSI (lower left) and high gamma PSI (lower right); and the difference of familiar object theta signal directionality and the novel object theta directionality (upper right) with the long-term memory performance.

5.2.5. Summary of encoding and disruption of memory acquisition, working memory and long-term memory

Across all the experiments conducted, we observed that sPCP decreased gamma power and theta-gamma coupling in the HPC and increased theta and high gamma power in the PFC. These effects were non-specific as they were independent of brain state and cognitive task (Table 2 and Fig. 5.2.5.1).

However, from the large dataset at hand where we did identify biomarkers that correlated with specific memory demands and were disrupted by sPCP, we tried to determine the essential neurophysiological mechanisms encoding the different types of memory. Overall, major biomarkers encoding memory were associated with inter-regional exchange of information at theta and gamma frequencies, that is, directionality of the signals. We validated the results reported above by shuffling the data obtained from the PFC and the HPC using surrogates (see Methods). During memory acquisition, we found that PFC-to-HPC slow theta directionality emerged as the animals encountered novelty (early visits) whereas HPC-to-PFC slow theta signals emerged as the memories for the objects were encoded (late visits) ([shuffle corrected: early, late,

difference]: p = 0.02, 0.065, 0.015; paired T tests). Consistently, the PFC-to-HPC theta directionality for novelty was partially conserved across the working memory (p = 0.071) and long-term memory tasks (p = 0.025) during baseline conditions. During working memory, PFC-to-HPC high gamma signal directionality was significantly different and correlated with good memory performance ([baseline familiar object explorations, familiar object explorations baseline vs sPCP]: p = 0.029, 0.001; [correlation of DI with signal directionality during familiar object explorations]: R = 0.7, p = 0.026). Lastly, during the long-term memory retrieval, the HPC-to-PFC signal directionality at theta (p = 0.024; [correlation of DI with signal directionality during familiar object explorationst in baseline mice]: R = -0.58, p = 0.037) and gamma ranges p = 0.024; [correlation of DI with signal directionality during familiar object explorations in baseline mice]: R = -0.52, p = 0.007) were correlated with the retrieval of long-term memory. All these biomarkers were disrupted by sPCP.

AREA	BAND(S)	QUIET	MA	WM	LTM
PFC	θ	✕			
	High γ				
HPC	γ				
	MI θ-γ				
PFC-HPC	MI θ-γ				
PFC-HPC	Slow θ				

ENCODED
INCREASED
DECREASED
✕ DISRUPTED

BIOMARKER	BAND(S)	MA	WM	LTM
PFC	θ	✕	✕	
HPC-PFC	MI δ-lγ			
PFC-HPC WPLI	θ			
PFC-HPC Directionalilty	High γ	✕	✕	✕
HPC	θ-γ			✕
PFC-HPC Directionality	θ	✕		
PFC-HPC Directionality	slow θ	✕	✕	
HCP → PFC Directionality Familiar object	Low γ			✕
PFC-HPC WPLI	Low γ			✕
PFC-HPC WPLI	HFO			✕

Table 2: PFC-HPC neurophysiological biomarkers encoding different types of memory and their disruption by sPCP. Acronyms: MA (memory acquisition), WM (working memory), LTM (long-term memory), **δ** (delta), **θ** (theta), ***γ*** (gamma), **θ-*γ*** (theta-gamma coupling) and HFO (high frequency oscillations).

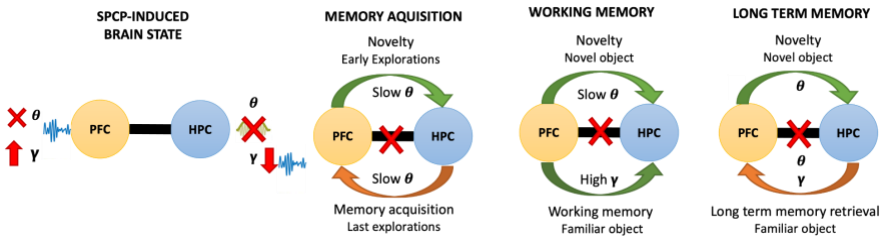

Figure 5.2.5.1: Schematic summary of the changes induced by sPCP in PFC-HPC neural dynamics during quiet wakefulness, memory acquisition, working memory

and long-term memory. Brain state refers to non-specific changes observed across all sessions.

5.3. Abnormal neural activity in the prefrontal cortex during auditory perception and attention

Patients with schizophrenia show deficits in auditory sensory processing (Javitt and Sweet, 2015) that can be tested using different non-operant auditory tasks based on event-related potentials (ERPs). Furthermore, these tasks are completely translatable to rodents (Schuelert et al., 2018; Scimemi et al., 2014; Wang et al., 2020). Rodents' ERPs are stable and similar to humans, however at a faster time scale due to the smaller size of their brain (Fig. 1.1.3.1.1). Therefore, we examined if the sPCP mouse model of schizophrenia presented sensory gating deficits similar to patients with schizophrenia. We specifically focused on the ERPs in the PFC in order to compare with the frontal cortical processes of the auditory stimuli. The tasks used for this study were as follows: the auditory evoked potential (AEP), the auditory state-steady response (ASSR) and the oddball paradigm to check mismatch negativity (MMN). Patients with schizophrenia exhibit anomalous EEG activities above the auditory and frontal cortices in the three tasks (Koshiyama et al., 2020; O'Donnell et al., 2013; Shen et al., 2020, p. 50). Anomalous neural activities have been

also reported in acute NMDAR hypofunction rodent models (Schuelert et al., 2018; Wang et al., 2020).

5.3.1. Auditory evoked potentials in the prefrontal cortex before and after sPCP

Auditory ERPs are evoked by blind sounds and can be readily seen in the LFP or EEG of the auditory and sensory processing areas, in our case the PFC. ERPs consist of distinct peaks (P) and negativities (N) at different time points that have been linked with several cognitive processes in humans and rodents: the P50 (humans) or P1 (rodents) assess pre-attentional filtering of sensory information; the N100 (humans) or N1 (rodents) assess the MMN or attention triggering; the P200 (humans) or P2 (rodents) assess attentional triggering and allocation processes; and finally the P300 (humans) or P3 (rodents) represents the information processing of the auditory signal and has been used as an index for cognitive processing (Turetsky et al., 2007). Here, we presented 100 sounds to the animals (see Methods) while neural activities were recorded in the PFC. Trials with clear artifacts in the LFP were discarded. Trials that presented an ERP were selected and averaged across trials and treatment groups. The

response index was calculated by dividing the trials that presented an ERP by the total number of trials presented (i.e., percentage of ERP response).

In order to do a better characterization of the auditory evoked potentials, we analysed the ERPs combining the LFP signals and the multi-unit spiking activity (MUA). First, we characterized the ERP generated in the PFC of mice during baseline (n = 9 mice, Fig. 5.3.1.1, represented in blue). Remarkably, the sound generated two peaks of spiking activity that corresponded with the positive components of the ERP (P1 and P2), suggesting a relationship between increased spiking activity with the processing of the auditory stimuli.

Next, we investigated any alteration in the ERPs produced by sPCP (Fig. 5.3.1.1). The response index decreased after the sPCP treatment (n = 9 mice) but not after the saline (n = 4 mice) ([index of response: baseline vs. sPCP, sPCP vs saline]: p = 0.024, 0.024, dependent and independent T test, respectively) indicating impaired processing of auditory stimuli in the cortex. Furthermore, sPCP induced alterations in the late components of the ERP, P2 and P3, with respect to the baseline, leaving the early components unaffected. The P2 component presented less spiking activity

after the sPCP treatment ([MUA: baseline vs. sPCP, sPCP vs. saline]: p = 0.013, 0.068), whereas the P3 was reduced in amplitude and spiking activity ([P3 amplitude: baseline vs. sPCP, sPCP vs. saline]: p = 0.015, 0.055; [MUA: baseline vs. sPCP, sPCP vs. saline]: p = 0.024, 0.06). Together, sPCP produced alterations in the response rate and the P2 and P3 components of the ERP, indicating impaired processing of the auditory signals.

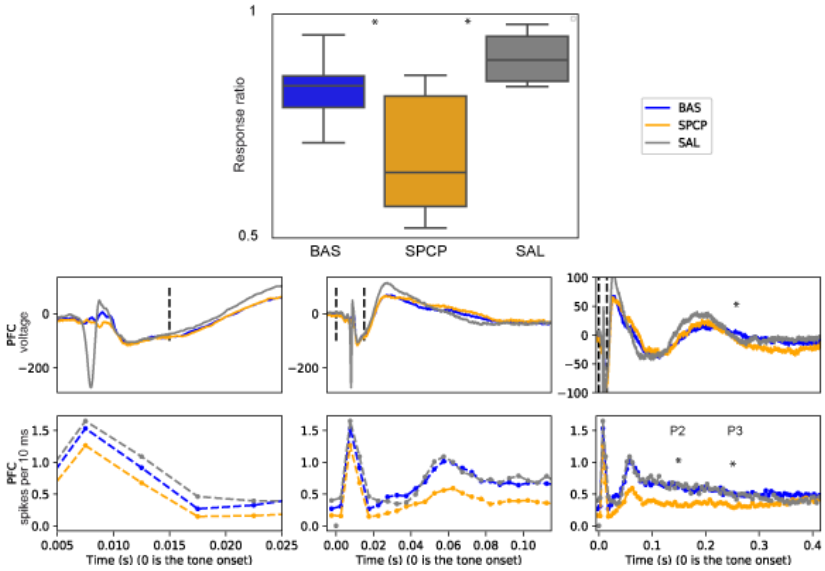

Figure 5.3.1.1: PFC auditory evoked potentials comparing baseline, sPCP and saline groups. The upper panel shows the response rate of ERPs in each group. The lower panels represent the mean ERPs (middle, voltage) and the corresponding multi-unit activities (lower, spikes per 10 ms) at different time scales.

5.3.2. Auditory steady-state responses in the prefrontal cortex before and after sPCP

The auditory steady-state response (ASSR) is a type of ERP based on the synchronous response of the brain to clicking sounds at one stable frequency. The test reflects the propensity of neurons to oscillate at 40-Hz induced by an external periodic stimulation. Of relevance here, the ASSR is reduced in patients with schizophrenia and NMDAR hypofunction rodent models of schizophrenia (O'Donnell et al., 2013; Wang et al., 2020). The ASSR was analysed looking at the power and inter-trial coherence of the responses (see Methods), which is the average power between 38-42 Hz across 50 trials. After the sPCP treatment we observed a mild reduction in the power or the inter-trial coherence that was not significantly different than baseline (Fig. 5.3.2.1).

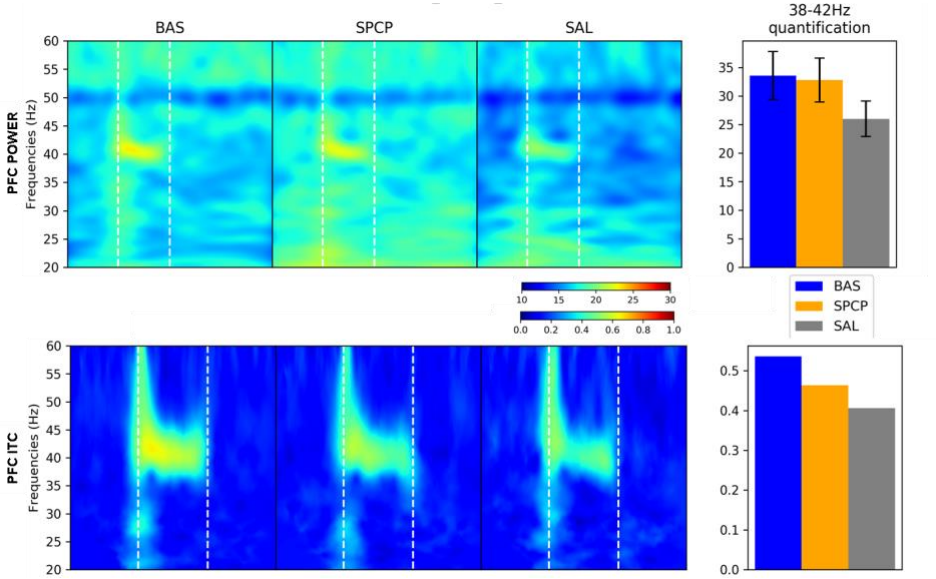

Figure 5.3.2.1: PFC auditory state-steady response comparing baseline, sPCP and saline groups. Mean power between the trials is represented in the upper panels and the inter-trial coherence is shown in the lower panels. The right panels represent the quantification. Baseline results are shown in the left or blue, sPCP results are shown in the middle or orange and saline results are shown in the right or grey.

5.3.3. Neurophysiological correlates of the attentional oddball paradigm (MMN) in the prefrontal cortex before and after sPCP

Finally, we examined the mismatch negativity (MMN) effects in sPCP-treated mice (n = 9 mice for baseline and sPCP group and n = 4 for saline controls) using a passive oddball paradigm that differed in the frequency of the stimuli (6000 Hz or 8000 Hz as target or standard) (Fig. 5.3.3.1).

The oddball paradigm consists of presentations of standard stimuli that are infrequently interrupted by a target or deviant stimulus (see Methods). Patients with schizophrenia show a reduced MMN that may reflect NMDAR hypofunction (Koshiyama et al., 2020). In order to calculate the MMN, we subtracted the averaged ERP evoked by the standard tone from the averaged ERP evoked by the target tone at a specific frequency, that is target-standard ERPs for the 6 kHz and 8 kHz tones separately. To make sure that the same number of ERPs were compared, we only used the standard ERPs recorded prior to the target tones (see Methods). We quantified the MMN measuring the area under the curve representing the MMN 25 ms before and after the MMN peak as done in Schuelert et al., 2018.

In the baseline and saline-treated mice, the MMN was only present in the tones at 6000 Hz but not in the tones at 8000 Hz. Furthermore, the MMN was reduced after the sPCP treatment ($p = 0.021$; paired T test) during presentation of tones at 6000 Hz. These results indicated that MMN was reduced after sPCP treatment as in patients with schizophrenia.

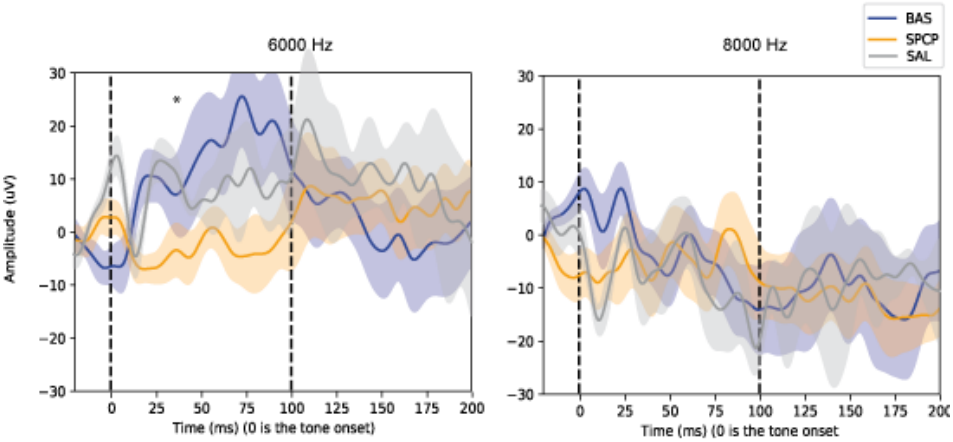

Figure 5.3.3.1: PFC mismatch negativity (MMN) response comparing baseline, sPCP and saline groups. The left panel represents the 6000 Hz MMN and the right panel represents the 8000 Hz MMN.

Overall, the sPCP treatment altered auditory perception by reducing two important biomarkers of schizophrenia: the last components of the auditory evoked potential and the MMN. However, there were no significant alterations in the neural signals evoked by the ASSR paradigm (Table 3).

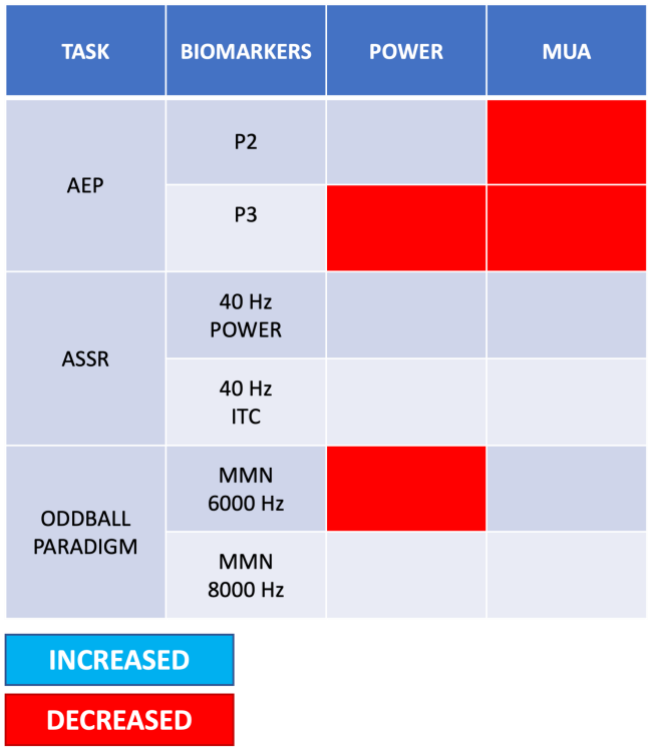

Table 3: Summary of the sPCP-induced changes in auditory perception and processing. ITC, intertrial coherence.

6. CHAPTER III. NEURAL CORRELATES OF COGNITIVE AMELIORATION IN sPCP-TREATED MICE BY CHRONIC RISPERIDONE

6. CHAPTER III. NEURAL CORRELATES OF COGNITIVE AMELIORATION IN sPCP-TREATED MICE BY CHRONIC RISPERIDONE

This chapter discusses our investigations on whether a chronic treatment with the atypical antipsychotic drug risperidone (0.5 mg/kg, i.p., 14 consecutive days) rescues abnormal PFC-HPC circuits in the sPCP mouse model of schizophrenia. Acute risperidone has proved to be effective in restoring cognitive deficits in the sPCP mouse model of schizophrenia (Grayson et al., 2007; Meltzer and Huang, 2008). However, the effects of a chronic treatment in memory impairment had not been studied. We started the chronic risperidone or saline treatments (controls) when the animals finished the sPCP characterization (Fig. 3.8.1). Open field explorations, NOR and auditory task characterizations were implemented within 48 hours after finishing the treatments.

6.1. Amelioration of sPCP-induced neural activity alterations during quiet wakefulness

First, we investigated whether chronic risperidone could rescue the sPCP-induced PFC-HPC circuit alterations during quiet wakefulness (n = 8 mice) (Fig. 6.1.1). Risperidone could only partially restore the local theta-gamma

coupling in the HPC ([baseline, sPCP and risperidone]: $F_{2,16} = 2.45$, $p = 0.125$; repeated measures ANOVA with treatment as factor), while the rest of sPCP-mediated alterations remained unaffected. Importantly, the pathological correlations between theta oscillations and synchrony and poor long-term memory performance that emerged after sPCP subsided after the chronic risperidone treatment ([correlations: PFC theta power, theta phase synchrony]: $R = 0.21, 0.42$, $p = 0.6, 0.26$).

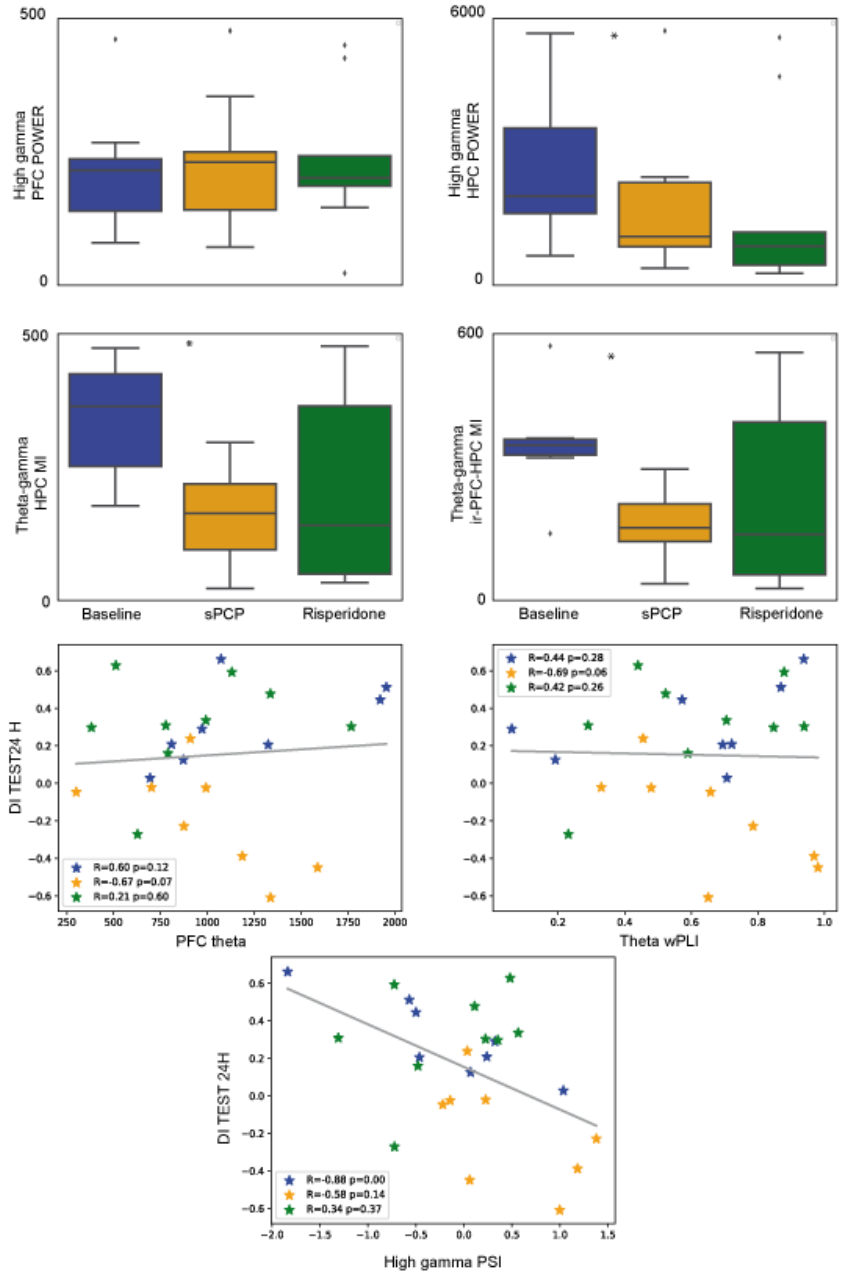

Figure 6.1.1: Effects of chronic risperidone on sPCP-induced neural activity alterations of PFC-HPC circuits during quiet wakefulness. The upper panels show quantifications of high gamma power of PFC (left) and HPC (right). Middle upper panels

show the modulation index changes of local (left) and interregional (right) theta-gamma coupling. The lower panels correspond to the correlations between long-term memory and PFC theta, theta wPLI and high gamma directionality. Note the color used: blue for baseline, orange for sPCP and green for risperidone.

Because the accumulated time of the sPCP+cRIS protocol was long (at least 30 days), we investigated any age-dependent and stress-dependent alterations in PFC-HPC neural dynamics in animals only treated with saline during both epochs of the protocol (n = 7 mice). We did not observe any significant alterations in this group of animals (Fig 6.1.2).

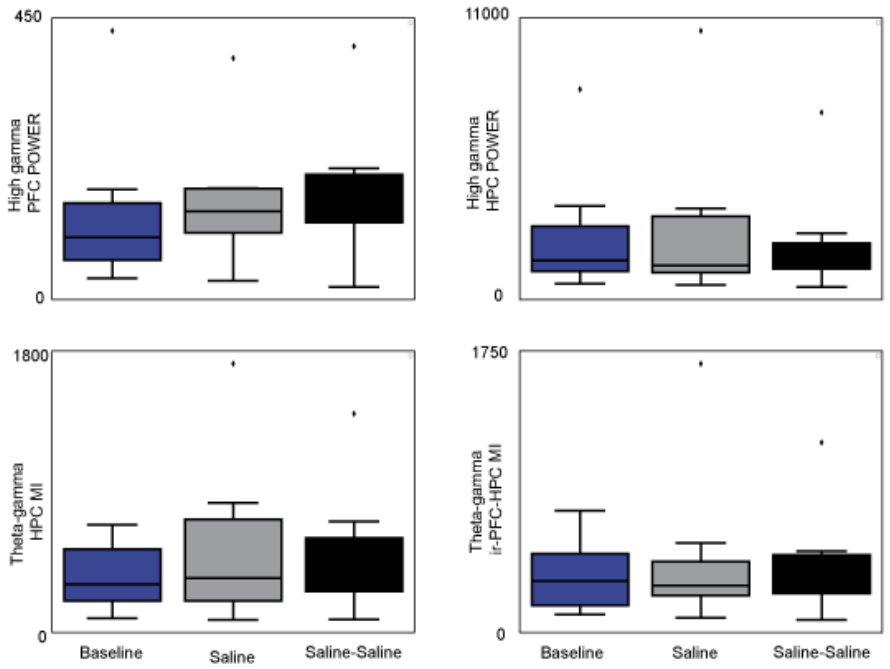

Figure 6.1.2: Effects of age and stress in the PFC-HPC neurophysiological biomarkers altered by sPCP via saline controls. PFC and HPC high gamma power is

shown in the upper panels, respectively. Local HPC and interregional theta gamma modulation index is shown on the lower panels. Note the color used: blue for baseline, grey for the first saline treatment and black for the second saline treatment.

6.2. Neural substrates of memory rescue by chronic risperidone

Next we investigated the neural substrates of the cognitive amelioration produced by the chronic risperidone treatment. We quantified performance in the working memory and long-term memory tasks using the same NOR protocol previously described (see Methods).

6.2.1. Recognition memory recovery with the chronic risperidone treatment

Risperidone rescued memory deficits in the working memory (Fig. 6.2.1.1, n = 4 mice, DI = 0.42 +- 0.1) and long-term memory tasks (Fig. 6.2.1.2, n = 6 mice, DI = 0.37 +- 0.07) ([working memory, long-term memory]: $F_{2,6}$ = 16.64, 15.15, p = 0.004, < 0.0005, repeated measures ANOVA with treatment condition as factor; $F_{2,24}$ = 5.11, 15.76, p = 0.017, < 0.0005, one-way ANOVA with sPCP-risperidone, sPCP-saline and saline-saline groups). Intriguingly, mice chronically treated with saline (saline-saline) presented impaired long-term memory performance (n = 5 mice, DI = 0.04

+- 0.07), most likely due to the chronic stress caused by the multiple injections.

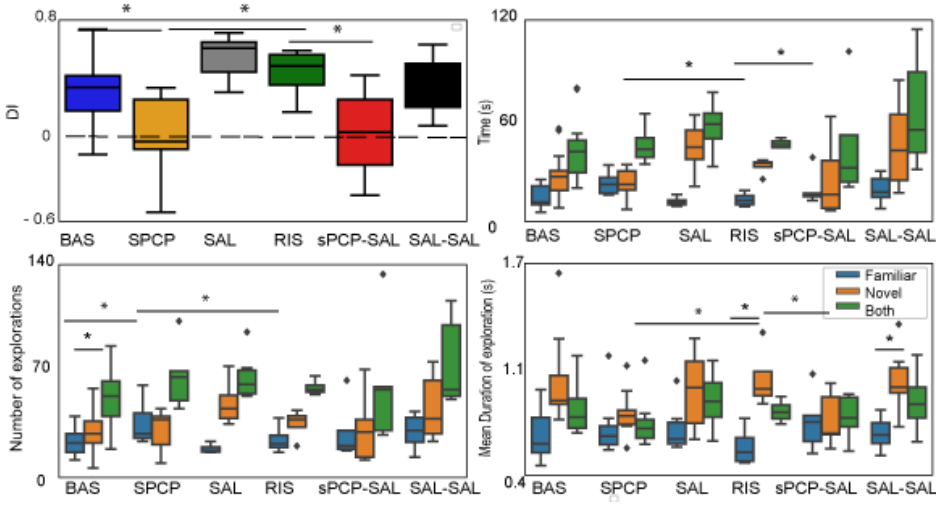

Figure 6.2.1.1: Working memory performance during baseline (BAS), sPCP-treated (SPCP), saline treated (SAL), risperidone treated after sPCP (RIS), saline treated after sPCP (sPCP-SAL) and saline after saline (SAL-SAL) conditions. Discriminations indexes (DIs) (top left panel) during baseline (blue), sPCP (orange), saline (grey), risperidone (green), saline after sPCP (red) and saline after saline (black) mice; total duration of explorations (top right panel), number of explorations (lower left panel) and mean duration of explorations (lower right panel) of familiar objects (blue), novel objects (red) and the combination of both (green).

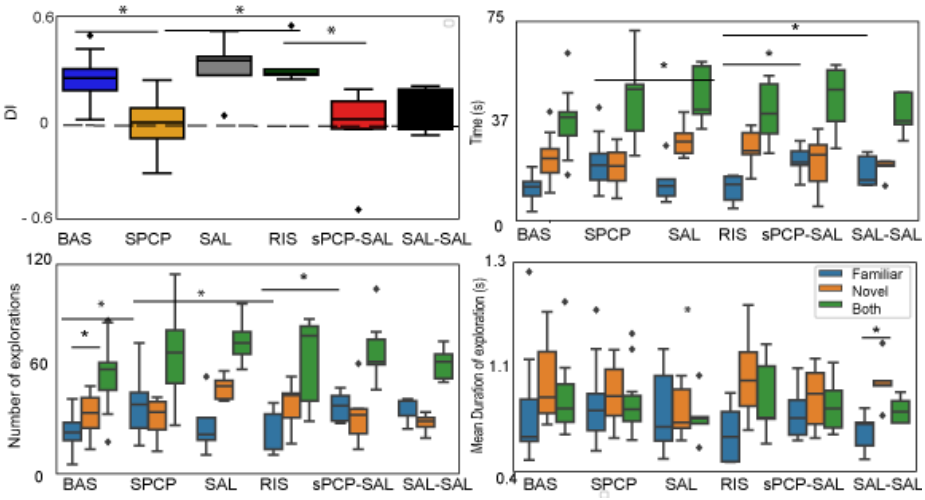

Figure 6.2.1.2: Long-term memory performance during baseline (BAS), sPCP-treated (SPCP), saline treated (SAL), risperidone treated after sPCP (RIS), saline treated after sPCP (sPCP-SAL) and saline after saline (SAL-SAL) conditions. Discriminations indexes (DIs) (top left panel) during baseline (blue), sPCP (orange), saline (grey), risperidone (green), saline after sPCP (red) and saline after saline (black) mice; total duration of explorations (top right panel), number of explorations (lower left panel) and mean duration of explorations (lower right panel) of familiar objects (blue), novel objects (red) and the combination of both (green).

During the working memory test, risperidone-treated animals explored the familiar objects less amount of time than sPCP-treated mice, but in comparable levels than the baseline and the saline-saline groups ([time exploring familiar objects: one-way ANOVA baseline vs sPCP vs risperidone, two-way ANOVA sPCP-risperidone vs. sPCP-saline vs. saline-saline]: $F_{2,6} = 24.54$, $p = 0.001$, $F_{2,24} = 4.97$, $p = 0.083$). Risperidone-

treated mice also spent more time exploring the novel objects than sPCP-treated mice ($F_{2,6} = 6.98$, $p = 0.027$). Furthermore, risperidone-treated mice visited the familiar objects fewer times and for shorter periods of time than sPCP-treated mice ([number of visits, mean individual time per visit]: $F_{2,6} = 5.87, 4.82$, $p = 0.038, 0.056$). Moreover, they also explored the novel objects for longer periods of time ($F_{2,24} = 5.83$, $p = 0.011$). The changes between the mean individual periods of time exploring the familiar objects were more apparent during the early visits ($F_{2,19} = 7.07$, $p = 0.005$; repeated measures two-way ANOVA within time and between treatments), in which risperidone-treated mice explored the familiar objects for shorter periods of time than the novel objects ($F_{2,16} = 51.93$, $p < 0.0005$) (Fig. 6.2.1.3). We note that the group of risperidone-treated mice was small (n = 4 mice) due to the long protocol (several animals lost their implant during the experiment) and the strict criteria used to include a behavioral test in the analyses of the NOR task (see Methods).

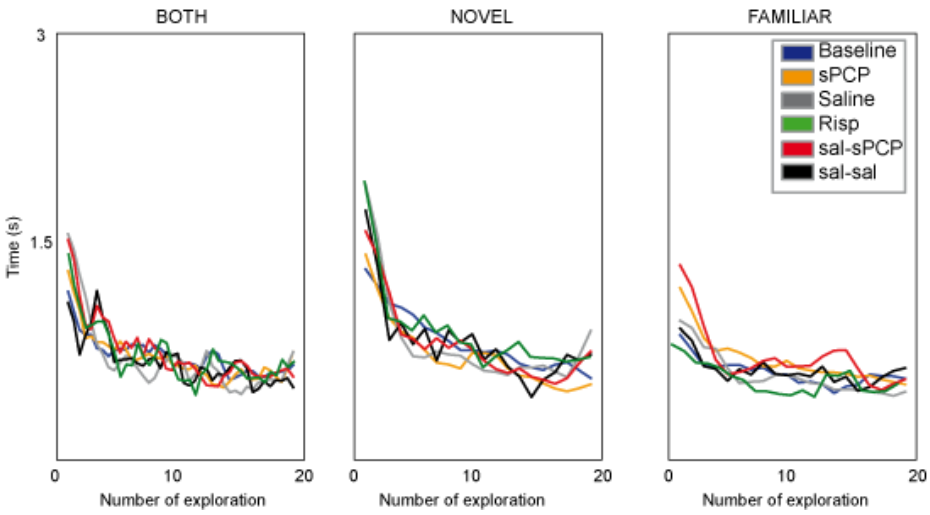

Figure 6.2.1.3: Mean duration of individual visits to novel and familiar objects over time during the working memory test. The first 20 explorations are shown for both objects combined (left), the novel object (middle) and the familiar object (left). Data from baseline is shown in blue, sPCP is shown in orange, saline is shown in grey, risperidone is shown in green, saline after sPCP is shown in red and saline after saline treatment is shown in black.

During the long-term memory test, risperidone-treated mice recovered the memory performance also by reducing the time exploring the familiar object compared with the sPCP-treated mice ([time exploring familiar object: baseline vs sPCP vs risperidone, sPCP-risperidone vs. sPCP-saline vs. saline-saline]: $F_{2,18} = 7.37$, $p = 0.005$, $F_{2,24} = 7.37$, $p = 0.003$). Risperidone-treated mice visited fewer times the familiar object ([number

of visits comparing: baseline vs sPCP vs. risperidone, risperidone vs. saline-sPCP vs. saline-saline]: $F_{2,18} = 3.64$, $p = 0.047$, $F_{2,24} = 4.03$, $p = 0.031$) and more times the novel object ($F_{2,18} = 5.74$, $p = 0.012$) (Fig. 6.2.1.2 and Fig. 6.2.1.4).

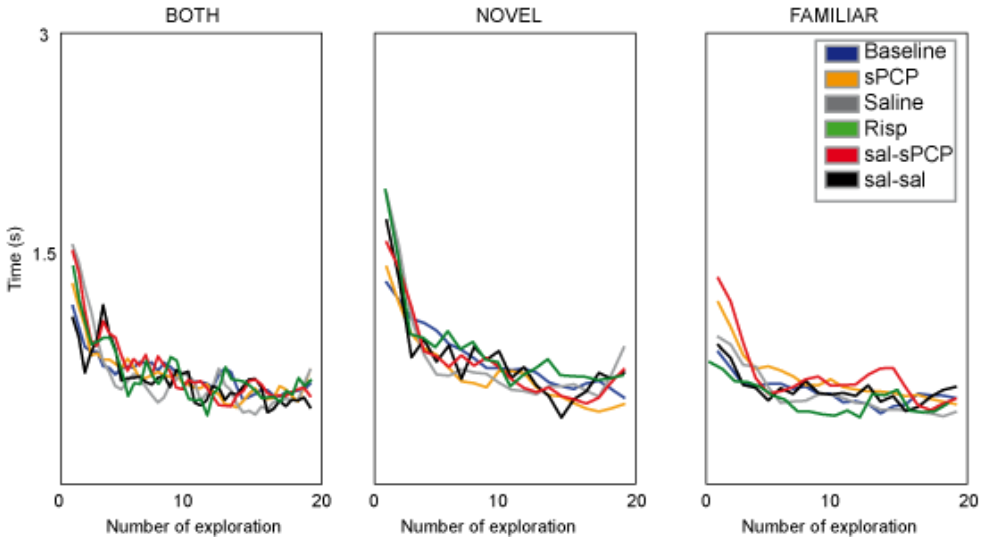

Figure 6.2.1.4: Mean duration of individual visits to novel and familiar objects over time during the long-term memory test. The first 20 explorations are shown for both objects combined (left), the novel object (middle) and the familiar object (left). Data from baseline is shown in blue, sPCP is shown in orange, saline is shown in grey, risperidone is shown in green, saline after sPCP is shown in red and saline after saline treatment is shown in black.

6.2.2. Neural substrates of memory acquisition, working memory and long-term memory rescue by risperidone

Next, we investigated the neural signatures of memory rescue by risperidone, specifically in memory acquisition, working memory and long-term memory (Fig. 6.2.2.1). Risperidone had minimal effects on the sPCP-induced non-specific "brain-state" reductions of HPC high gamma power ([familiarization, working memory and long-term memory test] $F_{2,10}$ = 5.74, 1.3, 3.78, p = 0.036, 0.34, 0.06; repeated measures two-way ANOVA within object or time and treatments; differences with baseline and not sPCP-treated) and theta-gamma coupling both locally ($F_{2,10}$ = 12.23, 1.32, 7.14, p = 0.006, 0,33, 0.023; differences with baseline and not sPCP-treated) and at the circuit level ($F_{2,10}$ = 12.68, 0.72, 8.5, p = 0.005, 0.45, 0.011; differences with baseline but not with sPCP-treated mice) during all the NOR phases.

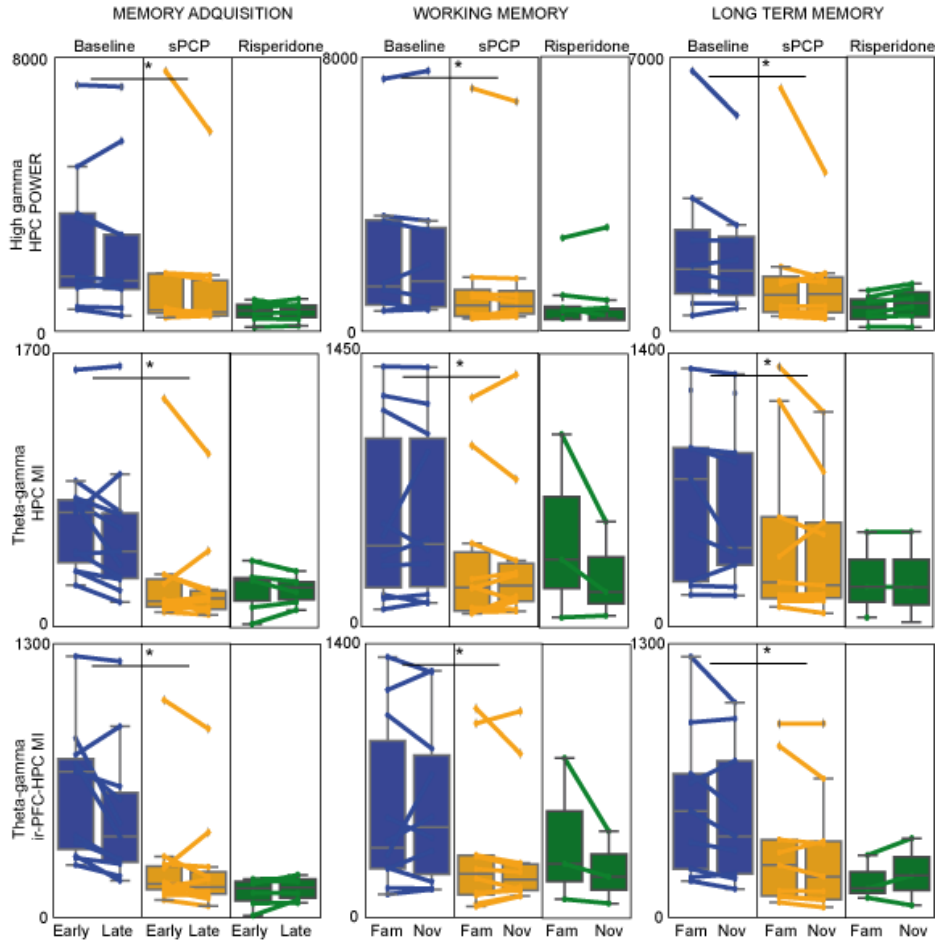

Figure 6.2.2.1: Risperidone had minimal effects on sPCP-induced PFC-HPC network deficits during memory acquisition, working memory and long-term memory. Baseline biomarkers are depicted in blue, sPCP-biomarkers in orange and risperidone-biomarkers in green. Each line corresponds to one mouse.

During memory acquisition (n = 6 mice), risperidone could partially recover the transitions from early PFC-to-HPC signals to late HPC-to-PFC signals at slow theta and theta (p = 0.059, 0.054; dependent T test between

early and late explorations) because PFC-to-HPC theta signals during early visits was restored ($p = 0.015$). Risperidone also partially corrected the high gamma HPC-to-PFC signals during early explorations and the PFC-to-HPC signals during late explorations, together with a reduction of the general increase in PFC theta power (Fig. 6.2.2.2).

During working memory ($n = 4$ mice), the risperidone treatment did not recover the previously mentioned neurophysiological biomarkers (Fig. 6.2.2.3). It should be noted that for the working memory test only 4 animals followed all the criteria needed to analyze the task.

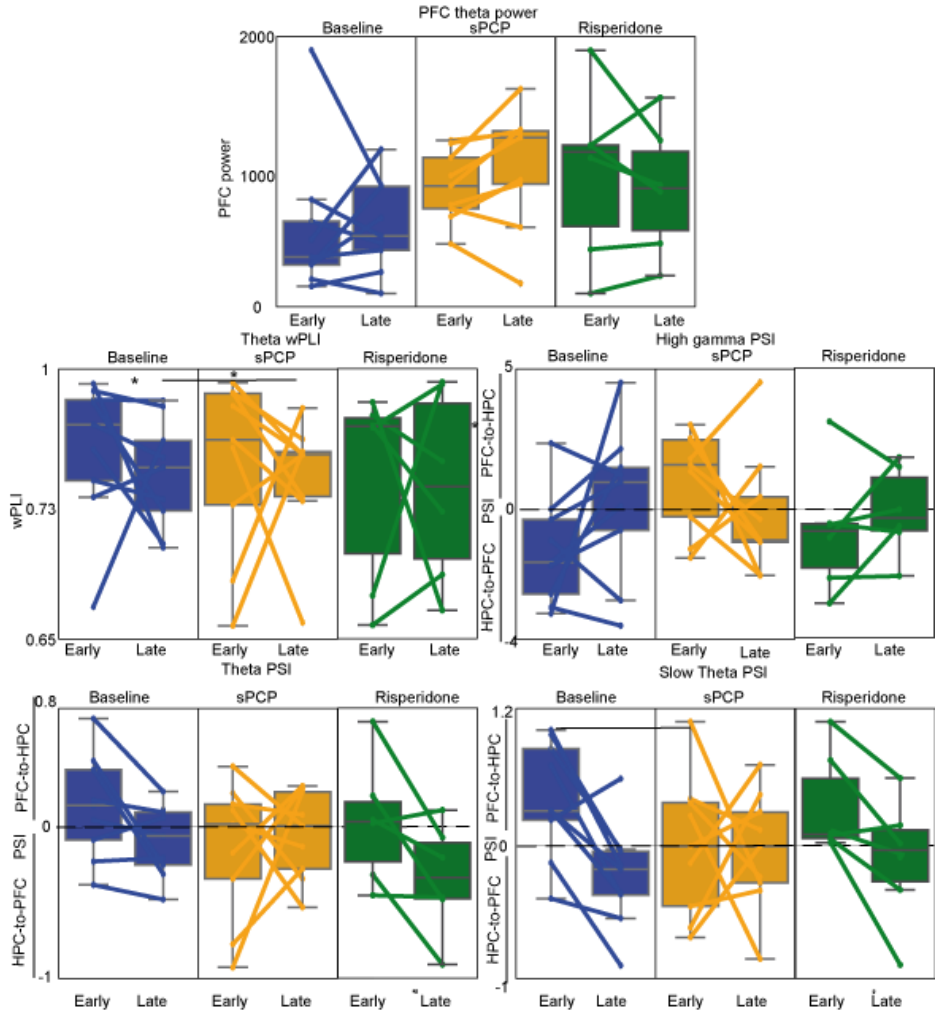

Figure 6.2.2.2: PFC-HPC circuit activity during memory acquisition in baseline, sPCP and risperidone groups. The upper panel shows the PFC theta power (left). Changes between early and late interactions of theta wPLI (middle left), theta PSI (lower left), slow theta PSI (lower right) and high gamma (middle right) are shown in the lower panels of the figure. Note the color used: blue for baseline, orange for sPCP and green for risperidone. Dashed lines represent no change in signal directionality. Each line corresponds to one mouse.

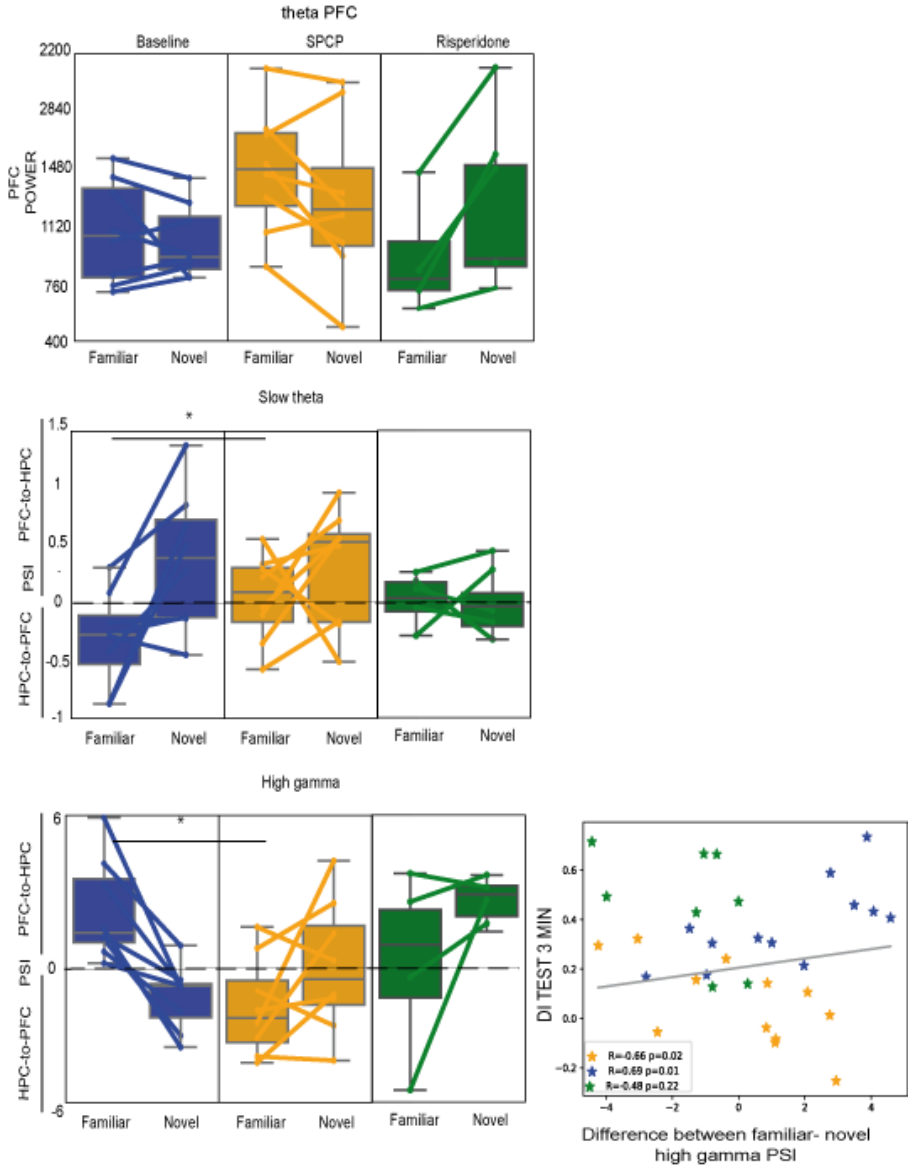

Figure 6.2.2.3: PFC-HPC circuit activity during the working memory task in baseline, sPCP and risperidone groups. The panels present the changes between familiar and novel explorations of PFC theta power (upper), slow theta PSI (middle) and high gamma PSI (lower). Correlation between the difference of familiar and novel objects of high gamma directionality and the discrimination index of the working memory task is

shown in the lower right panel. Note the color used: blue for baseline, orange for sPCP and green for saline. The dashed line represents the 0 or change of the signal directionality. Dashed lines represent no change in signal directionality. Each line corresponds to one mouse.

During the long-term memory task (n = 6 mice), the risperidone treatment could only recover the increased low gamma phase synchrony found in the novel object explorations ($p = 0.014$). Interestingly, a greater difference in low gamma phase synchrony between familiar and novel object explorations was partially associated with a superior long-term memory performance ($R = -0.77$, $p = 0.074$), indicating that the recovery of this neurophysiological biomarker may be related to risperidone's pro-cognitive effects (Fig. 6.2.2.4). These results indicate that risperidone's pro-cognitive effects relied on the increased phase synchronization of low gamma as a compensatory mechanism for the sPCP-induced effects.

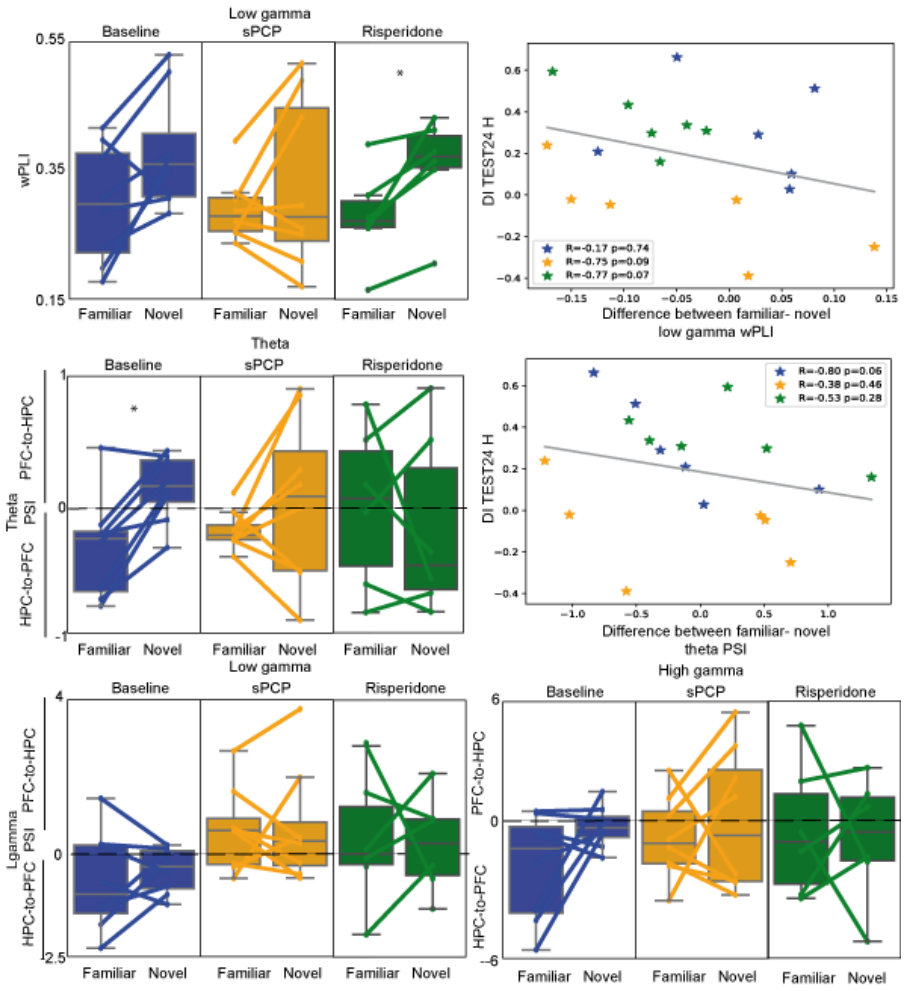

Figure 6.2.2.4: PFC-HPC circuit activity during long-term memory in baseline, sPCP and risperidone groups. The upper panels present the changes between familiar and novel object interactions of low gamma wPLI (upper left) and the correlation between the difference of familiar and novel object low gamma wPLI with the long-term memory performance (upper right). The middle panels represent the theta PSI (middle left) and the correlation between the difference of familiar and novel object theta PSI with the long-term memory performance (middle right). The lower panels present the low gamma PSI (lower left) and high gamma PSI (lower right). Note the color used: blue for baseline,

orange for sPCP and green for risperidone. Dashed lines represent no change in signal directionality. Each line corresponds to one mouse.

These results also evidenced that risperidone was unable to recover the non-specific disruptions of PFC-HPC circuits produced by sPCP, especially in the HPC (Table 4 and Fig. 6.2.2.5). However, risperidone selectively rescued specific biomarkers linked to the encoding of memories, which may have favored its improvement of memory performance. For instance, during memory acquisition, risperidone could restore the theta directionality ([shuffle corrected]: $p = 0.051$) by recovering the PFC-to-HPC signal directionality during the first explorations ($p = 0.035$). During long-term memory, the increased low gamma phase synchrony during novel object explorations compared to familiar object explorations could be a potential biomarker of memory retrieval after the chronic risperidone treatment for the memory retrieval ([shuffle corrected]: $p = 0.008$).

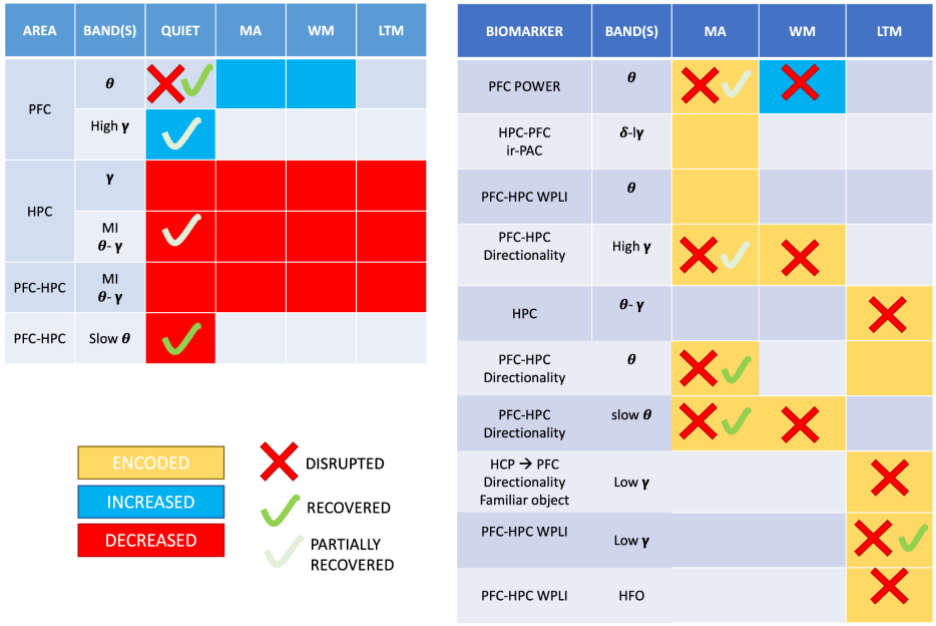

Table 4: Effects of chronic risperidone on the PFC-HPC neural activity changes induced by sPCP and the PFC-HPC neurophysiological biomarkers encoding different types of memory. Acronyms: MA (memory acquisition), WM (working memory), LTM (long-term memory), **δ** (delta), **θ** (theta), ***γ*** (gamma), **θ-*γ*** (theta-gamma coupling) and HFO (high frequency oscillations).

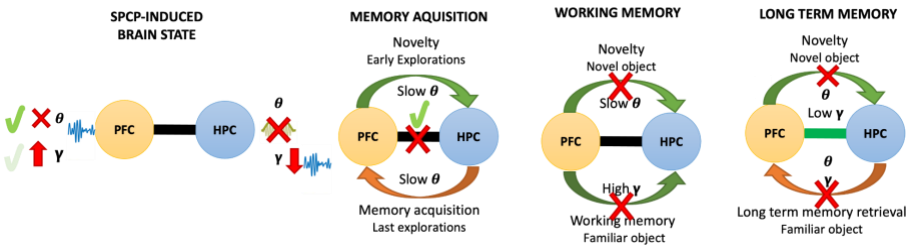

Figure 6.2.2.5: Schematic summary of risperidone effects insPCP-induced alterations and in PFC-HPC neural dynamics during memory acquisition, working memory and long-term memory. Note that the green tick represents total recovery while

the light green partial recovery. Note that in the long-term memory plot the recovery of low gamma phase synchrony is marked by the green line that connects both areas.

6.3. Amelioration of prefrontal cortex alterations during perception and attention

Finally, we investigated whether the risperidone treatment (n = 5 mice) corrected the sPCP-induced aberrant sensory processing in the PFC. We assessed risperidone's effects on the three auditory tasks 48 hours after the last injection of the treatment (Table 5).

First, risperidone could partially recover the response rate with respect to sPCP treatment alone during the auditory evoked potential task ($F_{1,4}$ = 4.55, p = 0.048, repeated measures ANOVA within baseline, sPCP and risperidone), indicating improved auditory processing. Furthermore, risperidone partially rescued the decreased spiking activity associated with P2 ($F_{2,10}$ = 2.49, p = 0.076) and the reduced amplitude and spiking activity associated with the P3 component ([amplitude, spiking activity]: $F_{1,4}$ = 3.92, 2.28, p = 0.065, 0.097). Altogether, these results suggested a partial recovery of auditory processing with respect to sPCP (Fig. 6.3.1).

However, risperidone could not correct the reduced MMN in the 6000 Hz protocol produced by sPCP (Fig. 6.3.2).

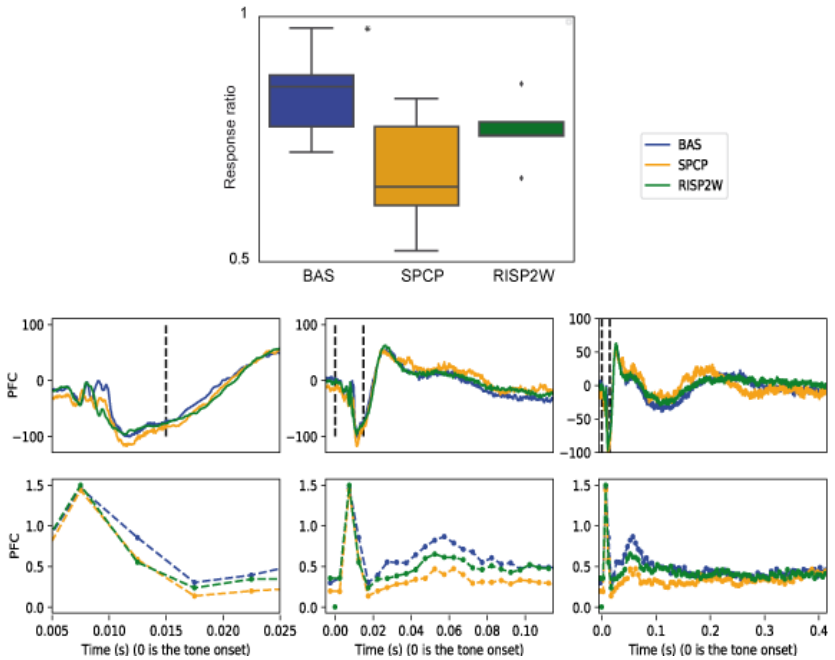

Figure 6.3.1: PFC auditory evoked potential comparing baseline, sPCP and risperidone groups. The upper panel shows the response rate of the auditory evoked potential. The lower panels represent the auditory evoked potentials (middle, voltage) and multi-unit activity (lower, spikes per 10 ms) at different time scales.

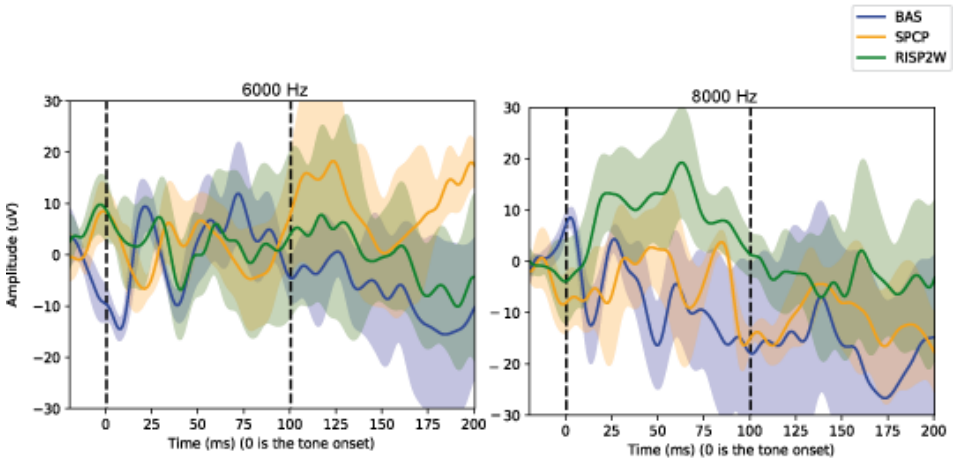

Figure 6.3.2: PFC mismatch negativity (MMN) response comparing baseline, sPCP and risperidone groups. The left panel represents the 6000 Hz MMN and the right panel represents the 8000 Hz MMN.

TASK	BIOMARKERS	POWER	MUA
AEP	P2		✓
	P3	✓	✓
ASSR	40 Hz POWER		
	40 Hz ITC		
ODDBALL PARADIGM	MMN 6000 Hz		
	MMN 8000 Hz		

INCREASED
DECREASED
RECOVERED
PARTIALLY RECOVERED

Table 5: Summary of risperidone's effects on the sPCP-induced changes in auditory perception and processing.

7. DISCUSSION

7. DISCUSSION

7.1. Discussion of chapter I: Neural correlates of psychosis-like states induced by acute phencyclidine and rescuing effects by antipsychotic medication

In the first project of the thesis we found that the psychotomimetic effects of PCP were associated with hypersynchronization and disordered communication of PFC-HPC pathways. Acute PCP induced major alterations in the PFC: it boosted oscillatory power at atypical frequencies within delta, gamma and high frequency ranges and generated delta-HFO coupling that suggested the presence of hypersynchronous cortical microcircuits. Inter-regional coupling and phase coherence of equivalent bands were also enhanced, reflecting increased synchronization of the circuit. PCP also diverted intrinsic HPC-to-PFC theta signals into fast delta rhythms traveling in the opposite direction, from the PFC to the HPC. PFC-HPC circuits were initially governed by fast delta rhythms following the administration of PCP. The circuit later transitioned into a state dominated by aberrant rhythms at higher frequencies while the delta drive was attenuated. These events disrupted the normal function of the circuit, weakening inherent HPC theta oscillations, theta-gamma coupling and

theta connectivity. The two atypical antipsychotic drugs, risperidone and clozapine, but not the classical antipsychotic drug haloperidol, reduced the aberrant power, coupling and circuit connectivity produced by PCP. In fact, haloperidol exacerbated several PCP-induced alterations, including PFC fast delta and fast delta-HFO coupling, HPC high gamma oscillations, and cortical delta signals. This suggests that PFC-HPC pathways may be a major target for atypical antipsychotic drugs, but not typical antipsychotic drugs, to elicit antipsychotic actions. Notably, clozapine was the only drug that fully rescued the signal directionality within the circuit, which is a crucial point considering that disrupted circuit communication is a hallmark of schizophrenia (Godsil et al., 2013; Hunt et al., 2017b). It should be noted that to differentiate between basal and pathological processes we have named slow theta or fast delta, respectively, the intermediate frequencies between delta and theta. Fast delta was an aberrant band produced by acute PCP that corresponded with a broader enhancement of delta frequencies, 2-7 Hz, whereas slow theta, in the next chapter, corresponded to a specific band within the theta range, 4-8 Hz, which was associated with cognitive processes in basal conditions.

The fast delta rhythms observed after the administration of acute PCP support the proposed mechanism of a large-scale delta connectivity in schizophrenia (Hunt et al., 2017b; Hunt and Kasicki, 2013). Brain wide aberrant delta activity is commonly found in patients with schizophrenia during wakefulness (Siekmeier and Stufflebeam, 2010), for example, interhemispheric delta coupling is observed during hallucinations (Spencer et al., 2009). Delta oscillations in the cortex arise from intrinsically bursting layer 5 pyramidal cells that are mediated between $GABA_B$ receptor inhibition and recurrent excitation (Hunt et al., 2017b). Therefore excessive delta power may be a biomarker of disinhibition of pyramidal neurons due to NMDAR hypofunction in GABAergic interneurons. Interestingly, here atypical antipsychotic drugs, but not haloperidol, enhanced slower delta rhythms while decreasing fast delta rhythms that correlated with sedative states. Sedation was also observed following the administration of the 5-HT_{2A}R antagonist M100907, which is consistent with previous studies suggesting that antipsychotic drugs-induced sedation depends on 5-HT_{2A}R transmission (Joshi et al., 2017; Williams et al., 2012). In fact, we have recently shown that sedative effects by antipsychotic drugs may result from the cooperation between 5-HT_{2A}/D2R antagonism and 5-HT_{1A} agonism (Gener et al., 2019). Overall,

synchronization at fast delta was associated with psychosis-like states whereas synchronization at slow delta was associated with sedative states.

Fast delta synchronization produced by acute PCP entrained aberrant network activities at high gamma and HFOs, consequently boosting their power, coupling, and circuit coherence. Cortical gamma increases emerge during psychosis in healthy individuals and patients diagnosed with schizophrenia and are subsequently recovered by antipsychotic drugs (Jones et al., 2012; Shaw et al., 2015; Uhlhaas and Singer, 2010). In rodents, NMDAR antagonists also increase gamma oscillations in cortical regions and this increase can also be rescued by antipsychotic drugs (Ahnaou et al., 2017; Caixeta et al., 2013; Hunt et al., 2017b; Phillips et al., 2012). We found that risperidone, clozapine and the serotonergic drugs reduced acute PCP-amplified PFC high gamma power, while haloperidol did not. This finding suggests that 5-HT_{2A}R antagonism and 5-HT_{1A}R agonism play causal roles in atypical antipsychotic drugs' ability to attenuate aberrant cortical gamma power. HFOs (<100 Hz) have been investigated in humans in the context of epilepsy but much less in psychosis, likely due to the technical limitations of detecting HFOs by scalp EEG and MEG (Zijlmans et al., 2012). Therefore, an association

between psychosis and HFOs still needs to be established at a clinical level. Intracerebral recordings in rodents show that the NMDAR antagonists, PCP and ketamine, produce substantial increases in the power of HFOs and HFO coupling with delta waves in several brain regions including cortical areas, the HPC, and the nucleus accumbens (Hunt et al., 2017b, 2015; Pittman-Polletta et al., 2018). Previous studies have shown that mesolimbic theta and delta oscillations that modulate HFO amplitude are driven by rhythmic activity generated in HPC and PFC, respectively, in which both compete for the control of the circuit (Pittman-Polletta et al., 2018). Accordingly, we also found that acute PCP produced significant increases in PFC HFO power and coupling of HFOs with delta oscillations, which were subsequently reduced by risperidone but not by haloperidol or clozapine. Additionally, M100907 and 8-OH-DPAT rescued PCP-induced HFOs, which suggests that 5-HT_{2A}R antagonism and 5-HT_{1A}R agonism may mediate risperidone' ability to recover PFC HFOs.

Previous studies suggest that abnormal activity of parvalbumin-expressing (PV+) interneurons may be responsible for the increase of gamma oscillations in schizophrenia. In support of this, postmortem studies of schizophrenia patients report reduced GABA synthesis in PV+ neurons

(Gonzalez-Burgos et al., 2015). Moreover, mice lacking NMDARs on PV+ neurons have increased spontaneous gamma power in the HPC and cortex (Carlén et al., 2012; Guyon et al., 2021; Korotkova et al., 2010a). Therefore, in our study the blockade of NMDARs on PV+ neurons by acute PCP may have been critically involved in the amplification of high gamma oscillations. Importantly, different subpopulations of PV+ neurons in the PFC express 5-HT_{1A}R and 5-HT_{2A}R (Puig et al., 2010), rendering these neurons key elements in the gamma reduction mediated by atypical antipsychotic drugs. In contrast, the neural mechanisms underlying PCP-mediated HFO are not clear. A recent study has found a close correlation between the firing rates of PV+ neurons and HFOs in the medial PFC of healthy animals, although a causal relationship could not be established (Yao et al., 2020). Moreover, local blockade of NMDARs in the nucleus accumbens increases the power of HFOs (Hunt et al., 2010), although the neurons involved in generating these HFOs are unknown. Thus, the exact neural mechanisms underlying psychosis-associated HFOs in the PFC and HPC and their response to antipsychotic drugs will need further investigation.

Our results demonstrate that 5-HT_{2A}R antagonism and 5-HT_{1A}R agonism exert strong influences on PFC-HPC pathways under psychotic-like states and suggest that they likely contributed to the actions of risperidone and clozapine. In particular, the way in which the 5-HT_{2A}R antagonist, M100907, and risperidone blocked PCP's actions appeared to be similar, which likely reflects risperidone's strong affinity for 5-HT_{2A}Rs. Conversely, D2R antagonism by haloperidol produced little changes on the circuit's neural dynamics. This suggests that atypical antipsychotic drugs, but not typical antipsychotic drugs, target PFC-HPC pathways to elicit antipsychotic action.

In conclusion, the two atypical antipsychotic drugs, risperidone and clozapine, but not the typical antipsychotic drug, haloperidol, reduced PCP-induced hypersynchronization and disrupted circuit communication, which may point to a fundamentally different neural mechanism by which atypical antipsychotic drugs and typical antipsychotic drugs treat the core positive, negative and cognitive symptoms in schizophrenia. These differential effects likely reflect the different affinity of atypical antipsychotic drugs and haloperidol for serotonin and dopamine receptors. Our findings show that understanding how antipsychotic drugs affect PFC-

HPC neural dynamics in animal models may prove useful to gain insight into the cognitive and negative symptoms in schizophrenia and is imperative to make progress in the development of novel therapeutic interventions for neuropsychiatric diseases.

7.2. Discussion of chapter II and III: Neural substrates of sPCP-induced cognitive impairment and rescuing effects of risperidone

In the second project of this thesis, we observed that sPCP disrupted PFC-HPC neural circuitry that in turn impaired working memory, long-term memory, auditory evoked potential and the mismatch negativity (MMN). Across all experiments conducted, sPCP decreased local, HPC gamma power and local, HPC, and circuit, PFC_{phase}-HPC_{amp}, theta-gamma coupling. These results indicate that sPCP generated non-specific changes in PFC-HPC neural substrates that were independent of the brain state and cognitive task. Working memory and long-term memory were impaired by sPCP and this was accompanied by a disruption of PFC-HPC interregional flow of information at theta and gamma frequency ranges. In baseline conditions, these neurophysiological biomarkers were found to be associated with the encoding of memory. sPCP also disrupted the late

components of the auditory evoked potential and the MMN in the PFC, while there was no effect on the ASSR task. Finally, chronic risperidone rescued memory impairment and the late components of the auditory evoked potential. However, it was unable to restore sPCP-induced disruptions in PFC-HPC neural dynamics, only rescuing some neurophysiological biomarkers for memory. These results suggest that risperidone may use different compensatory circuits to recover the memory performance without reinstating the basal circuit activity.

sPCP produced non-selective gamma power alterations in the HPC and the PFC that were independent of brain state and cognitive task. These results support studies in patients with schizophrenia, in which alterations in gamma oscillations were found to be a key biomarker of the disorder (Uhlhaas and Singer, 2010). Previous studies have also shown that sPCP treatment causes a reduction of PV-interneuron density in the HPC (Abdul-Monim et al., 2007), accompanied by a reduction in pyramidal neuron firing rates (Korotkova et al., 2010b), which may underlie decreases in HPC gamma power in sPCP mice. In sPCP-treated mice we also observed the decrease in HPC gamma power was accompanied by the disruption of the local, HPC, and circuit, PFC_{phase}-HPC_{amp}, theta-gamma coupling. We

controlled for movement influencing the change in theta-gamma coupling by analyzing epochs with similar levels of movement. Notably, the disruption in HPC gamma power was correlated with the reduction of local and circuit theta-gamma coupling, which could suggest that the disruption of both neurophysiological biomarkers was caused by a common mechanism. Furthermore, sPCP also enhanced gamma power in the PFC during quiet wakefulness, which may have been due to the disinhibition of pyramidal neurons caused by the NMDAR hypofunction in PV-interneurons (Sigurdsson, 2016). Gamma alterations were found in both the acute and subchronic PCP treatment, indicating that the PCP induced NMDAR antagonism produced a strong disruption of the PV-interneuron activity. Moreover, alterations in gamma oscillations in the PFC and the HPC induced by NMDAR hypofunction, has also been correlated with cognitive impairment, including tasks assessing working memory and object recognition (Carlén et al., 2012; Korotkova et al., 2010b).

During quiet wakefulness, PFC theta oscillations and PFC-HPC theta phase synchrony negatively correlated with long-term memory performance in sPCP mice. Interestingly, a negative correlation between PFC theta power and long-term memory performance was also found in another mouse model of cognitive impairment (Alemany-González et al.,

2020). These results suggest that PFC theta oscillations during quiet wakefulness could be a potential biomarker of long-term memory performance in models of cognitive impairment. Despite that PFC and PFC-HPC theta oscillatory function correlated with poor long-term memory performance, we did not observe significant differences between PFC theta power or theta synchrony before and after the sPCP treatment. This could suggest that there is one mechanism generating pathological theta rhythms found in sPCP mice that correlates with poor memory performance, and a separate mechanism generating basal theta rhythms found in baseline and saline conditions, which does not correlate with memory performance. Theta oscillations are modulated by interneurons and the dopaminergic system (Benchenane et al., 2011), which can be altered by sPCP (Cadinu et al., 2018; Sigurdsson, 2016). Therefore, sPCP induced alterations in interneuron activity and the dopaminergic system may underlie the generation of pathological theta oscillations that are correlated with impaired long-term memory in sPCP mice.

Our results from the NOR task in baseline conditions suggest that memories were encoded through the flow of information throughout the PFC-HPC circuit at theta and gamma frequency ranges. PFC-to-HPC gamma signals encoded working memory, whereas HPC-to-PFC gamma

signals encoded long-term memory retrieval. A previous study also found that HPC-to-PFC gamma directionality was relevant for long-term memory retrieval in wild-type mice, further supporting our findings (Alemany-González et al., 2020). PFC-to-HPC theta directionality encoded novelty during all phases of the NOR, whereas HPC-to-PFC theta directionality was associated with the acquisition and retrieval of long-term memories. Previous studies show that novel experiences initiate molecular signaling in the PFC producing modifications in synaptic connectivity. Moreover, these modifications in synaptic connectivity are connected with neural activity in the HPC (Takehara-Nishiuchi, 2020), where the memory is stored (Eichenbaum, 2004). The disruption of the synaptic connectivity leads to impaired memory formation (Takehara-Nishiuchi, 2020), further suggesting that memory encoding and retrieval is dependent on PFC-HPC pathways. To conclude, our results suggest that the new information (novelty) or the information stored recently (working memory) uses PFC-to-HPC connectivity at theta or gamma frequency ranges, respectively, to encode the recognition of a novel or recent familiar object, whereas HPC-to-PFC flow of information may be associated with acquisition and retrieval of the memory.

Various studies have shown that sPCP treatment produces disruptions in recognition memory during the NOR task (Cadinu et al., 2018; Castañé et al., 2015; Rajagopal et al., 2016b), which we replicated in this thesis. We found that sPCP-treated animals exhibited impaired performance in NOR tasks assessing working and long-term memory. Poor performance resulted from an equal number of visits to the familiar and novel objects, which suggests the animal encoded both objects as novel and thus did not recognize the familiar object. Previous studies show that the increase of HPC gamma oscillations is important for memory load in humans (van Vugt et al., 2010) and rodents (Zheng et al., 2016). Moreover, patients with schizophrenia also show decreased HPC recruitment during default mode network which is associated with memory encoding (Gurler et al., 2021). Therefore, the constant disruption of HPC gamma oscillations in sPCP-treated animals could be a mechanism underlying their memory impairment. In addition, sPCP treatment also disrupted PFC-HPC flow of information at theta and gamma frequency ranges, which we found to be important neurophysiological biomarkers in memory recognition. In conclusion, sPCP mice exhibit impairments in working and long-term memory due to the sPCP induced disruption in the neurophysiological biomarkers relevant for the encoding of memories.

Patients with schizophrenia present impairments in auditory perception and processing that are related with positive symptoms (Galderisi et al., 2014) and cognitive disability (Javitt and Sweet, 2015). Our results show that in the PFC of sPCP treated mice there were similar disturbances in the late components of the auditory evoked potential and the mismatch negativity (MMN), but not in the early component of the auditory-evoked potential or the ASSR. During the auditory evoked potential tests, we found disruptions in the P3 component that corresponded with decreased spiking activity after the sPCP treatment. Alterations in the P3 component have been associated with attention-mediated processing deficits and it's one of the most replicated findings in patients with schizophrenia (Hamilton et al., 2019; Turetsky et al., 2015). Another relevant biomarker of schizophrenia is a reduction in the MMN, a measure that has been related with cognitive and psychosocial abilities (Fitzgerald and Todd, 2020; Koshiyama et al., 2020). We found sPCP-treated mice replicated these alterations, suggesting they also have impairments in cognitive processing and attention. However, sPCP-treated mice did not present deficits on the ASSR biomarker, which is also a classical biomarker in patients with schizophrenia (O'Donnell et al., 2013). These results indicate that sPCP mice conserved the evoked gamma activities in the PFC.

Furthermore, we did not observe alterations in the early components of the auditory evoked potential, which have been associated with positive symptoms (Galderisi et al., 2014). Electrophysiological recordings in the auditory cortex would be necessary to confirm these results as the auditory cortex has shown more consistent alterations in the early components of the auditory evoked potential and the ASSR in patients and rodent models (Wang et al., 2020).

Chronic risperidone rescued memory impairment and the late components of the auditory evoked potential. However, it was unable to restore sPCP-induced anomalous PFC-HPC neural dynamics. Acute risperidone has proved to be effective in restoring cognitive deficits in the sPCP mouse model of schizophrenia (Cadinu et al., 2018; Grayson et al., 2007; Meltzer et al., 2011). In our project, we also showed that a chronic treatment also reversed the memory deficits induced by sPCP treatment. Furthermore, clinical studies investigating schizophrenic patients treated with risperidone demonstrate that risperidone can mildly improve cognition (Houthoofd et al., 2008) and partially rescue the auditory processing (Umbricht et al., 1999). Moreover, antipsychotic medication modulates the decreased HPC recruitment during the memory encoding (Gurler et al., 2021). In our study, we found that risperidone rescued memory impairment

and the late components of the auditory evoked potential as well as some of the neurophysiological biomarkers relevant for the memory performance. However, the chronic risperidone treatment was unable to reverse sPCP-induced anomalous PFC-HPC neural dynamics. The incomplete rescue of the circuit by risperidone may be due to irreversible changes produced by the sPCP treatment. In conclusion, our results suggest that risperidone recovered memory impairments through correcting certain neurophysiological biomarkers or by activating compensatory mechanisms that involved other areas, however it was unable to recover the most relevant sPCP-induced changes.

We note that this thesis presents several limitations that should be taken into account when interpreting the results. First, all the treatments consisted of a series of injections which may have caused stress in the mice and resulted in behavioral deficits such as depression or anxiety which may have influenced memory performance (Lezak et al., 2017; Strekalova and Steinbusch, 2010). Mice treated with two consecutive saline treatments conserved the baseline PFC-HPC circuit neural dynamics, and performance on the auditory and working memory tasks, however they exhibited an impairment in long-term memory. Mice treated with one saline treatment conserved most baseline neural dynamics and

performance and did not exhibit any impairments. This suggests that most of the alterations produced by the sPCP and risperidone treatment were not affected by stress, however some neurophysiological biomarkers could possibly be disrupted by chronic stress and cause memory impairment. Moreover, further analyses and experiments looking at the single unit activity or involving optogenetic manipulations need to be performed in order to understand the cellular mechanisms that caused the sPCP-induced deficits and partial recovery by, with emphasis on the involvement of PV-interneurons.

In conclusion, the sPCP treatment produced alterations in gamma and theta oscillations which were associated with impaired memory and auditory processes, similarly to the observations found in patients with schizophrenia. The chronic risperidone treatment could ameliorate memory performance by rescuing some of the neurophysiological PFC-HPC biomarkers or activating compensatory mechanisms, but it was unable to restore the sPCP-induced abnormal neural activity within PFC-HPC circuits. Finally, our findings showed that understanding the neural substrates of PFC-HPC circuits during cognitive tasks in a pharmacological model of schizophrenia and how they are affected by atypical antipsychotic treatments may be useful to gain insight into the

cognitive symptoms in schizophrenia, which in turn could help further the development of new therapeutic interventions for neuropsychiatric diseases.

8. CONCLUSIONS

8. CONCLUSIONS

1. Acute PCP administration produced hypersynchronization and disruption of connectivity of PFC-HPC circuits.
2. Atypical antipsychotic drugs reduced PFC-HPC hypersynchronization and disrupted connectivity induced by PCP. However, the classical antipsychotic drug, haloperidol, was unable to restore the PCP-induced aberrant neural dynamics.
3. Atypical antipsychotic drugs' greater affinity for serotonin 1A and 2A receptors may explain their differential effects with haloperidol.
4. sPCP treatment produced non-specific brain state alterations in gamma oscillatory activity and theta-gamma modulation.
5. PFC theta power and PFC-HPC theta synchrony during quiet wakefulness may be potential biomarkers of long-term memory performance in mouse models of cognitive impairment.
6. In basal conditions, theta and gamma functional connectivity, especially the signal directionality between PFC-HPC circuits, correlated strongly with the encoding of novelty, memory acquisition, memory retrieval and working memory.

7. After the sPCP treatment, working memory and long-term memory performance was disrupted, along with the PFC-HPC neurophysiological biomarkers that encoded it.
8. sPCP treatment also disrupted the late components of the auditory evoked potential and the MMN. These results are comparable to alterations in auditory and attentional processing observed in patients with schizophrenia. However, there was no change in the ASSR task, indicating no alterations in evoked gamma activity.
9. Chronic risperidone rescued memory impairment and the late components of the auditory evoked potential. However, it was unable to restore sPCP-induced anomalous PFC-HPC neural dynamics, only rescuing some neurophysiological biomarkers for memory. This implicates other compensatory mechanisms outside the PFC-HPC axis that will need further elucidation.

9. BIBLIOGRAPHY

9. BIBLIOGRAPHY

Delgado-Sallent, C., Nebot P., Gener T., Timplalexi M., Fath A.B., Puig M.V. (2021). Phencyclidine-induced psychosis causes hypersynchronization and disruption of connectivity within prefrontal-hippocampal circuits that is rescued by antipsychotic drugs. ***bioRxiv*****. 2021.02.03.429582**

Bibliography

Abdul-Monim, Z., Neill, J.C., Reynolds, G.P., 2007. Sub-chronic psychotomimetic phencyclidine induces deficits in reversal learning and alterations in parvalbumin-immunoreactive expression in the rat. J. Psychopharmacol. Oxf. Engl. 21, 198–205. https://doi.org/10.1177/0269881107067097

Ahnaou, A., Huysmans, H., Van de Casteele, T., Drinkenburg, W.H.I.M., 2017. Cortical high gamma network oscillations and connectivity: a translational index for antipsychotics to normalize aberrant neurophysiological activity. Transl. Psychiatry 7, 1285–1285. https://doi.org/10.1038/s41398-017-0002-9

Alemany-González, M., Gener, T., Nebot, P., Vilademunt, M., Dierssen, M., Puig, M.V., 2020. Prefrontal-hippocampal functional

connectivity encodes recognition memory and is impaired in intellectual disability. Proc. Natl. Acad. Sci. 117, 11788–11798. https://doi.org/10.1073/pnas.1921314117
Alkan, E., Davies, G., Evans, S.L., 2021. Cognitive impairment in schizophrenia: relationships with cortical thickness in fronto-temporal regions, and dissociability from symptom severity. Npj Schizophr. 7, 1–9. https://doi.org/10.1038/s41537-021-00149-0
Allen, R.M., Young, S.J., 1978. Phencyclidine-induced psychosis. Am. J. Psychiatry 135, 1081–1084. https://doi.org/10.1176/ajp.135.9.1081
Amad, A., Cachia, A., Gorwood, P., Pins, D., Delmaire, C., Rolland, B., Mondino, M., Thomas, P., Jardri, R., 2014. The multimodal connectivity of the hippocampal complex in auditory and visual hallucinations. Mol. Psychiatry 19, 184–191. https://doi.org/10.1038/mp.2012.181
Aru, Juhan, Aru, Jaan, Priesemann, V., Wibral, M., Lana, L., Pipa, G., Singer, W., Vicente, R., 2015. Untangling cross-frequency coupling in neuroscience. Curr. Opin. Neurobiol. 31, 51–61. https://doi.org/10.1016/j.conb.2014.08.002
Bastos, A.M., Schoffelen, J.-M., 2015. A Tutorial Review of Functional Connectivity Analysis Methods and Their Interpretational Pitfalls. Front. Syst. Neurosci. 9, 175. https://doi.org/10.3389/fnsys.2015.00175
Benchenane, K., Tiesinga, P.H., Battaglia, F.P., 2011. Oscillations in the prefrontal cortex: a gateway to memory and attention. Curr. Opin. Neurobiol., Behavioural and cognitive neuroscience 21, 475–485. https://doi.org/10.1016/j.conb.2011.01.004
Berumen, L.C., Rodríguez, A., Miledi, R., García-Alcocer, G., 2012. Serotonin receptors in hippocampus. ScientificWorldJournal 2012, 823493. https://doi.org/10.1100/2012/823493
Blair, D.T., Dauner, A., 1992. Extrapyramidal symptoms are serious side-effects of antipsychotic and other drugs. Nurse Pract. 17, 56, 62–64, 67. https://doi.org/10.1097/00006205-199211000-00018
Bostwick, J.R., Guthrie, S.K., Ellingrod, V.L., 2009. Antipsychotic-induced hyperprolactinemia. Pharmacotherapy 29, 64–73. https://doi.org/10.1592/phco.29.1.64
Brincat, S.L., Miller, E.K., 2015. Frequency-specific hippocampal-prefrontal interactions during associative learning. Nat. Neurosci. 18, 576–581. https://doi.org/10.1038/nn.3954
Bruijnzeel, D., Suryadevara, U., Tandon, R., 2014. Antipsychotic

treatment of schizophrenia: An update. Asian J. Psychiatry, This issue includes a Special Section on Classification of Psychiatric Disorders 11, 3–7. https://doi.org/10.1016/j.ajp.2014.08.002
Buzsáki, G., Chrobak, J.J., 1995. Temporal structure in spatially organized neuronal ensembles: a role for interneuronal networks. Curr. Opin. Neurobiol. 5, 504–510. https://doi.org/10.1016/0959-4388(95)80012-3
Buzsáki, G., Draguhn, A., 2004. Neuronal oscillations in cortical networks. Science 304, 1926–1929. https://doi.org/10.1126/science.1099745
Cadinu, D., Grayson, B., Podda, G., Harte, M.K., Doostdar, N., Neill, J.C., 2018. NMDA receptor antagonist rodent models for cognition in schizophrenia and identification of novel drug treatments, an update. Neuropharmacology 142, 41–62. https://doi.org/10.1016/j.neuropharm.2017.11.045
Caixeta, F.V., Cornélio, A.M., Scheffer-Teixeira, R., Ribeiro, S., Tort, A.B.L., 2013. Ketamine alters oscillatory coupling in the hippocampus. Sci. Rep. 3, 2348. https://doi.org/10.1038/srep02348
Canetta, S.E., Brown, A.S., 2012. PRENATAL INFECTION, MATERNAL IMMUNE ACTIVATION, AND RISK FOR SCHIZOPHRENIA. Transl. Neurosci. 3, 320–327. https://doi.org/10.2478/s13380-012-0045-6
Canolty, R.T., Edwards, E., Dalal, S.S., Soltani, M., Nagarajan, S.S., Kirsch, H.E., Berger, M.S., Barbaro, N.M., Knight, R.T., 2006. High Gamma Power Is Phase-Locked to Theta Oscillations in Human Neocortex. Science 313, 1626–1628. https://doi.org/10.1126/science.1128115
Carlén, M., Meletis, K., Siegle, J.H., Cardin, J.A., Futai, K., Vierling-Claassen, D., Rühlmann, C., Jones, S.R., Deisseroth, K., Sheng, M., Moore, C.I., Tsai, L.-H., 2012. A critical role for NMDA receptors in parvalbumin interneurons for gamma rhythm induction and behavior. Mol. Psychiatry 17, 537–548. https://doi.org/10.1038/mp.2011.31
Castañé, A., Santana, N., Artigas, F., 2015. PCP-based mice models of schizophrenia: differential behavioral, neurochemical and cellular effects of acute and subchronic treatments. Psychopharmacology (Berl.) 232, 4085–4097. https://doi.org/10.1007/s00213-015-3946-6
Celada, Pau, Puig, M.V., Artigas, F., 2013. Serotonin modulation of

cortical neurons and networks. Front. Integr. Neurosci. 7, 25. https://doi.org/10.3389/fnint.2013.00025
Celada, P., Puig, M.V., Artigas, F., 2013. Serotonin modulation of cortical neurons and networks. Front. Integr. Neurosci. https://doi.org/10.3389/fnint.2013.00025
Cho, K.K.A., Hoch, R., Lee, A.T., Patel, T., Rubenstein, J.L.R., Sohal, V.S., 2015. Gamma rhythms link prefrontal interneuron dysfunction with cognitive inflexibility in Dlx5/6(+/-) mice. Neuron 85, 1332–1343. https://doi.org/10.1016/j.neuron.2015.02.019
Choi, S., Yu, E., Lee, S., Llinás, R.R., 2015. Altered thalamocortical rhythmicity and connectivity in mice lacking CaV3.1 T-type Ca2+ channels in unconsciousness. Proc. Natl. Acad. Sci. U. S. A. 112, 7839–7844. https://doi.org/10.1073/pnas.1420983112
Colgin, L.L., 2015. Do slow and fast gamma rhythms correspond to distinct functional states in the hippocampal network? Brain Res. 1621, 309–315. https://doi.org/10.1016/j.brainres.2015.01.005
Condé, F., Maire-Lepoivre, E., Audinat, E., Crépel, F., 1995. Afferent connections of the medial frontal cortex of the rat. II. Cortical and subcortical afferents. J. Comp. Neurol. 352, 567–593. https://doi.org/10.1002/cne.903520407
Conn, K.-A., Burne, T.H.J., Kesby, J.P., 2020. Subcortical Dopamine and Cognition in Schizophrenia: Looking Beyond Psychosis in Preclinical Models. Front. Neurosci. 14, 542. https://doi.org/10.3389/fnins.2020.00542
Correll, C.U., Schooler, N.R., 2020. Negative Symptoms in Schizophrenia: A Review and Clinical Guide for Recognition, Assessment, and Treatment. Neuropsychiatr. Dis. Treat. 16, 519–534. https://doi.org/10.2147/NDT.S225643
Cosgrove, J., Newell, T.G., 1991. Recovery of neuropsychological functions during reduction in use of phencyclidine. J. Clin. Psychol. 47, 159–169. https://doi.org/10.1002/1097-4679(199101)47:1<159::aid-jclp2270470125>3.0.co;2-o
Coyle, J.T., 2012. NMDA receptor and schizophrenia: a brief history. Schizophr. Bull. 38, 920–926. https://doi.org/10.1093/schbul/sbs076
Cruz, J.F.O. da, Gomis-Gonzalez, M., Maldonado, R., Marsicano, G., Ozaita, A., Busquets-Garcia, A., 2020. An Alternative Maze to Assess Novel Object Recognition in Mice. Bio-Protoc. 10, e3651–e3651.

Dickerson, D.D., Bilkey, D.K., 2013. Aberrant neural synchrony in the maternal immune activation model: using translatable measures to explore targeted interventions. Front. Behav. Neurosci. 7, 217. https://doi.org/10.3389/fnbeh.2013.00217

Duan, A.R., Varela, C., Zhang, Y., Shen, Y., Xiong, L., Wilson, M., Lisman, J., 2015. Delta frequency optogenetic stimulation of a thalamic nucleus reuniens is sufficient to produce working memory deficits; relevance to schizophrenia. Biol. Psychiatry 77, 1098–1107. https://doi.org/10.1016/j.biopsych.2015.01.020

Ehrlich, S., Brauns, S., Yendiki, A., Ho, B.-C., Calhoun, V., Schulz, S.C., Gollub, R.L., Sponheim, S.R., 2012. Associations of Cortical Thickness and Cognition in Patients With Schizophrenia and Healthy Controls. Schizophr. Bull. 38, 1050–1062. https://doi.org/10.1093/schbul/sbr018

Eichenbaum, H., 2004. Hippocampus: cognitive processes and neural representations that underlie declarative memory. Neuron 44, 109–120. https://doi.org/10.1016/j.neuron.2004.08.028

Fett, A.-K.J., Velthorst, E., Reichenberg, A., Ruggero, C.J., Callahan, J.L., Fochtmann, L.J., Carlson, G.A., Perlman, G., Bromet, E.J., Kotov, R., 2020. Long-term Changes in Cognitive Functioning in Individuals With Psychotic Disorders: Findings From the Suffolk County Mental Health Project. JAMA Psychiatry 77, 387–396. https://doi.org/10.1001/jamapsychiatry.2019.3993

Fitzgerald, K., Todd, J., 2020. Making Sense of Mismatch Negativity. Front. Psychiatry 11, 468. https://doi.org/10.3389/fpsyt.2020.00468

Fletcher, P.C., Frith, C.D., 2009. Perceiving is believing: a Bayesian approach to explaining the positive symptoms of schizophrenia. Nat. Rev. Neurosci. 10, 48–58. https://doi.org/10.1038/nrn2536

Flores, F.J., Ching, S., Hartnack, K., Fath, A.B., Purdon, P.L., Wilson, M.A., Brown, E.N., 2015. A PK-PD model of ketamine-induced high-frequency oscillations. J. Neural Eng. 12, 056006. https://doi.org/10.1088/1741-2560/12/5/056006

Ford, J.M., Dierks, T., Fisher, D.J., Herrmann, C.S., Hubl, D., Kindler, J., Koenig, T., Mathalon, D.H., Spencer, K.M., Strik, W., van Lutterveld, R., 2012. Neurophysiological studies of auditory verbal hallucinations. Schizophr. Bull. 38, 715–723. https://doi.org/10.1093/schbul/sbs009

Ford, J.M., Roach, B.J., Faustman, W.O., Mathalon, D.H., 2007. Synch before you speak: auditory hallucinations in schizophrenia. Am. J.

Psychiatry 164, 458–466. https://doi.org/10.1176/ajp.2007.164.3.458
Fries, P., 2015. Rhythms for Cognition: Communication through Coherence. Neuron 88, 220–235. https://doi.org/10.1016/j.neuron.2015.09.034
Friese, U., Köster, M., Hassler, U., Martens, U., Trujillo-Barreto, N., Gruber, T., 2013. Successful memory encoding is associated with increased cross-frequency coupling between frontal theta and posterior gamma oscillations in human scalp-recorded EEG. NeuroImage 66, 642–647. https://doi.org/10.1016/j.neuroimage.2012.11.002
Frohlich, J., Van Horn, J.D., 2014. Reviewing the ketamine model for schizophrenia. J. Psychopharmacol. Oxf. Engl. 28, 287–302. https://doi.org/10.1177/0269881113512909
Galderisi, S., Vignapiano, A., Mucci, A., Boutros, N.N., 2014. Physiological correlates of positive symptoms in schizophrenia. Curr. Top. Behav. Neurosci. 21, 103–128. https://doi.org/10.1007/7854_2014_322
Gardoni, F., Bellone, C., 2015. Modulation of the glutamatergic transmission by Dopamine: a focus on Parkinson, Huntington and Addiction diseases. Front. Cell. Neurosci. 9, 25. https://doi.org/10.3389/fncel.2015.00025
Gener, T., Tauste Campo, A., Alemany-González, M., Nebot, P., Delgado-Sallent, C., Chanovas, J., Puig, M.V., 2019. Serotonin 5-HT1A, 5-HT2A and dopamine D2 receptors strongly influence prefronto-hippocampal neural networks in alert mice: Contribution to the actions of risperidone. Neuropharmacology 158, 107743–107743. https://doi.org/10.1016/j.neuropharm.2019.107743
Godsil, B.P., Kiss, J.P., Spedding, M., Jay, T.M., 2013. The hippocampal–prefrontal pathway: The weak link in psychiatric disorders? Eur. Neuropsychopharmacol. 23, 1165–1181. https://doi.org/10.1016/j.euroneuro.2012.10.018
Goldsmith, D.R., Rapaport, M.H., 2020. Inflammation and Negative Symptoms of Schizophrenia: Implications for Reward Processing and Motivational Deficits. Front. Psychiatry 11, 46. https://doi.org/10.3389/fpsyt.2020.00046
Gonzalez-Burgos, G., Cho, R.Y., Lewis, D.A., 2015. Alterations in cortical network oscillations and parvalbumin neurons in schizophrenia. Biol. Psychiatry 77, 1031–1040.

https://doi.org/10.1016/j.biopsych.2015.03.010
Gramfort, A., Luessi, M., Larson, E., Engemann, D., Strohmeier, D., Brodbeck, C., Goj, R., Jas, M., Brooks, T., Parkkonen, L., Hämäläinen, M., 2013. MEG and EEG data analysis with MNE-Python. Front. Neurosci. 7, 267. https://doi.org/10.3389/fnins.2013.00267
Grayson, B., Idris, N., Neill, J., 2007. Atypical antipsychotics attenuate a sub-chronic PCP-induced cognitive deficit in the novel object recognition task in the rat. Behav. Brain Res. 184, 31–38. https://doi.org/10.1016/j.bbr.2007.06.012
Green, M.F., Kern, R.S., Braff, D.L., Mintz, J., 2000. Neurocognitive Deficits and Functional Outcome in Schizophrenia: Are We Measuring the "Right Stuff"? Schizophr. Bull. 26, 119–136. https://doi.org/10.1093/oxfordjournals.schbul.a033430
Guderian, S., Schott, B.H., Richardson-Klavehn, A., Düzel, E., 2009. Medial temporal theta state before an event predicts episodic encoding success in humans. Proc. Natl. Acad. Sci. 106, 5365–5370. https://doi.org/10.1073/pnas.0900289106
Gulinello, M., Mitchell, H.A., Chang, Q., Timothy O'Brien, W., Zhou, Z., Abel, T., Wang, L., Corbin, J.G., Veeraragavan, S., Samaco, R.C., Andrews, N.A., Fagiolini, M., Cole, T.B., Burbacher, T.M., Crawley, J.N., 2019. Rigor and reproducibility in rodent behavioral research. Neurobiol. Learn. Mem. 165, 106780. https://doi.org/10.1016/j.nlm.2018.01.001
Gurler, D., White, D.M., Kraguljac, N.V., Ver Hoef, L., Martin, C., Tennant, B., Lahti, A.C., 2021. Neural Signatures of Memory Encoding in Schizophrenia are Modulated by Antipsychotic Treatment. Neuropsychobiology 80, 12–24. https://doi.org/10.1159/000506402
Guyon, N., Zacharias, L.R., Oliveira, E.F. de, Kim, H., Leite, J.P., Lopes-Aguiar, C., Carlén, M., 2021. Network asynchrony underlying increased broadband gamma power. J. Neurosci. https://doi.org/10.1523/JNEUROSCI.2250-20.2021
Hamilton, H.K., D'Souza, D.C., Ford, J.M., Roach, B.J., Kort, N.S., Ahn, K.-H., Bhakta, S., Ranganathan, M., Mathalon, D.H., 2018a. Interactive effects of an N-methyl-d-aspartate receptor antagonist and a nicotinic acetylcholine receptor agonist on mismatch negativity: Implications for schizophrenia. Schizophr. Res. 191, 87–94. https://doi.org/10.1016/j.schres.2017.06.040
Hamilton, H.K., Perez, V.B., Ford, J.M., Roach, B.J., Jaeger, J.,

Mathalon, D.H., 2018b. Mismatch Negativity But Not P300 Is Associated With Functional Disability in Schizophrenia. Schizophr. Bull. 44, 492–504. https://doi.org/10.1093/schbul/sbx104
Hamilton, H.K., Woods, S.W., Roach, B.J., Llerena, K., McGlashan, T.H., Srihari, V.H., Ford, J.M., Mathalon, D.H., 2019. Auditory and Visual Oddball Stimulus Processing Deficits in Schizophrenia and the Psychosis Risk Syndrome: Forecasting Psychosis Risk With P300. Schizophr. Bull. 45, 1068–1080. https://doi.org/10.1093/schbul/sby167
Hardmeier, M., Hatz, F., Bousleiman, H., Schindler, C., Stam, C.J., Fuhr, P., 2014. Reproducibility of functional connectivity and graph measures based on the phase lag index (PLI) and weighted phase lag index (wPLI) derived from high resolution EEG. PloS One 9, e108648–e108648. https://doi.org/10.1371/journal.pone.0108648
Hartung, H., Cichon, N., De Feo, V., Riemann, S., Schildt, S., Lindemann, C., Mulert, C., Gogos, J.A., Hanganu-Opatz, I.L., 2016. From Shortage to Surge: A Developmental Switch in Hippocampal-Prefrontal Coupling in a Gene-Environment Model of Neuropsychiatric Disorders. Cereb. Cortex N. Y. N 1991 26, 4265–4281. https://doi.org/10.1093/cercor/bhw274
Hashimoto, K., Fujita, Y., Shimizu, E., Iyo, M., 2005. Phencyclidine-induced cognitive deficits in mice are improved by subsequent subchronic administration of clozapine, but not haloperidol. Eur. J. Pharmacol. 519, 114–117. https://doi.org/10.1016/j.ejphar.2005.07.002
Heckers, S., Konradi, C., 2010. Hippocampal pathology in schizophrenia. Curr. Top. Behav. Neurosci. 4, 529–553. https://doi.org/10.1007/7854_2010_43
Hentschke, H., Perkins, M.G., Pearce, R.A., Banks, M.I., 2007. Muscarinic blockade weakens interaction of gamma with theta rhythms in mouse hippocampus. Eur. J. Neurosci. 26, 1642–1656. https://doi.org/10.1111/j.1460-9568.2007.05779.x
Hoffman, D.C., Donovan, H., 1995. Catalepsy as a rodent model for detecting antipsychotic drugs with extrapyramidal side effect liability. Psychopharmacology (Berl.) 120, 128–133. https://doi.org/10.1007/BF02246184
Homayoun, H., Moghaddam, B., 2007. NMDA receptor hypofunction produces opposite effects on prefrontal cortex interneurons and pyramidal neurons. J. Neurosci. Off. J. Soc. Neurosci. 27, 11496–

11500. https://doi.org/10.1523/JNEUROSCI.2213-07.2007
Hong, L.E., Summerfelt, A., Mitchell, B.D., O'Donnell, P., Thaker, G.K., 2012. A shared low-frequency oscillatory rhythm abnormality in resting and sensory gating in schizophrenia. Clin. Neurophysiol. 123, 285–292. https://doi.org/10.1016/j.clinph.2011.07.025
Horiguchi, M., Hannaway, K.E., Adelekun, A.E., Jayathilake, K., Meltzer, H.Y., 2012. Prevention of the Phencyclidine-Induced Impairment in Novel Object Recognition in Female Rats by Co-Administration of Lurasidone or Tandospirone, a 5-HT1A Partial Agonist. Neuropsychopharmacology 37, 2175–2183. https://doi.org/10.1038/npp.2012.64
Houthoofd, S.A.M.K., Morrens, M., Sabbe, B.G.C., 2008. Cognitive and psychomotor effects of risperidone in schizophrenia and schizoaffective disorder. Clin. Ther. 30, 1565–1589. https://doi.org/10.1016/j.clinthera.2008.09.014
Hunt, M.J., Falinska, M., Łęski, S., Wójcik, D.K., Kasicki, S., 2010. Differential effects produced by ketamine on oscillatory activity recorded in the rat hippocampus, dorsal striatum and nucleus accumbens: J. Psychopharmacol. (Oxf.). https://doi.org/10.1177/0269881110362126
Hunt, M.J., Kasicki, S., 2013. A systematic review of the effects of NMDA receptor antagonists on oscillatory activity recorded in vivo. J. Psychopharmacol. (Oxf.) 27, 972–986. https://doi.org/10.1177/0269881113495117
Hunt, M.J., Kopell, N.J., Traub, R.D., Whittington, M.A., 2017a. Aberrant Network Activity in Schizophrenia. Trends Neurosci. 40, 371–382. https://doi.org/10.1016/j.tins.2017.04.003
Hunt, M.J., Kopell, N.J., Traub, R.D., Whittington, M.A., 2017b. Aberrant network activity in schizophrenia. Trends Neurosci. 40, 371–382. https://doi.org/10.1016/j.tins.2017.04.003
Hunt, M.J., Olszewski, M., Piasecka, J., Whittington, M.A., Kasicki, S., 2015. Effects of NMDA receptor antagonists and antipsychotics on high frequency oscillations recorded in the nucleus accumbens of freely moving mice. Psychopharmacology (Berl.) 232, 4525–4535. https://doi.org/10.1007/s00213-015-4073-0
Itil, T., Keskiner, A., Kiremitci, N., Holden, J.M., 1967. Effect of phencyclidine in chronic schizophrenics. Can. Psychiatr. Assoc. J. 12, 209–212. https://doi.org/10.1177/070674376701200217
Javitt, D.C., Sweet, R.A., 2015. Auditory dysfunction in schizophrenia: integrating clinical and basic features. Nat. Rev. Neurosci. 16,

535–550. https://doi.org/10.1038/nrn4002
Jensen, O., Colgin, L.L., 2007. Cross-frequency coupling between neuronal oscillations. Trends Cogn. Sci. 11, 267–269. https://doi.org/10.1016/j.tics.2007.05.003
Jones, N.C., Reddy, M., Anderson, P., Salzberg, M.R., O'Brien, T.J., Pinault, D., 2012. Acute administration of typical and atypical antipsychotics reduces EEG γ power, but only the preclinical compound LY379268 reduces the ketamine-induced rise in γ power. Int. J. Neuropsychopharmacol. 15, 657–68. https://doi.org/10.1017/S1461145711000848
Joshi, R.S., Quadros, R., Drumm, M., Ain, R., Panicker, M.M., 2017. Sedative effect of Clozapine is a function of 5-HT2A and environmental novelty. Eur. Neuropsychopharmacol. 27, 70–81. https://doi.org/10.1016/j.euroneuro.2016.10.007
Joyce, J.N., Millan, M.J., 2005. Dopamine D3 receptor antagonists as therapeutic agents. Drug Discov. Today 10, 917–925. https://doi.org/10.1016/S1359-6446(05)03491-4
Kaar, S.J., Angelescu, I., Marques, T.R., Howes, O.D., 2019. Pre-frontal parvalbumin interneurons in schizophrenia: a meta-analysis of post-mortem studies. J. Neural Transm. Vienna Austria 1996 126, 1637–1651. https://doi.org/10.1007/s00702-019-02080-2
Kao, H.-Y., Dvořák, D., Park, E., Kenney, J., Kelemen, E., Fenton, A.A., 2017. Phencyclidine Discoordinates Hippocampal Network Activity But Not Place Fields. J. Neurosci. Off. J. Soc. Neurosci. 37, 12031–12049. https://doi.org/10.1523/JNEUROSCI.0630-17.2017
Kaplan, R., Bush, D., Bonnefond, M., Bandettini, P.A., Barnes, G.R., Doeller, C.F., Burgess, N., 2014. Medial prefrontal theta phase coupling during spatial memory retrieval. Hippocampus 24, 656–665. https://doi.org/10.1002/hipo.22255
Kesby, J.P., Eyles, D.W., McGrath, J.J., Scott, J.G., 2018. Dopamine, psychosis and schizophrenia: the widening gap between basic and clinical neuroscience. Transl. Psychiatry 8, 1–12. https://doi.org/10.1038/s41398-017-0071-9
Kocsis, B., Brown, R.E., McCarley, R.W., Hajos, M., 2013. Impact of ketamine on neuronal network dynamics: translational modeling of schizophrenia-relevant deficits. CNS Neurosci. Ther. 19, 437–447. https://doi.org/10.1111/cns.12081
Korotkova, T., Fuchs, E.C., Ponomarenko, A., von Engelhardt, J., Monyer, H., 2010a. NMDA receptor ablation on parvalbumin-

positive interneurons impairs hippocampal synchrony, spatial representations, and working memory. Neuron 68, 557–569. https://doi.org/10.1016/j.neuron.2010.09.017
Korotkova, T., Fuchs, E.C., Ponomarenko, A., von Engelhardt, J., Monyer, H., 2010b. NMDA Receptor Ablation on Parvalbumin-Positive Interneurons Impairs Hippocampal Synchrony, Spatial Representations, and Working Memory. Neuron 68, 557–569. https://doi.org/10.1016/j.neuron.2010.09.017
Koshiyama, D., Kirihara, K., Tada, M., Nagai, T., Fujioka, M., Usui, K., Araki, T., Kasai, K., 2020. Reduced Auditory Mismatch Negativity Reflects Impaired Deviance Detection in Schizophrenia. Schizophr. Bull. 46, 937–946. https://doi.org/10.1093/schbul/sbaa006
Krystal, J.H., Karper, L.P., Seibyl, J.P., Freeman, G.K., Delaney, R., Bremner, J.D., Heninger, G.R., Bowers, M.B., Charney, D.S., 1994. Subanesthetic effects of the noncompetitive NMDA antagonist, ketamine, in humans. Psychotomimetic, perceptual, cognitive, and neuroendocrine responses. Arch. Gen. Psychiatry 51, 199–214. https://doi.org/10.1001/archpsyc.1994.03950030035004
Krzystanek, M., Pałasz, A., 2019. NMDA Receptor Model of Antipsychotic Drug-Induced Hypofrontality. Int. J. Mol. Sci. 20, 1442. https://doi.org/10.3390/ijms20061442
Kumar, S., Soren, S., Chaudhury, S., 2009. Hallucinations: Etiology and clinical implications. Ind. Psychiatry J. 18, 119–126. https://doi.org/10.4103/0972-6748.62273
Lahti, A.C., Koffel, B., LaPorte, D., Tamminga, C.A., 1995. Subanesthetic doses of ketamine stimulate psychosis in schizophrenia. Neuropsychopharmacol. Off. Publ. Am. Coll. Neuropsychopharmacol. 13, 9–19. https://doi.org/10.1016/0893-133X(94)00131-I
Lancaster, G., Iatsenko, D., Pidde, A., Ticcinelli, V., Stefanovska, A., 2018. Surrogate data for hypothesis testing of physical systems. Phys. Rep., Surrogate data for hypothesis testing of physical systems 748, 1–60. https://doi.org/10.1016/j.physrep.2018.06.001
Lee, G., Zhou, Y., 2019. NMDAR Hypofunction Animal Models of Schizophrenia. Front. Mol. Neurosci. 12, 185. https://doi.org/10.3389/fnmol.2019.00185
Lee, J., Hudson, M.R., O'Brien, T.J., Nithianantharajah, J., Jones, N.C., 2017. Local NMDA receptor hypofunction evokes generalized

effects on gamma and high-frequency oscillations and behavior. Neuroscience 358, 124–136. https://doi.org/10.1016/j.neuroscience.2017.06.039
Leger, M., Quiedeville, A., Bouet, V., Haelewyn, B., Boulouard, M., Schumann-Bard, P., Freret, T., 2013. Object recognition test in mice. Nat. Protoc. 8, 2531–2537. https://doi.org/10.1038/nprot.2013.155
Lewis, D.A., Hashimoto, T., Volk, D.W., 2005. Cortical inhibitory neurons and schizophrenia. Nat. Rev. Neurosci. 6, 312–324. https://doi.org/10.1038/nrn1648
Lewis, D.A., Levitt, P., 2002. Schizophrenia as a disorder of neurodevelopment. Annu. Rev. Neurosci. 25, 409–432. https://doi.org/10.1146/annurev.neuro.25.112701.142754
Lezak, K.R., Missig, G., Carlezon Jr, W.A., 2017. Behavioral methods to study anxiety in rodents. Dialogues Clin. Neurosci. 19, 181–191.
Li, L., Vlisides, P.E., 2016. Ketamine: 50 Years of Modulating the Mind. Front. Hum. Neurosci. 10, 612. https://doi.org/10.3389/fnhum.2016.00612
Lladó-Pelfort, L., Troyano-Rodriguez, E., van den Munkhof, H.E., Cervera-Ferri, A., Jurado, N., Núñez-Calvet, M., Artigas, F., Celada, P., 2016. Phencyclidine-induced disruption of oscillatory activity in prefrontal cortex: Effects of antipsychotic drugs and receptor ligands. Eur. Neuropsychopharmacol. 26, 614–625. https://doi.org/10.1016/j.euroneuro.2015.11.015
Lyne, J., O'Donoghue, B., Roche, E., Renwick, L., Cannon, M., Clarke, M., 2018. Negative symptoms of psychosis: A life course approach and implications for prevention and treatment. Early Interv. Psychiatry 12, 561–571. https://doi.org/10.1111/eip.12501
Mäki-Marttunen, T., Krull, F., Bettella, F., Hagen, E., Næss, S., Ness, T.V., Moberget, T., Elvsåshagen, T., Metzner, C., Devor, A., Edwards, A.G., Fyhn, M., Djurovic, S., Dale, A.M., Andreassen, O.A., Einevoll, G.T., 2019. Alterations in Schizophrenia-Associated Genes Can Lead to Increased Power in Delta Oscillations. Cereb. Cortex N. Y. N 1991 29, 875–891. https://doi.org/10.1093/cercor/bhy291
Marder, S.R., Meibach, R.C., 1994. Risperidone in the treatment of schizophrenia. Am. J. Psychiatry 151, 825–835. https://doi.org/10.1176/ajp.151.6.825
McDonald-McGinn, D.M., Sullivan, K.E., Marino, B., Philip, N., Swillen, A., Vorstman, J.A.S., Zackai, E.H., Emanuel, B.S.,

Vermeesch, J.R., Morrow, B.E., Scambler, P.J., Bassett, A.S., 2015. 22q11.2 deletion syndrome. Nat. Rev. Dis. Primer 1, 15071. https://doi.org/10.1038/nrdp.2015.71

McKibben, C.E., Jenkins, T.A., Adams, H.N., Harte, M.K., Reynolds, G.P., 2010. Effect of pretreatment with risperidone on phencyclidine-induced disruptions in object recognition memory and prefrontal cortex parvalbumin immunoreactivity in the rat. Behav. Brain Res. 208, 132–136. https://doi.org/10.1016/j.bbr.2009.11.018

Mechelli, A., Allen, P., Amaro, E., Fu, C.H.Y., Williams, S.C.R., Brammer, M.J., Johns, L.C., McGuire, P.K., 2007. Misattribution of speech and impaired connectivity in patients with auditory verbal hallucinations. Hum. Brain Mapp. 28, 1213–1222. https://doi.org/10.1002/hbm.20341

Meltzer, H., Massey, B., 2011. The role of serotonin receptors in the action of atypical antipsychotic drugs. Curr. Opin. Pharmacol. 11, 59–67. https://doi.org/10.1016/j.coph.2011.02.007

Meltzer, H.Y., 2012. Serotonergic Mechanisms as Targets for Existing and Novel Antipsychotics, in: Gross, G., Geyer, M.A. (Eds.), Current Antipsychotics, Handbook of Experimental Pharmacology. Springer, Berlin, Heidelberg, pp. 87–124. https://doi.org/10.1007/978-3-642-25761-2_4

Meltzer, H.Y., Horiguchi, M., Massey, B.W., 2011. The role of serotonin in the NMDA receptor antagonist models of psychosis and cognitive impairment. Psychopharmacology (Berl.) 213, 289–305. https://doi.org/10.1007/s00213-010-2137-8

Meltzer, H.Y., Huang, M., 2008. In vivo actions of atypical antipsychotic drug on serotonergic and dopaminergic systems, in: Di Giovann, G., Di Matteo, V., Esposito, E. (Eds.), Progress in Brain Research, Serotonin–Dopamine Interaction: Experimental Evidence and Therapeutic Relevance. Elsevier, pp. 177–197. https://doi.org/10.1016/S0079-6123(08)00909-6

Merritt, K., Mcguire, P., Egerton, A., 2013. Relationship between Glutamate Dysfunction and Symptoms and Cognitive Function in Psychosis. Front. Psychiatry 4, 151. https://doi.org/10.3389/fpsyt.2013.00151

Millan, M.J., Andrieux, A., Bartzokis, G., Cadenhead, K., Dazzan, P., Fusar-Poli, P., Gallinat, J., Giedd, J., Grayson, D.R., Heinrichs, M., Kahn, R., Krebs, M.-O., Leboyer, M., Lewis, D., Marin, O., Marin, P., Meyer-Lindenberg, A., McGorry, P., McGuire, P.,

Owen, M.J., Patterson, P., Sawa, A., Spedding, M., Uhlhaas, P., Vaccarino, F., Wahlestedt, C., Weinberger, D., 2016. Altering the course of schizophrenia: progress and perspectives. Nat. Rev. Drug Discov. 15, 485–515. https://doi.org/10.1038/nrd.2016.28

Miller, E.K., 2000. The prefontral cortex and cognitive control. Nat. Rev. Neurosci. 1, 59–65. https://doi.org/10.1038/35036228

Minzenberg, M.J., Laird, A.R., Thelen, S., Carter, C.S., Glahn, D.C., 2009. Meta-analysis of 41 functional neuroimaging studies of executive function in schizophrenia. Arch. Gen. Psychiatry 66, 811–822. https://doi.org/10.1001/archgenpsychiatry.2009.91

Modi, M.E., Sahin, M., 2017. Translational use of event-related potentials to assess circuit integrity in ASD. Nat. Rev. Neurol. 13, 160–170. https://doi.org/10.1038/nrneurol.2017.15

Moran, R.J., Jones, M.W., Blockeel, A.J., Adams, R.A., Stephan, K.E., Friston, K.J., 2015. Losing Control Under Ketamine: Suppressed Cortico-Hippocampal Drive Following Acute Ketamine in Rats. Neuropsychopharmacology 40, 268–277. https://doi.org/10.1038/npp.2014.184

Mouri, A., Koseki, T., Narusawa, S., Niwa, M., Mamiya, T., Kano, S., Sawa, A., Nabeshima, T., 2012. Mouse strain differences in phencyclidine-induced behavioural changes. Int. J. Neuropsychopharmacol. 15, 767–779. https://doi.org/10.1017/S146114571100085X

Nandi, B., Swiatek, P., Kocsis, B., Ding, M., 2019. Inferring the direction of rhythmic neural transmission via inter-regional phase-amplitude coupling (ir-PAC). Sci. Rep. 9, 6933. https://doi.org/10.1038/s41598-019-43272-w

Negrón-Oyarzo, I., Espinosa, N., Aguilar-Rivera, M., Fuenzalida, M., Aboitiz, F., Fuentealba, P., 2018. Coordinated prefrontal-hippocampal activity and navigation strategy-related prefrontal firing during spatial memory formation. Proc. Natl. Acad. Sci. U. S. A. 115, 7123–7128. https://doi.org/10.1073/pnas.1720117115

Neill, J.C., Harte, M.K., Haddad, P.M., Lydall, E.S., Dwyer, D.M., 2014. Acute and chronic effects of NMDA receptor antagonists in rodents, relevance to negative symptoms of schizophrenia: A translational link to humans. Eur. Neuropsychopharmacol., Negative symptoms of schizophrenia: clinical characteristics and their measurement, experimental modelling, and opportunities for improved treatment 24, 822–835. https://doi.org/10.1016/j.euroneuro.2013.09.011

Nestler, E.J., Hyman, S.E., 2010. Animal models of neuropsychiatric disorders. Nat. Neurosci. 13, 1161–1169. https://doi.org/10.1038/nn.2647

Nolte, G., Ziehe, A., Nikulin, V.V., Schlögl, A., Krämer, N., Brismar, T., Müller, K.-R., 2008. Robustly estimating the flow direction of information in complex physical systems. Phys Rev Lett 100, 234101–234101. https://doi.org/10.1103/PhysRevLett.100.234101

O'Donnell, B.F., Vohs, J.L., Krishnan, G.P., Rass, O., Hetrick, W.P., Morzorati, S.L., 2013. The auditory steady-state response (ASSR): a translational biomarker for schizophrenia. Suppl. Clin. Neurophysiol. 62, 101–112. https://doi.org/10.1016/b978-0-7020-5307-8.00006-5

Onslow, A.C.E., Bogacz, R., Jones, M.W., 2011. Quantifying phase-amplitude coupling in neuronal network oscillations. Prog. Biophys. Mol. Biol. 105, 49–57. https://doi.org/10.1016/j.pbiomolbio.2010.09.007

Owen, M.J., Sawa, A., Mortensen, P.B., 2016. Schizophrenia. The Lancet 388, 86–97. https://doi.org/10.1016/S0140-6736(15)01121-6

Phillips, K.G., Cotel, M.C., McCarthy, A.P., Edgar, D.M., Tricklebank, M., O'Neill, M.J., Jones, M.W., Wafford, K.A., 2012. Differential effects of NMDA antagonists on high frequency and gamma EEG oscillations in a neurodevelopmental model of schizophrenia. Neuropharmacology, Schizophrenia 62, 1359–1370. https://doi.org/10.1016/j.neuropharm.2011.04.006

Phillips, W.A., Silverstein, S.M., 2003. Convergence of biological and psychological perspectives on cognitive coordination in schizophrenia. Behav. Brain Sci. 26, 65–137. https://doi.org/10.1017/S0140525X03000025

Pittman-Polletta, B., Hu, K., Kocsis, B., 2018. Subunit-specific NMDAR antagonism dissociates schizophrenia subtype-relevant oscillopathies associated with frontal hypofunction and hippocampal hyperfunction. Sci. Rep. 8, 11588. https://doi.org/10.1038/s41598-018-29331-8

Puig, M.V., Gener, T., 2015. Serotonin Modulation of Prefronto-Hippocampal Rhythms in Health and Disease. ACS Chem. Neurosci. 6, 1017–1025. https://doi.org/10.1021/cn500350e

Puig, M.V., Gulledge, A.T., 2011. Serotonin and prefrontal cortex function: neurons, networks, and circuits. Mol. Neurobiol. 44, 449–464. https://doi.org/10.1007/s12035-011-8214-0

Puig, M.V., Miller, E.K., 2015. Neural Substrates of Dopamine D2 Receptor Modulated Executive Functions in the Monkey Prefrontal Cortex. Cereb. Cortex 25, 2980–2987. https://doi.org/10.1093/cercor/bhu096

Puig, M.V., Watakabe, A., Ushimaru, M., Yamamori, T., Kawaguchi, Y., 2010. Serotonin modulates fast-spiking interneuron and synchronous activity in the rat prefrontal cortex through 5-HT1A and 5-HT2A receptors. J. Neurosci. 30, 2211–2222. https://doi.org/10.1523/JNEUROSCI.3335-09.2010

Puighermanal, E., Biever, A., Espallergues, J., Gangarossa, G., De Bundel, D., Valjent, E., 2015. drd2-cre:ribotag mouse line unravels the possible diversity of dopamine d2 receptor-expressing cells of the dorsal mouse hippocampus. Hippocampus 25, 858–875. https://doi.org/10.1002/hipo.22408

Rajagopal, L., Massey, B.W., Michael, E., Meltzer, H.Y., 2016a. Serotonin (5-HT)1A receptor agonism and 5-HT7 receptor antagonism ameliorate the subchronic phencyclidine-induced deficit in executive functioning in mice. Psychopharmacology (Berl.) 233, 649–660. https://doi.org/10.1007/s00213-015-4137-1

Rajagopal, L., Massey, B.W., Michael, E., Meltzer, H.Y., 2016b. Serotonin (5-HT)1A receptor agonism and 5-HT7 receptor antagonism ameliorate the subchronic phencyclidine-induced deficit in executive functioning in mice. Psychopharmacology (Berl.) 233, 649–660. https://doi.org/10.1007/s00213-015-4137-1

Rapoport, J., Giedd, J., Gogtay, N., 2012. Neurodevelopmental model of schizophrenia: update 2012. Mol. Psychiatry 17, 1228–1238. https://doi.org/10.1038/mp.2012.23

Ripke, S., Neale, B.M., Corvin, A., Walters, J.T., Farh, K.-H., Holmans, P.A., Lee, P., Bulik-Sullivan, B., Collier, D.A., Huang, H., Pers, T.H., Agartz, I., Agerbo, E., Albus, M., Alexander, M., Amin, F., Bacanu, S.A., Begemann, M., Belliveau, R.A., Bene, J., Bergen, S.E., Bevilacqua, E., Bigdeli, T.B., Black, D.W., Bruggeman, R., Buccola, N.G., Buckner, R.L., Byerley, W., Cahn, W., Cai, G., Campion, D., Cantor, R.M., Carr, V.J., Carrera, N., Catts, S.V., Chambert, K.D., Chan, R.C., Chan, R.Y., Chen, E.Y., Cheng, W., Cheung, E.F., Chong, S.A., Cloninger, C.R., Cohen, D., Cohen, N., Cormican, P., Craddock, N., Crowley, J.J., Curtis, D., Davidson, M., Davis, K.L., Degenhardt, F., Del Favero, J., Demontis, D., Dikeos, D., Dinan, T., Djurovic, S., Donohoe, G., Drapeau, E., Duan, J., Dudbridge, F., Durmishi, N., Eichhammer,

P., Eriksson, J., Escott-Price, V., Essioux, L., Fanous, A.H., Farrell, M.S., Frank, J., Franke, L., Freedman, R., Freimer, N.B., Friedl, M., Friedman, J.I., Fromer, M., Genovese, G., Georgieva, L., Giegling, I., Giusti-Rodríguez, P., Godard, S., Goldstein, J.I., Golimbet, V., Gopal, S., Gratten, J., de Haan, L., Hammer, C., Hamshere, M.L., Hansen, M., Hansen, T., Haroutunian, V., Hartmann, A.M., Henskens, F.A., Herms, S., Hirschhorn, J.N., Hoffmann, P., Hofman, A., Hollegaard, M.V., Hougaard, D.M., Ikeda, M., Joa, I., Julià, A., Kahn, R.S., Kalaydjieva, L., Karachanak-Yankova, S., Karjalainen, J., Kavanagh, D., Keller, M.C., Kennedy, J.L., Khrunin, A., Kim, Y., Klovins, J., Knowles, J.A., Konte, B., Kucinskas, V., Kucinskiene, Z.A., Kuzelova-Ptackova, H., Kähler, A.K., Laurent, C., Lee, J., Lee, S.H., Legge, S.E., Lerer, B., Li, M., Li, T., Liang, K.-Y., Lieberman, J., Limborska, S., Loughland, C.M., Lubinski, J., Lönnqvist, J., Macek, M., Magnusson, P.K., Maher, B.S., Maier, W., Mallet, J., Marsal, S., Mattheisen, M., Mattingsdal, M., McCarley, R.W., McDonald, C., McIntosh, A.M., Meier, S., Meijer, C.J., Melegh, B., Melle, I., Mesholam-Gately, R.I., Metspalu, A., Michie, P.T., Milani, L., Milanova, V., Mokrab, Y., Morris, D.W., Mors, O., Murphy, K.C., Murray, R.M., Myin-Germeys, I., Müller-Myhsok, B., Nelis, M., Nenadic, I., Nertney, D.A., Nestadt, G., Nicodemus, K.K., Nikitina-Zake, L., Nisenbaum, L., Nordin, A., O'Callaghan, E., O'Dushlaine, C., O'Neill, F.A., Oh, S.-Y., Olincy, A., Olsen, L., Van Os, J., Pantelis, C., Papadimitriou, G.N., Papiol, S., Parkhomenko, E., Pato, M.T., Paunio, T., Pejovic-Milovancevic, M., Perkins, D.O., Pietiläinen, O., Pimm, J., Pocklington, A.J., Powell, J., Price, A., Pulver, A.E., Purcell, S.M., Quested, D., Rasmussen, H.B., Reichenberg, A., Reimers, M.A., Richards, A.L., Roffman, J.L., Roussos, P., Ruderfer, D.M., Salomaa, V., Sanders, A.R., Schall, U., Schubert, C.R., Schulze, T.G., Schwab, S.G., Scolnick, E.M., Scott, R.J., Seidman, L.J., Shi, J., Sigurdsson, E., Silagadze, T., Silverman, J.M., Sim, K., Slominsky, P., Smoller, J.W., So, H.-C., Spencer, C.C.A., Stahl, E.A., Stefansson, H., Steinberg, S., Stogmann, E., Straub, R.E., Strengman, E., Strohmaier, J., Stroup, T.S., Subramaniam, M., Suvisaari, J., Svrakic, D.M., Szatkiewicz, J.P., Söderman, E., Thirumalai, S., Toncheva, D., Tosato, S., Veijola, J., Waddington, J., Walsh, D., Wang, D., Wang, Q., Webb, B.T., Weiser, M., Wildenauer, D.B., Williams, N.M., Williams, S.,

Witt, S.H., Wolen, A.R., Wong, E.H., Wormley, B.K., Xi, H.S., Zai, C.C., Zheng, X., Zimprich, F., Wray, N.R., Stefansson, K., Visscher, P.M., Adolfsson, R., Andreassen, O.A., Blackwood, D.H., Bramon, E., Buxbaum, J.D., Børglum, A.D., Cichon, S., Darvasi, A., Domenici, E., Ehrenreich, H., Esko, T., Gejman, P.V., Gill, M., Gurling, H., Hultman, C.M., Iwata, N., Jablensky, A.V., Jönsson, E.G., Kendler, K.S., Kirov, G., Knight, J., Lencz, T., Levinson, D.F., Li, Q.S., Liu, J., Malhotra, A.K., McCarroll, S.A., McQuillin, A., Moran, J.L., Mortensen, P.B., Mowry, B.J., Nöthen, M.M., Ophoff, R.A., Owen, M.J., Palotie, A., Pato, C.N., Petryshen, T.L., Posthuma, D., Rietschel, M., Riley, B.P., Rujescu, D., Sham, P.C., Sklar, P., St Clair, D., Weinberger, D.R., Wendland, J.R., Werge, T., Daly, M.J., Sullivan, P.F., O'Donovan, M.C., 2014. Biological Insights From 108 Schizophrenia-Associated Genetic Loci. Nature 511, 421–427. https://doi.org/10.1038/nature13595

Rissling, A.J., Light, G.A., 2010. Neurophysiological measures of sensory registration, stimulus discrimination, and selection in schizophrenia patients. Curr. Top. Behav. Neurosci. 4, 283–309. https://doi.org/10.1007/7854_2010_59

Santana, N., Mengod, G., Artigas, F., 2009. Quantitative analysis of the expression of dopamine D1 and D2 receptors in pyramidal and GABAergic neurons of the rat prefrontal cortex. Cereb. Cortex N. Y. N 1991 19, 849–860. https://doi.org/10.1093/cercor/bhn134

Sauseng, P., Griesmayr, B., Freunberger, R., Klimesch, W., 2010. Control mechanisms in working memory: a possible function of EEG theta oscillations. Neurosci. Biobehav. Rev. 34, 1015–1022. https://doi.org/10.1016/j.neubiorev.2009.12.006

Scheffer-Teixeira, R., Tort, A.B.L., 2017. Unveiling fast field oscillations through comodulation. eneuro. https://doi.org/10.1523/ENEURO.0079-17.2017

Schuelert, N., Dorner-Ciossek, C., Brendel, M., Rosenbrock, H., 2018. A comprehensive analysis of auditory event-related potentials and network oscillations in an NMDA receptor antagonist mouse model using a novel wireless recording technology. Physiol. Rep. 6, e13782. https://doi.org/10.14814/phy2.13782

SCIMEMI, P., SANTARELLI, R., SELMO, A., MAMMANO, F., 2014. Auditory brainstem responses to clicks and tone bursts in C57 BL/6J mice. Acta Otorhinolaryngol. Ital. 34, 264–271.

Shaw, A.D., Saxena, N., E. Jackson, L., Hall, J.E., Singh, K.D.,

Muthukumaraswamy, S.D., 2015. Ketamine amplifies induced gamma frequency oscillations in the human cerebral cortex. Eur. Neuropsychopharmacol. 25, 1136–1146. https://doi.org/10.1016/j.euroneuro.2015.04.012
Shen, C.-L., Chou, T.-L., Lai, W.-S., Hsieh, M.H., Liu, C.-C., Liu, C.-M., Hwu, H.-G., 2020. P50, N100, and P200 Auditory Sensory Gating Deficits in Schizophrenia Patients. Front. Psychiatry 11, 868. https://doi.org/10.3389/fpsyt.2020.00868
Siafis, S., Tzachanis, D., Samara, M., Papazisis, G., 2018. Antipsychotic Drugs: From Receptor-binding Profiles to Metabolic Side Effects. Curr. Neuropharmacol. 16, 1210–1223. https://doi.org/10.2174/1570159X15666170630163616
Siekmeier, P.J., Stufflebeam, S.M., 2010. Patterns of spontaneous magnetoencephalographic activity in patients with schizophrenia. J. Clin. Neurophysiol. Off. Publ. Am. Electroencephalogr. Soc. 27, 179–190. https://doi.org/10.1097/WNP.0b013e3181e0b20a
Sigurdsson, T., 2016. Neural circuit dysfunction in schizophrenia: Insights from animal models. Neuroscience 321, 42–65. https://doi.org/10.1016/j.neuroscience.2015.06.059
Sigurdsson, T., Duvarci, S., 2016. Hippocampal-Prefrontal Interactions in Cognition, Behavior and Psychiatric Disease. Front. Syst. Neurosci. 9. https://doi.org/10.3389/fnsys.2015.00190
Sigurdsson, T., Stark, K.L., Karayiorgou, M., Gogos, J.A., Gordon, J.A., 2010. Impaired hippocampal–prefrontal synchrony in a genetic mouse model of schizophrenia. Nature 464, 763–767. https://doi.org/10.1038/nature08855
Skene, N.G., Bryois, J., Bakken, T.E., Breen, G., Crowley, J.J., Gaspar, H.A., Giusti-Rodriguez, P., Hodge, R.D., Miller, J.A., Muñoz-Manchado, A.B., O'Donovan, M.C., Owen, M.J., Pardiñas, A.F., Ryge, J., Walters, J.T.R., Linnarsson, S., Lein, E.S., Sullivan, P.F., Hjerling-Leffler, J., 2018. Genetic identification of brain cell types underlying schizophrenia. Nat. Genet. 50, 825–833. https://doi.org/10.1038/s41588-018-0129-5
Spellman, T., Rigotti, M., Ahmari, S.E., Fusi, S., Gogos, J.A., Gordon, J.A., 2015. Hippocampal-prefrontal input supports spatial encoding in working memory. Nature 522, 309–314. https://doi.org/10.1038/nature14445
Spencer, K.M., Nestor, P.G., Niznikiewicz, M.A., Salisbury, D.F., Shenton, M.E., McCarley, R.W., 2003. Abnormal neural synchrony in schizophrenia. J. Neurosci. Off. J. Soc. Neurosci.

23, 7407–7411.
Spencer, K.M., Niznikiewicz, M.A., Nestor, P.G., Shenton, M.E., McCarley, R.W., 2009. Left auditory cortex gamma synchronization and auditory hallucination symptoms in schizophrenia. BMC Neurosci. 10, 85. https://doi.org/10.1186/1471-2202-10-85
Stam, C.J., Nolte, G., Daffertshofer, A., 2007. Phase lag index: assessment of functional connectivity from multi channel EEG and MEG with diminished bias from common sources. Hum. Brain Mapp. 28, 1178–93. https://doi.org/10.1002/hbm.20346
Stassen, H.H., Coppola, R., Gottesman, I.I., Torrey, E.F., Kuny, S., Rickler, K.C., Hell, D., 1999. EEG differences in monozygotic twins discordant and concordant for schizophrenia. Psychophysiology 36, 109–117. https://doi.org/10.1017/s0048577299970713
Strekalova, T., Steinbusch, H.W.M., 2010. Measuring behavior in mice with chronic stress depression paradigm. Prog. Neuropsychopharmacol. Biol. Psychiatry 34, 348–361. https://doi.org/10.1016/j.pnpbp.2009.12.014
Sturgeon, R.D., Fessler, R.G., Meltzer, H.Y., 1979. Behavioral rating scales for assessing phencyclidine-induced locomotor activity, stereotyped behavior and ataxia in rats. Eur. J. Pharmacol. 59, 169–179. https://doi.org/10.1016/0014-2999(79)90279-6
Sur, S., Sinha, V.K., 2009. Event-related potential: An overview. Ind. Psychiatry J. 18, 70–73. https://doi.org/10.4103/0972-6748.57865
Takehara-Nishiuchi, K., 2020. Prefrontal–hippocampal interaction during the encoding of new memories. Brain Neurosci. Adv. 4, 2398212820925580. https://doi.org/10.1177/2398212820925580
Tamura, M., Spellman, T.J., Rosen, A.M., Gogos, J.A., Gordon, J.A., 2017. Hippocampal-prefrontal theta-gamma coupling during performance of a spatial working memory task. Nat. Commun. 8, 2182. https://doi.org/10.1038/s41467-017-02108-9
Tandon, R., MD, 2011. Antipsychotics in the Treatment of Schizophrenia: An Overview. J. Clin. Psychiatry 72, 0–0. https://doi.org/10.4088/JCP.10075su1.01
Tavares, L.C., Tort, A.B., 2020. Hippocampal-prefrontal interactions during spatial decision-making. bioRxiv 2020.06.24.168732. https://doi.org/10.1101/2020.06.24.168732
Tomelleri, L., Jogia, J., Perlini, C., Bellani, M., Ferro, A., Rambaldelli, G., Tansella, M., Frangou, S., Brambilla, P., 2009. Brain

structural changes associated with chronicity and antipsychotic treatment in schizophrenia. Eur. Neuropsychopharmacol. 19, 835–840. https://doi.org/10.1016/j.euroneuro.2009.07.007
Tort, A.B.L., Komorowski, R.W., Manns, J.R., Kopell, N.J., Eichenbaum, H., 2009. Theta–gamma coupling increases during the learning of item–context associations. Proc. Natl. Acad. Sci. 106, 20942–20947. https://doi.org/10.1073/pnas.0911331106
Tort, A.B.L., Kramer, M.A., Thorn, C., Gibson, D.J., Kubota, Y., Graybiel, A.M., Kopell, N.J., 2008. Dynamic cross-frequency couplings of local field potential oscillations in rat striatum and hippocampus during performance of a T-maze task. Proc Natl Acad Sci U A 105, 20517–20522.
Trimper, J.B., Galloway, C.R., Jones, A.C., Mandi, K., Manns, J.R., 2017. Gamma Oscillations in Rat Hippocampal Subregions Dentate Gyrus, CA3, CA1, and Subiculum Underlie Associative Memory Encoding. Cell Rep. 21, 2419–2432. https://doi.org/10.1016/j.celrep.2017.10.123
Turetsky, B.I., Calkins, M.E., Light, G.A., Olincy, A., Radant, A.D., Swerdlow, N.R., 2007. Neurophysiological endophenotypes of schizophrenia: the viability of selected candidate measures. Schizophr. Bull. 33, 69–94. https://doi.org/10.1093/schbul/sbl060
Turetsky, B.I., Dress, E.M., Braff, D.L., Calkins, M.E., Green, M.F., Greenwood, T.A., Gur, R.E., Gur, R.C., Lazzeroni, L.C., Nuechterlein, K.H., Radant, A.D., Seidman, L.J., Siever, L.J., Silverman, J.M., Sprock, J., Stone, W.S., Sugar, C.A., Swerdlow, N.R., Tsuang, D.W., Tsuang, M.T., Light, G., 2015. The Utility of P300 as a Schizophrenia Endophenotype and Predictive Biomarker: Clinical and Socio-Demographic Modulators in COGS-2. Schizophr. Res. 163, 53–62. https://doi.org/10.1016/j.schres.2014.09.024
Uhlhaas, P.J., Singer, W., 2010. Abnormal neural oscillations and synchrony in schizophrenia. Nat. Rev. Neurosci. 11, 100–113. https://doi.org/10.1038/nrn2774
Umbricht, D., Javitt, D., Novak, G., Bates, J., Pollack, S., Lieberman, J., Kane, J., 1999. Effects of risperidone on auditory event-related potentials in schizophrenia. Int. J. Neuropsychopharmacol. 2, 299–304. https://doi.org/10.1017/S1461145799001595
Vallat, R., 2018. Pingouin: statistics in Python. J. Open Source Softw. 3, 1026. https://doi.org/10.21105/joss.01026
Valli, I., Stone, J., Mechelli, A., Bhattacharyya, S., Raffin, M., Allen, P.,

Fusar-Poli, P., Lythgoe, D., O'Gorman, R., Seal, M., McGuire, P., 2011. Altered Medial Temporal Activation Related to Local Glutamate Levels in Subjects with Prodromal Signs of Psychosis. Biol. Psychiatry 69, 97–99. https://doi.org/10.1016/j.biopsych.2010.08.033

van Vugt, M.K., Schulze-Bonhage, A., Litt, B., Brandt, A., Kahana, M.J., 2010. Hippocampal Gamma Oscillations Increase with Memory Load. J. Neurosci. 30, 2694–2699. https://doi.org/10.1523/JNEUROSCI.0567-09.2010

Vertes, R.P., 2006. Interactions among the medial prefrontal cortex, hippocampus and midline thalamus in emotional and cognitive processing in the rat. Neuroscience 142, 1–20. https://doi.org/10.1016/j.neuroscience.2006.06.027

Vinck, M., Oostenveld, R., Wingerden, M.V., Battaglia, F., Pennartz, C.M.A., 2011. An improved index of phase-synchronization for electrophysiological data in the presence of volume-conduction , noise and sample-size bias. NeuroImage 55, 1548–1565. https://doi.org/10.1016/j.neuroimage.2011.01.055

Wang, X., Li, Y., Chen, J., Li, Z., Li, J., Qin, L., 2020. Aberrant Auditory Steady-State Response of Awake Mice After Single Application of the NMDA Receptor Antagonist MK-801 Into the Medial Geniculate Body. Int. J. Neuropsychopharmacol. 23, 459–468. https://doi.org/10.1093/ijnp/pyaa022

Warburton, E.C., Brown, M.W., 2015. Neural circuitry for rat recognition memory. Behav. Brain Res. 285, 131–139. https://doi.org/10.1016/j.bbr.2014.09.050

Williams, A.A., Ingram, W.M., Levine, S., Resnik, J., Kamel, C.M., Lish, J.R., Elizalde, D.I., Janowski, S.A., Shoker, J., Kozlenkov, A., González-Maeso, J., Gallitano, A.L., 2012. Reduced levels of serotonin 2A receptors underlie resistance of Egr3-deficient mice to locomotor suppression by clozapine. Neuropsychopharmacol. Off. Publ. Am. Coll. Neuropsychopharmacol. 37, 2285–98. https://doi.org/10.1038/npp.2012.81

Wilson, C., Terry, A.V., 2010. Neurodevelopmental Animal Models of Schizophrenia: Role in Novel Drug Discovery and Development. Clin. Schizophr. Relat. Psychoses 4, 124–137. https://doi.org/10.3371/CSRP.4.2.4

Winson, J., 1978. Loss of hippocampal theta rhythm results in spatial memory deficit in the rat. Science 201, 160–163. https://doi.org/10.1126/science.663646

Winters, B.D., Saksida, L.M., Bussey, T.J., 2010. Implications of animal object memory research for human amnesia. Neuropsychologia 48, 2251–2261. https://doi.org/10.1016/j.neuropsychologia.2010.01.023

Yang, A.C., Tsai, S.-J., 2017. New Targets for Schizophrenia Treatment beyond the Dopamine Hypothesis. Int. J. Mol. Sci. 18, E1689. https://doi.org/10.3390/ijms18081689

Yao, Y., Wu, M., Wang, L., Lin, L., Xu, J., 2020. Phase coupled firing of prefrontal parvalbumin interneuron with high frequency oscillations. Front. Cell. Neurosci. 14, 610741. https://doi.org/10.3389/fncel.2020.610741

Young, J.W., Powell, S.B., Risbrough, V., Marston, H.M., Geyer, M.A., 2009. Using the MATRICS to guide development of a preclinical cognitive test battery for research in schizophrenia. Pharmacol. Ther. 122, 150–202. https://doi.org/10.1016/j.pharmthera.2009.02.004

Zhang, C., Li, H., Han, R., 2020. An open-source video tracking system for mouse locomotor activity analysis. BMC Res. Notes 13, 48. https://doi.org/10.1186/s13104-020-4916-6

Zhang, X., Zhong, W., Brankačk, J., Weyer, S.W., Müller, U.C., Tort, A.B.L., Draguhn, A., 2016. Impaired theta-gamma coupling in APP-deficient mice. Sci Rep 1–10. https://doi.org/10.1038/srep21948

Zheng, C., Bieri, K.W., Hwaun, E., Colgin, L.L., 2016. Fast Gamma Rhythms in the Hippocampus Promote Encoding of Novel Object-Place Pairings. eNeuro 3, ENEURO.0001-16.2016. https://doi.org/10.1523/ENEURO.0001-16.2016

Zijlmans, M., Jiruska, P., Zelmann, R., Leijten, F.S.S., Jefferys, J.G.R., Gotman, J., 2012. High-Frequency Oscillations as a New Biomarker in Epilepsy. Ann. Neurol. 71, 169–178. https://doi.org/10.1002/ana.22548